

UNIVERSITÀ DEGLI STUDI DI PADOVA

DIPARTIMENTO DI INGEGNERIA INDUSTRIALE

CORSO DI LAUREA MAGISTRALE IN INGEGNERIA CHIMICA E DEI PROCESSI
INDUSTRIALI

Tesi di Laurea Magistrale in
Ingegneria Chimica e dei Processi Industriali

**SEGREGATION AND MIXING OF PARTICLES OF
DIFFERENT SIZE AND SHAPE IN A ROTATING DRUM**

Relatore: Prof. Andrea Claudio Santomaso

Correlatore: Prof. Marco Ramaioli

Laureando: CLAUDIA PIACENZA

ANNO ACCADEMICO 2016–2017

Abstract

In this work, the segregation of particles with different properties is experimentally studied. The main attention is focused on mixtures of particles of different shapes, but also differently sized particles are considered. The experimental tests have been run with spherical particles of different size and with two types of ellipsoids as non-spherical particles. The mixer that has been used is a rotating drum with a very low thickness that allowed to consider only radial phenomena. The analysis of the mixtures in the drum has been carried out by a specific image analysis procedure developed with the open-source ImageJ software. It is shown that the shape determines segregation phenomena that occur with a dynamic similar to size segregation phenomena. The phenomenon does not depend neither on the initial configuration of the system nor on the rotational speed of the drum and its filling level.

The experimental work has been conducted at the Chemical and Process Engineering Department of the University of Surrey.

Contents

INTRODUCTION	1
CHAPTER 1 – MIXING AND SEGREGATION	3
1.1 Mixture classification	3
1.2 Mixing mechanisms.....	4
1.3 Types of mixers	5
1.3.1 Tumbling or diffusive mixers.....	5
1.3.2 Agitated or convective mixers.....	6
1.4 Flow regimes in the rotating drum	6
1.4.1 Slipping motion.....	7
1.4.2 Cascading (or tumbling) motion	7
1.4.3 Cataracting motion	8
1.5 Segregation phenomena.....	9
1.6 Literature review.....	11
1.6.1 Size segregation.....	11
1.6.2 Shape segregation.....	16
1.6.3 Summary of previous studies	21
CHAPTER 2 – MATERIALS AND METHODS	23
2.1 Materials	23
2.1.1 Spherical particles	23
2.1.2 Ellipsoids.....	25
2.1.3 Density measurement	28
2.1.3.1 The gas pycnometer	28
2.1.3.2 Density measurement procedure	29
2.1.4 3D printing	31
2.2 Experimental equipment.....	33

2.2.1	The rotating drum.....	33
2.2.2	The recording system	34
2.2.3	Velocity calculation.....	35
2.3	Experimental plan.....	37
2.3.1	Mixtures of particles of different shapes.....	37
2.3.2	Mixtures of particles of different sizes.....	38
2.4	Particles analysis	39
2.5	Drum analysis	44
2.5.1	Binary mixtures of spheres and ellipsoids with AR=1.5.....	44
2.5.2	Mixtures with ellipsoids with AR=3.5	46
2.6	Image analysis procedure	48
2.6.1	Procedure.....	48
2.6.2	Filling level evaluation.....	52
2.6.3	Angle evaluation	52
CHAPTER 3 – RESULTS AND DISCUSSION		55
3.1	Mixtures of particles of different shapes	55
3.1.1	Spheres and ellipsoids AR=1.5, $\omega=4.22$ rpm, $\phi=25\%$	55
3.1.2	Spheres and ellipsoids AR=3.5, $\omega=4.22$ rpm, $\phi=25\%$	61
3.1.3	Spheres and ellipsoids AR=1.5, $\omega=4.22$ rpm, $\phi=47\%$	68
3.1.4	Spheres and ellipsoids AR=3.5, $\omega=4.22$ rpm, $\phi=47\%$	72
3.1.5	Mixtures of ellipsoids (AR=1.5 and AR=3.5).....	77
3.1.6	Spheres and ellipsoids AR=1.5, $\omega=11.5$ rpm.....	85
3.1.7	Spheres and ellipsoids AR=3.5, $\omega=11.5$ rpm.....	88
3.1.8	Discussion	90
3.2	Mixtures of particles of different sizes	93
3.2.1	Spheres with 8 mm and 3.81 mm diameter.....	93
3.2.2	Spheres with 8 mm and 6 mm diameter.....	95
3.2.3	Comparison and discussion.....	97

3.3 Evaluation of Maximum Angle of Stability, Angle of Repose and Dynamic Repose Angle	98
CONCLUSIONS.....	113
APPENDIX	115
REFERENCES	119

Introduction

Mixing is one of the most common operations carried out in industry. In particular, mixing of solids is a widespread unit operation in particulate processes where consistency and homogeneity of the product is a key requirement. A proper mixing of granular materials is fundamental, for example, in the drug formulation but also in many other industrial fields, such as the food one, in which quality specification must be ensured.

Generally, particulate materials are made of particles that have different properties (size, density, shape) and when they are mixed together segregation phenomena are experienced. Segregation, however, has to be avoided since most of the processes require homogeneous mixtures: it is of relevant importance to understand segregation phenomena and to know how they occur so to be able to control and even try to avoid them.

Many experimental studies exist about segregation; in particular, size-induced and density-induced segregation phenomena have been widely investigated. About shape segregation, instead, limited experimental studies have been developed and the phenomenon has been investigated mainly through numerical simulations. However, it is important to extend the experimental study also to different shaped particles, considering that in many practical cases particles have an irregular shape and the case of spherical shape, often assumed as a reference, is just an ideal one. For this reason, this work was mainly focused on the experimental investigation of mixtures made of particles of different shape. Ellipsoids were used as non-spherical particles, with the aim of understanding if mixtures of spherical and ellipsoidal particles segregate and which operative variable can affect the system; also, mixtures of ellipsoids were considered. Size segregation was experimented too, due to its relevance. The experimental study has been conducted in a rotating drum, which is one of the most common mixers among the ones industrially adopted. The considered drum had a very thin thickness, in order to realize only a monolayer of particles; therefore, it was possible to focus only on the study of radial segregation and no axial phenomena were considered. The analysis of the system was done through image analysis, with a procedure developed with the ImageJ software.

This work is divided into three chapters. The first one introduces the main concepts related to the topic in question: mixing and segregation mechanisms are presented, together with the mixers used industrially. Also, the previous studies developed about size and shape segregation in rotating drums are reported. In the second chapter, the used particles are described, together with all the equipment; the experimental procedure followed in the experimental tests is presented as well. Finally, the results are reported and discussed in the third chapter.

Chapter 1

Mixing and segregation

Mixing is a process operation aimed at obtaining a homogeneous system starting from two or more components. On the contrary, when there is a lack of homogeneity within the mixture segregation occurs. Segregation phenomena represent a relevant problem in the case of mixing processes.

In this chapter, the main concepts related to mixing and segregation will be presented. Also, previous studies about size and shape segregation in the rotating drum are reported.

1.1 Mixture classification

Three types of mixture can be defined:

1. **Perfect mixture:** mixture of two types of particles in which in each position of the space the composition is the composition of the whole mixture. This represents an ideal situation, not possible in reality.
2. **Perfect random mixture:** mixture in which there is the same probability of finding a particle of one component in each point of the mixture. This is the maximum degree of mixing realizable.
3. **Segregated mixture:** mixture in which there is a high probability of finding one component in a certain region of the considered space. This configuration occurs typically when the components of the mixture present different properties.

The three types of mixture are reported in Figure 1.1

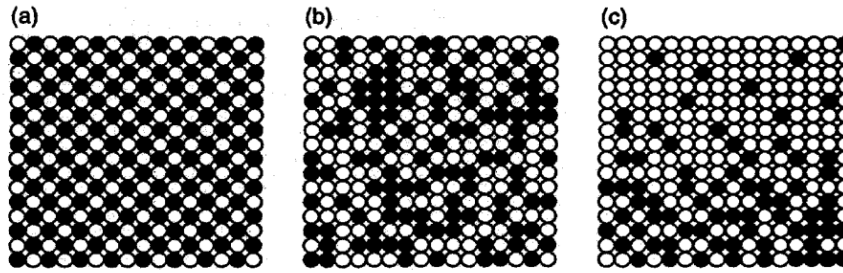


Figure 1.1. Three types of mixture: a) perfect mixture; b) perfect random mixture; c) segregated mixture (Rhodes, 2008).

Also, there is another type of mixture, the **structured or interactive mixture**, obtained when cohesive big particles are covered by fine particles with a homogeneous layer. In this case, if the interactions are very high segregated mixtures may form.

1.2 Mixing mechanisms

Differently from liquids and gases, solid particles are not thermal activated system and so in order to obtain a certain degree of mixing they need to be mechanically activated.

According to Rhodes (1998), three different mixing mechanisms can be distinguished:

1. **Dispersion:** it is analogous to diffusion in fluids. It involves single particles that randomly move due to collision between each other.
2. **Convection:** it involves a portion of the bulk material, with a precise direction and velocity.
3. **Shear mixing:** it is peculiar to granular solids and it is a combination of the two previous mechanisms. It combines a convective motion between layers of materials with and individual randomness across the planes.

In non-cohesive powders, dispersion and shear mixing affect segregation between particles; the convective mechanism instead is the main mixing mechanism.

1.3 Types of mixers

Powder mixers are relatively simple machines of low capital cost. They are classified into two types: tumbling mixers and agitated mixers.

1.3.1 Tumbling or diffusive mixers

Tumbling mixers are the simplest and the most common type. A totally enclosed vessel is rotated about an axis causing the particles within the mixer to tumble over each other on the mixture surface. In most cases the vessel is attached to a drive shaft and supported on one or two bearings; in the case of a horizontal cylinder, rotation can be effected by placing the cylinder on driving rollers.

The most common vessels of this type are:

- Horizontal drum.
- Double cone.
- V-tumbler.
- Y-tumbler.

They are shown in Figure 1.2:

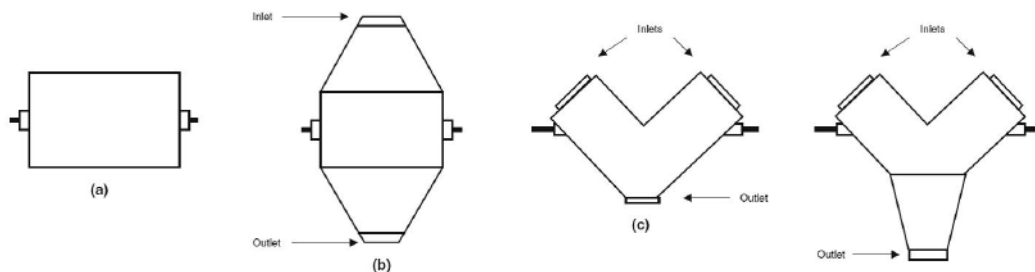


Figure 1.2 Tumbling mixers: a) horizontal drum; b) double cone mixer; c) V-mixers and Y-mixer (Rhodes, 2008).

Tumbling vessels provide low-shear environments and they are used when materials are shear sensitive or non-agglomerating.

To achieve better dispersion the presence of internal baffles is often required. In some cases, a high-speed impeller operating on the same axis of rotation as the shell can be used for extending the application of the tumblers to agglomerating and cohesive mixtures.

1.3.2 Agitated or convective mixers

Convective mixers are characterized by the action of impellers or paddles to move the powders around and generate a well-mixed product.

The most common types of convective mixers are:

- Ribbon mixer.
- Nauta mixer or orbiting screw mixer.
- Flow mixer.
- Paddle mixer.
- Horizontal double cone with baffles.

In these mixers, the mixing mechanism is the convective one. Convective mixers provide more shear into the mixture and tend to be utilized for cohesive materials.

1.4 Flow regimes in the rotating drum

Rotating drums are extensively used in the chemical and process industries; they are employed in the chemical, pharmaceutical, food, detergent and metallurgical industries to perform mixing, drying, decoating, heating and chemical reactions. With respect to mixing processes, rotating drums are used to study and understand mixing phenomena; as a result, many studies were developed about granular behaviour in rotating drums.

Different granular flow regimes can occur in the drum, each one with its specific flow behaviour. In particular, different flow regimes can be assessed by using the dimensionless Froude number which is defined by the following formula:

$$Fr = \frac{\omega^2 R}{g} \quad (1.1)$$

where ω [s^{-1}] is the drum rotation speed, R [m] the drum radius and g [m/s^2] the gravitational acceleration.

The different types of bed motion may be subdivided into three basic forms (Mellmann, 2001):

- Slipping motion.
- Cascading (or tumbling) motion.
- Cataracting motion.

Figure 1.3 illustrates the different flow regimes.

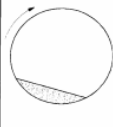
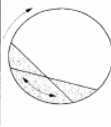

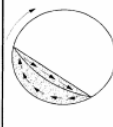

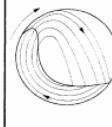
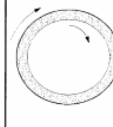
Basic form	Slipping motion		Cascading ("tumbling") motion			Catacting motion	
Subtype	Sliding	Surging	Slumping	Rolling	Cascading	Catacting	Centrifuging
Schematic							
Physical process	Slipping		Mixing			Crushing	Centrifuging
Froude number Fr [-]	$0 < Fr < 10^{-4}$		$10^{-5} < Fr < 10^{-3}$	$10^{-4} < Fr < 10^{-2}$	$10^{-3} < Fr < 10^{-1}$	$0.1 < Fr < 1$	$Fr \geq 1$
Filling degree f [-]	$f < 0.1$	$f > 0.1$	$f < 0.1$	$f > 0.1$		$f > 0.2$	
Wall friction coeff. μ_w [-]	$\mu_w < \mu_{w,c}$	$\mu_w \geq \mu_{w,c}$	$\mu_w > \mu_{w,c}$			$\mu_w > \mu_{w,c}$	
Application	no use		Rotary kilns and reactors; rotary dryers and coolers; mixing drums			Ball mills	no use

Figure 1.3. Forms of motion in rotating drums (Mellmann, 2001).

1.4.1 Slipping motion

Slipping motion can occur under favourable frictional conditions between the solid bed and the cylinder wall. There are two types of slipping motion:

- Sliding;
- Surging.

When the drum wall is very smooth, *sliding* regime may be observed in which the bed is constantly sliding from the wall. This can also occur at higher rotational speed and filling levels of the drum (Rutgers, 1965).

With higher wall friction, sliding turns into *surging*, characterized by periodic alternation between adhesive and kinetic friction of the bed on the wall. The solid bed adheres on the rotating wall up to a certain angle of deflection and subsequently slides back on the wall surface.

No mixing takes place in slipping motion and so this is usually an undesirable behaviour in practice that must be avoided by the use of rough walls or bars attached to the walls.

1.4.2 Cascading (or tumbling) motion

Cascading motion is observed when there is a sufficient wall friction. At different rotational speeds and with different particles size, three states of motion are possible:

- Slumping.

- Rolling.
- Cascading.

When the rotational speed is low, *slumping* of the bed may occur; the solid bed is continuously elevated, levelled off again and again by successive avalanches at the surface.

Increasing the rotational speed, a transition to *rolling* regime takes place. This motion is characterized by a uniform, steady flow of a particle layer on the surface (cascading layer) while the larger part of the bed (plug flow region) is moved upwards by solid rotation with the rotational speed of the wall. A uniform and good mixing is achievable with this type of motion, but when particle size distribution is very broad segregation can appear.

When the rotational speed of the drum further increases the surface starts to arch and *cascading* sets in.

Tumbling motion is the prevailing form of motion used in practice and undesired slipping motion can be prevented by creating enough wall friction conditions. The rolling bed is preferred, since it is the simplest regime providing favourable conditions for heat transfer and high quality of the product even when mass flow rates are large. However, there are also many industrial cases where drums are operated in cascading regime.

1.4.3 Cataracting motion

At higher rotational velocities, the cascading motion is so strongly pronounced that individual particles detach from the bed and are thrown off into the free space of the drum. The release of particles is a characteristic feature of cataracting motion which may be subdivided into the following states of motion:

- Cataracting.
- Centrifuging.

When particles are flung into the gas space, *cataracting* motion occurs.

With increasing the rotational speed, particles start to adhere to the wall and the extreme case of cataracting motion, *centrifuging* motion takes place. Centrifuging reaches its final state when all the solid material is in contact with the drum wall as a uniform film; this state is only reached at extremely high rotational speeds.

1.5 Segregation phenomena

When particles to be mixed have different properties such as different size, different density or different shape segregation can occur and so, especially considering long mixing times, the particles tend to separate. (Fitzpatrick, 2009). Difference in size is by far the most important cause of particle segregation.

Four mechanisms of segregation according to size can be identified (Williams, 1990):

1. **Trajectory mechanism:** according to the Stokes' law, the limiting distance (L) that a particle can travel is:

$$L = \frac{u \rho_p d_p^2}{18 \mu} \quad (1.2)$$

where u is the particle velocity, ρ_p the particle density, d_p the characteristic dimension of the particle and μ the viscosity of the fluid in which the particles move. So, the velocity of fine particles is lower than the velocity of big particles. This can cause segregation when particles move through air and it also happens when powders fall from the end of a conveyor belt.

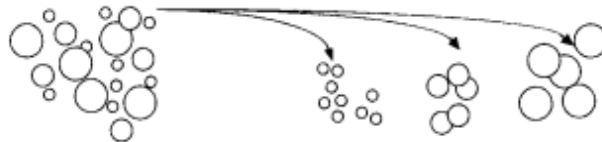


Figure 1.4. Segregation due to particles trajectories (Rhodes, 2008).

2. **Percolation mechanism:** if a mass of particles is disturbed in such a way that individual particles move, a rearrangement in the packing of particles occurs. If the powder is composed of particles of different size, it will be easier for fine particles to fall down and percolate in the void space between bigger particles

that instead can raise up. Segregation by percolation can occur whenever the mixture is disturbed, causing rearrangements of particles.

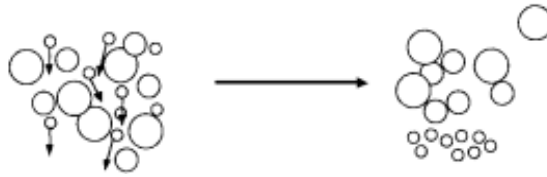


Figure 1.5. Segregation by percolation (Rhodes, 2008).

3. **Inertial mechanism:** it occurs typically in pouring and filling operations. The bigger particles tend to flow to the bottom of the pile of powders since they have a higher momentum; smaller particles instead have lower momentum so tend to accumulate in the centre.

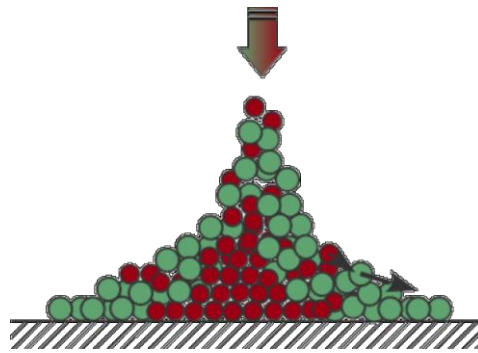


Figure 1.6. Inertial mechanism of segregation.

4. **Elutriation mechanism:** when very small and big particles are present, in presence of air the fine ones can remain in suspension after the larger ones have settled to the surface of the system. This occurs in charging storage vessels or hoppers.

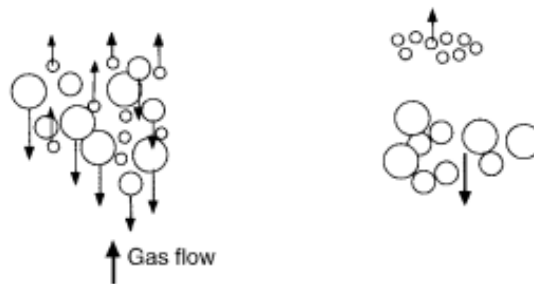


Figure 1.7. Segregation by elutriation (Rhodes, 2008).

1.6 Literature review

The existing literature related to size segregation and shape segregation in rotating drums is reviewed in this paragraph.

1.6.1 Size segregation

A homogeneous binary granular mixture in a two-dimensional rotating drum typically demonstrates radial segregation. This occurs typically due to differences in size and density. *Size-induced radial segregation* had been investigated by several authors.

Cantelaube and Bideau (1995) specifically studied radial segregation in a two-dimensional rotating drum where segregation by percolation was supposed to be absent. The drum was made of two glass disks, with a diameter of 60 cm, held together by an iron annulus. About 1400 disks, whose diameter varied from 6 to 22 mm, were used to fill half of the drum. The drum was moved by a motor at a rotation speed equal to 1.3 rpm that could be changed in order to maintain the continuous-flow regime. The system was filmed and the pictures were analysed by an image processing program. Small white and larger black disks were used. It was observed that the kinetics of segregation was very fast: the small white disks were localized in the centre of the packing in less than one revolution, as shown in Figure 1.8.

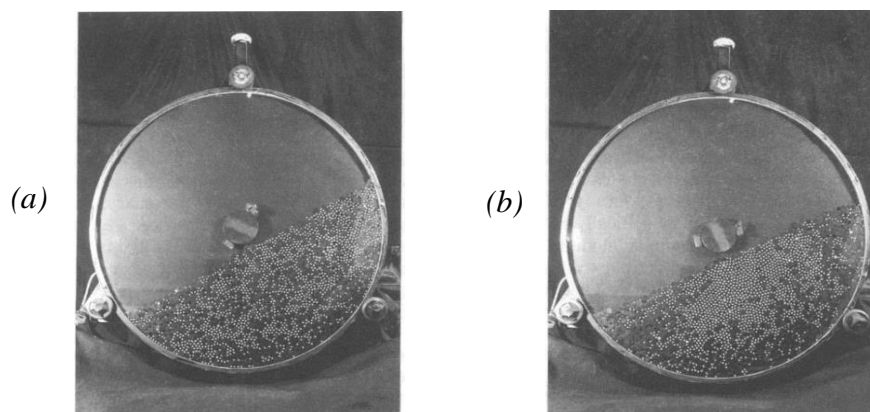


Figure 1.8. (a) Homogeneous mixture at $t=0$; (b) the same mixture after one revolution (Cantelaube and Bideau, 1995).

By adding tracer particles into the granular bulk, also Clément *et al.* (1995) showed size segregation. They used a cylinder partially filled with steel beads that have a diameter equal to 1.5 mm. The cylindrical drum had a diameter of 200 mm and rotated at constant

low speed (2 degrees/s) to keep the avalanche regime; the experimental set-up is reported in Figure 1.9. A tracer of the same material was placed in the system. The beads and the cylinder were treated to darken their surface while the test particle was steel bright. Tracer particles with different sizes were used (1 mm, 1.5 mm and 2 mm). By image processing the trajectories of tracer particles were followed. It was displayed that smaller particles are attracted to the centre of the drum; larger particles tend to move to the edge of the system and tracer particle of the same size of the beads mix homogeneously.

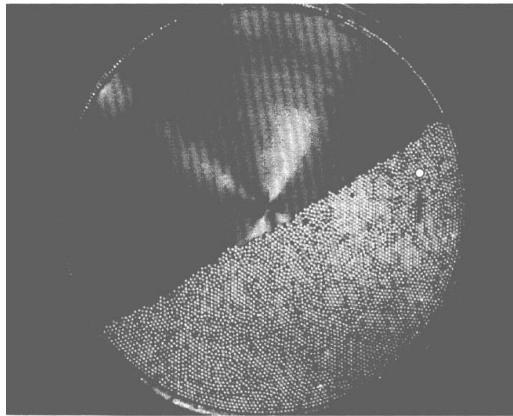


Figure 1.9. Bidimensional rotating drum (Clement et al., 1995).

Also, some mathematical models were developed, trying to predict segregation in the rotating drum.

Prigozhin and Kalman (1998) studied mixing and size segregation of a binary mixture in a partially filled rotating drum and proposed a mathematical model of material transport, considering free-surface segregation. Their cylindrical vessel had a 141 mm internal diameter and a 36 mm length. The binary mixture that filled the drum was made by spherical particles of two different sizes ($d_1=1.37$ mm and $d_2=2.51$ mm); all particles were made of zirconium oxide with a density of 4.14 g/cm³. Axial segregation was not considered and percolation was neglected; also, it was assumed that mixing and segregation occurred in a thin surface layer. Considering that the initial composition of the bulk was given, the mass transport equations were evaluated. These equations allowed to determine the material composition and the concentration in the filling surface layer. Also, the operator of segregation was defined and so the local composition of a general layer was determined. To find the constitutive equation governing the free surface segregation of binary mixtures the procedure developed by Prigozhin (Prigozhin, 1993)

was followed. A good agreement of theoretical and experimental data was found. The model obtained was able to predict the material distribution for various drum fillings and compositions, even if, due to its simplifications, the applicability is limited to slow rotational speed.

Van Puyelde *et al.* (2000) developed an empirical model, by conducting some experiments in order to study the effect of particle size ratios on both segregation dynamics and the final segregated configuration. Coloured shale was used in the experiments. Mean particle sizes were 0.89 mm, 1.70 mm, 2.51 mm, 3.44 mm and 5.08 mm; the density was not significantly different for all the particles and so segregation due to density differences would not occur. The particle size ratio varied from 5.7, for the 0.89 mm and 5.08 mm particles, to 1.37, for 2.51 mm and 3.44 material. The steel drum had a 570 mm inner diameter and a 50 mm thick cross section; two removable semi-circular 10 mm thick plate glass sections were attached to the frame. The rear section was connected to a shaft powered by a variable DC power supply. A camera allowed to take pictures of the beds and to derive the model by the use of image analysis. The fine material was coloured orange and the larger particles were coloured black. The initial configuration of the system was a well-mixed bed; rotation was started and images were taken from the initial state until the final segregated configuration. Images were taken every second for 60 seconds, with the drum in motion. In order to analyse the system, the bed was divided in two concentric layers: the inner layer had a radius of 50% of the bed radius from the centre and the remaining area of the bed represented the outer layer. For low rotational speed the segregation time was measured, but it was not possible at higher velocities, since the segregation occurred too fast to be observed. A concentration proportion was used to express the distribution of the segregating material and the final segregated concentration proportion was defined as the average concentration proportion in each layer when the bed was fully segregated. It was found that the fine material tended to move toward the centre of the bed for all experiments but this tendency was reduced with smaller particles ratios and higher active layer velocities. The concentration proportion could be determined with the following correlation:

$$P_j = m(PSR)\bar{V}_{AL} + i(PSR) \quad (1.3)$$

Where \bar{V}_{AL} was the mean active layer velocity $m(PSR)$ and $i(PSR)$ were the gradient and intercepts functions for the different particle size ratios respectively. It was found a small range of particle size ratio, close to 1, where segregation had not occurred and so the values of $m(PSR)$ and $i(PSR)$ were equal to the boundary condition values. A final upper limit value was observed for the larger particle size ratios, probably due to the onset of spontaneous segregation. The region between the lower and upper limits was linear, as shown in Figure 1.10.

Also, the amount of fine materials in each layer could be calculated by multiplying the concentration of each layer by the volume of the layer.

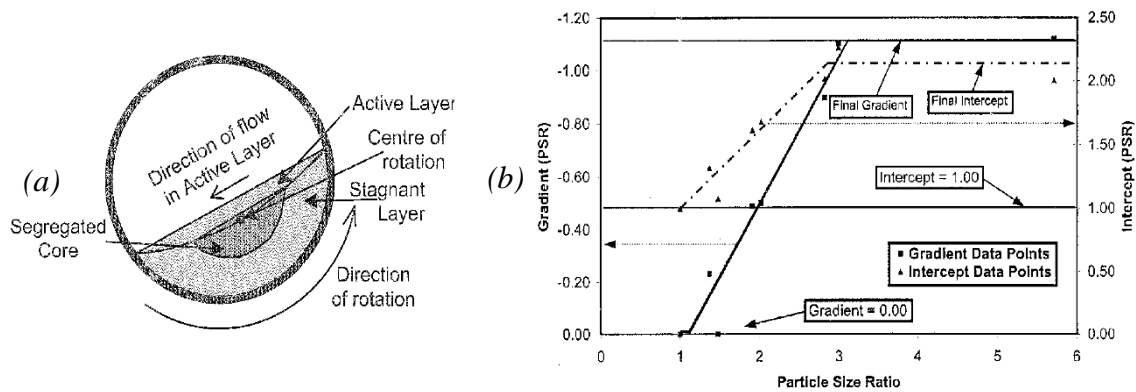


Figure 1.10. a) Rolling bed showing segregated core; b) modelling of $m(PSR)$ and $i(PSR)$ for the inner layer (Van Puyelde et al., 2000).

The half-filled rotating drum was investigated also by Thomas (2000). He studied the radial segregation in the system, considering glass beads with diameters between 45 μm and 7.5 mm and with density equal to 2.5 g/cm^3 . First, a drum with a length of 42 mm long and a diameter of 48.5 mm was considered; it was filled with small and large beads and rotated manually by rolling it on a plane. The rotation speed was between 0.04 and 0.09 s^{-1} . Experiments were conducted varying the diameters ratio. Some experiments were conducted with 16.6% large black beads ($d=710 \mu\text{m}$ or $d=3 \text{ mm}$) and small beads of different sizes. It was observed that large beads roll on the surface for small size ratios and rapidly sink for high size ratios; for very large size ratios, they move along the slope before reaching the surface and flow embedded in a layer of small beads. Using large particles with $d=710 \mu\text{m}$ and small particles with diameters $d=500 \mu\text{m}$ or $d=45-90 \mu\text{m}$, axial and radial segregation occurred. For size ratios lower than 2.3, the large beads were at the surface and at the periphery of the drum; for size ratios from 2.8 to 4.3, the large

beads were close to the periphery; for size ratios higher than 7.8, large beads were uniformly distributed inside. Some examples are reported in Figure 1.11, for different values of the particles size ratio.

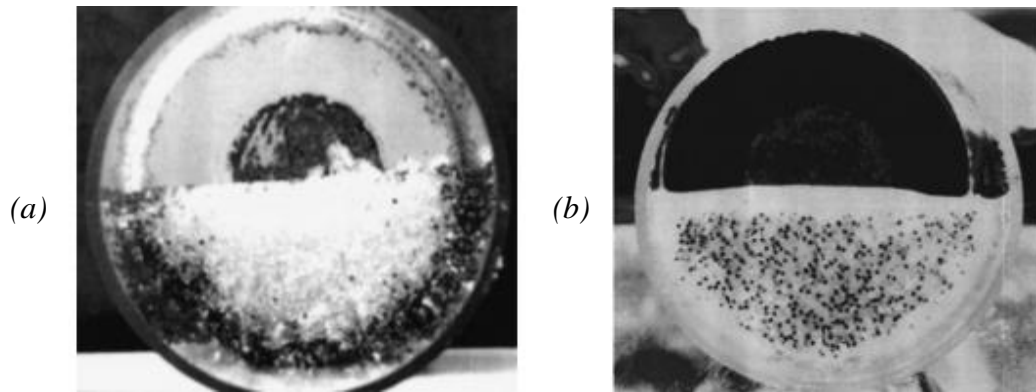


Figure 1.11. Cross section of the drum for (a) size ratio equal to 1.42 and (b) for size ratios larger than 7.8 (Thomas, 2000).

The same occurred with 3 mm large beads, demonstrating that the process does not depend on the diameter of the beads but on the size ratio. Other experiments were made with 3% of 3 mm large beads. Large beads tended to accumulate on a circle on a preferential distance from the centre and the circle moves from the walls when increasing the diameter ratio. Moreover, a variation by a factor of about 10 in the rotational speed was considered, finding that the results were very similar. Thus, speed seemed not to affect the results in the range of speed considered for the experiments. In addition, Thomas studied a clear plastic disk placed horizontally and rotating with a speed equal to 0.04 s^{-1} around its axis. The disk had a 3.5 mm thickness and a diameter equal to 81 mm; the large beads in the drum were 710 μm , 1.5 mm and 3 mm in diameter. The segregation patterns were the same as in the previous drum and the phenomenon occurred for the same diameter ratios. Again, it was observed that large beads seemed to have a constant vertical location compared to the free surface and their vertical relative position depend on the size ratio: starting from the free surface, the beads are then increasingly embedded when enlarging the diameter ratio. Considering 3-mm large beads, it was observed that they can act as plugs and strongly affect the flow in the system. In fact, when a 3-mm bead sinks in the bed and stops at a certain distance, it prevents the flow of the following small beads.

1.6.2 Shape segregation

The case of spherical particles is often assumed as a reference and many of the existing studies consider spherical particles only. However, also different geometries have to be considered since the particles shape has a strong influence on the dynamics of the system. There exist limited experimental investigations of non-spherical particles flow in rotating drums and also there is little knowledge about the granular dynamics of non-spherical particles inside the rotating drums.

Some experiments were conducted in a rotary kiln considering nickel oxide pellets, limestone, sand and gravel (Henein *et al.*, 1983, 1985): the effect of particle shape on bed motion was determined. Also, particles made from and with ovoid, shell and tube shapes were used to investigate the effects of particle type on mixing in the rotary kiln. (Woodle and Murno, 1993); it was shown that particle type has an effect on mixing time.

Considering the importance of partially filled rotating cylinders in practical applications, Boateng and Barr (1997) experimentally studied the behaviour of granular materials in rotary cylinders. To cover a large range of particle shapes, they considered spherical uniformly sized polyethylene pellets, ellipsoidal non-uniformly sized rice grains and unequally shaped and sized limestone particles. The rotary drum had a 1 m outer diameter and a 1 m length and it was rotated by an electrical motor with variable speed. Figure 1.12 reports their experimental set-up.

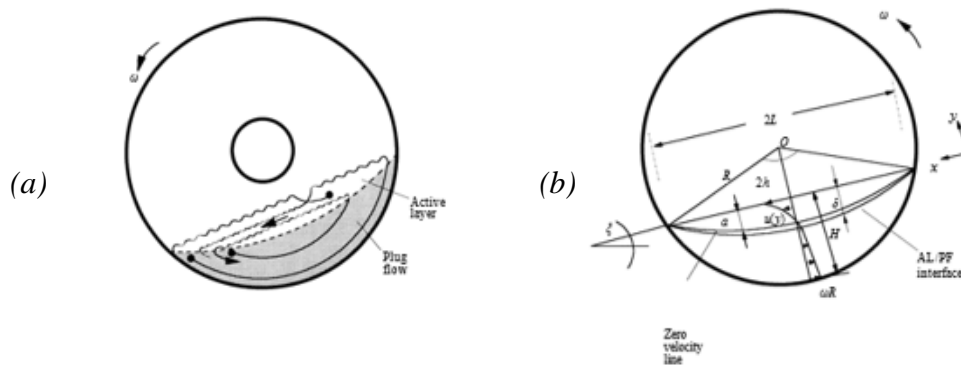


Figure 1.12. Schematic of experimental set-up: (a) transverse flow; (b) geometry of flow field. (Boateng and Barr, 1997).

Rotation rates between 1 and 5 rpm were used and the drum loading was varied from 3.3% to 29%. The rotational Froude number was between 5.4×10^{-4} and 1.3×10^{-2} . Particle size, particles density, static angle of repose, interparticle and particle-to-wall

coefficients of restitution were measured for the three different types of particles. The fibre-optic technique allowed to measure particle velocities within the bed and at the free surface. Two fonic sensor-probe were used: they were made by a light source connected to the probe tip by a transmitter and a light sensor which communicate with the probe tip. Two probes in parallel and 5 mm apart measured particles velocities: when the tip was aligned with the flow, the passage of a single particle produced an identical signal in each probe with a delay equal to the time required for the particle to travel the distance between the probes. Polyethylene was analysed with many different drum loadings (3.3%, 8.5%, 15% and 29%) and at the full range of rotational speeds; rice grains were loaded at 3.3%, 8.5% and 10% fills at 3 and 5 rpm only; limestone was run at a speed between 2 and 5 rpm with a loading not exceeding 8.5%. It was found that the spherical polyethylene pellets exhibit a lower angle of repose (25°) than rice grains (32°) and limestone (35°). Furthermore, some differences were found in the velocity profiles. At low drum loading all three materials show linear velocity profiles but at higher loadings non-spherical materials developed more parabolic profiles and the deviation from linearity seemed to increase with the rotation rate. This was explained considering the thermodynamics of the system and the collisions between particles. Between polyethylene particles elastic collision occur and a singular surface velocity profiles develop; inelastic collisions occur between rice grains and limestone particles giving rise to the build-up of material at the apex.

Ingram *et al.* (2005) used PEPT technique to characterize axial and radial dispersion of granular media in a rolling drum operated in batch and continuous mode. They used three drums with a length of 1000 mm and with internal diameters of 120, 240 and 390 mm; the drums were mounted on rollers driven by a variable speed motor. Sand and titanium dioxide were analysed, with a filling level between 10% and 30% and rotation speed up to about 6 rpm. Sand particles had a mass mean diameter of $475 \mu\text{m}$ and a bulk density of 1640 kg/m^3 ; titanium dioxide mass mean diameter was $1275 \mu\text{m}$ and its bulk density equal to 1575 kg/m^3 . The experiments displayed that drum speed, drum diameter and drum fill level does not affect the radial and axial dispersion coefficients. Particle shape seemed rather to affect the system but this factor was not considered in the study.

Santomaso *et al.* (2006) experimentally studied mixing processes in a horizontal rotating cylinder, considering materials with the same size and different angle of repose. The

horizontal cylinder that was used was 0.11 m long and had a radius of 0.046 m; the system was filled up to 30% in volume with two different materials completely axially segregated. Blue and white tetraacetylethylenediamine (tead) powders were mixed to allow composition quantification by image analysis; also, sodium percarbonate (sp) powders with a spheroidal and irregular shapes were used. A solidification technique of the mixture was used: after a fixed number of revolutions at low speed the mixture was saturated with molten wax, then solidified and cut into nine slices. Information about the radial composition distribution were obtained by image analysis of the slices, dividing the system into 12 rings and calculating the relative grey intensity on each ring. Radial segregation was observed and, for the blue and white tead, it was found to be a transient phenomenon that faded out at longer mixing times. When powders with not only different angle of repose but also different density were considered, much stronger radial segregation was observed; moreover, in some cases the phenomenon was found to be permanent. The kinetics and intensity of the segregation increased with increasing the initial difference of dynamic angle of repose.

The dependence of the dynamic angle of repose on particles shape was also investigated (Santomaso *et al.*, 2007) in a rotating drum partially filled with powders. The considered drum had an internal diameter of 0.192 m and a length of 0.1 m; it was placed on two steel rollers and rotated at different rotational speed between 1 and 8 rpm. The dynamic angle of repose of eight different materials was measured by taking pictures of the material by back lighting technique. The angle was found to be constant for all the materials except one. Also, a correlation for the angle was derived, relating the dynamic angle of repose to the Roundness and the Elongation, two parameters that quantify the particles shape.

The dynamics of non-spherical particles in rotating drums has been considered only recently (Dubè *et al.*, 2013). Dubè *et al.* used pharmaceutical tablets as non-spherical particles. Their rotating drum operated in the rolling regime and so two regions characterized the system: a passive layer near the walls and an active layer in which mixing and segregation mainly occur. The drum had a 0.3556 m internal length and a 0.2413 m internal diameter; it is schematically displayed in Figure 1.13.

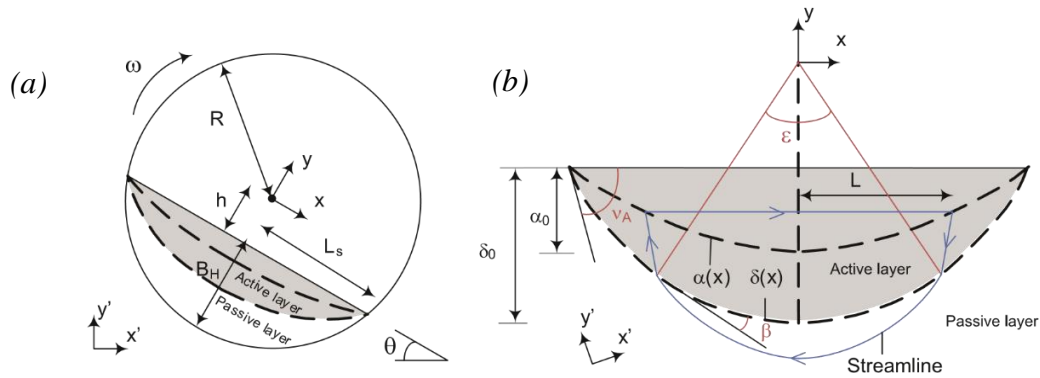


Figure 1.13. (a) Cross-section view of the drum; (b) a close-up on the active layer (Dubé et al., 2013).

Five different tablets were considered with a specific size and composition; for all the experiments 35 vol% as filling fraction was used. The tablets are schematically represented in Figure 1.14.

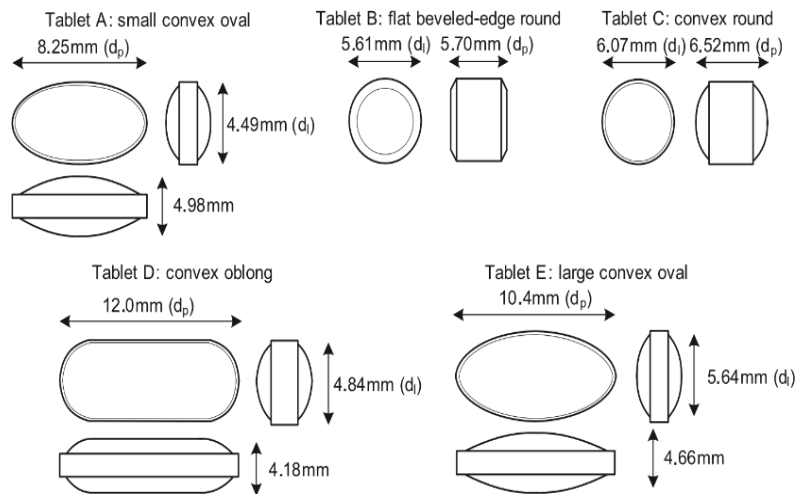


Figure 1.14. Schematic representation of the non-spherical tablets (Dubé et al., 2013).

The tablets had a density equal to 1.40, 1.58, 1.63, 1.54 and 1.29 g/cm³, respectively. They were tested individually, but also bi-dispersed mixtures of mono-shaped tablets and bi-disperse mixtures of bi-shaped tablets were studied. In the blends 85 vol% of the bigger tablet and 15 vol% of the smaller tablets were used. The drum rotational speed was 10 rpm; only one experiment was performed at 5 rpm in order to assess how the drum speed affects the particle dynamics. Furthermore, to compare non-spherical particles dynamics to the spherical one, three experiments were done with spherical glass beads. Radioactive

particle tracking (RPT) technique was used to follow the particle motion. A tracer was used which can emit isotropic γ -rays that are then used to show its trajectory. The static and dynamic repose angles were evaluated, finding significant differences between spherical particles and non-spherical ones. Tablets with a longer straight side can form stable structures near the wall and so they present a higher dynamic repose angles and even if they have a different aspect ratio, they show similar dynamic repose angles. Moreover, when tablets with similar dynamic repose angles are mixed the resulting angle is the same as the individual one. In all the experiments, a bed dilation was measured: this phenomenon is a characteristic of non-spherical granular flow and in fact was not displayed by spherical particles. It was found that all the individual tablets and blends show a higher velocity profile than the glass beads. Previously developed models used for spherical particles adequately describe the velocity profile of non-spherical particles, except when the non-spherical particles have an aspect ratio higher than two.

Alan and Scheper (2016) conducted experiment using rice particles and spherocylindrical steel particles, finding that spherocylinders do not have the same segregation mechanism as spherical particles. First, some experiments were conducted with rice particles. A wooden drum was used, with a radius of 125 mm and a depth of 25 mm which rotated at 4 rpm. The drum was 45% filled with a premixed mixture of two particles of different size. All rice particles were coloured with a food dye to have a high contrast for the optical analysis. A camera was used to take pictures of the mixtures and, in particular, every rotation a picture was taken to compare the mixing state; the PEPT technique was used to obtain the location of the particles. Another experiment was done with a wooden drum with a 260 mm diameter rotating at 4 rpm and 45% filled with steel rollers. The particles had a diameter which varies from 1.5 to 4 mm and a length between 7.8 and 19.8 mm; their density varied from 323.1 to 7800 kg/m³. Pictures of the mixtures were taken after 0, 2 5 and 10 rotations. The steel rollers started in a segregated state and reached an equilibrium mixed state after only 5 rotations; the rollers also showed a tendency to form cluster of the same constituents. In the experiments, no segregation was observed on a large scale; a possible explanation to this non-segregation behaviour is the fact that particles form clusters and so they segregate just on a smaller scale.

1.6.3 Summary of previous studies

Size segregation was widely observed experimentally. Considering a rotating drum operating in the rolling regime filled with particles of different sizes, bigger particles mainly tend to the edge of the system, while smaller particles are attracted to the centre of the drum. The phenomenon occurs very fast and the rotational speed of the drum seems not to affect the phenomenon; the size ratio of the particles is, instead, the parameter that mainly affects size segregation phenomena.

Most of the experimental investigations about segregation in the rotating drum involved spherical or nearly-spherical particles; the experimental studies of the flow of non-spherical particles are, in fact, rather limited. The shape of the particles, however, strongly influences the motion in the system. In particular, the static and dynamic angles of repose of non-spherical particles are found to be very different from the ones measured for spherical particles. Moreover, for mixtures of non-spherical particles a dilation of the granular bed is observed, finding it to be a characteristic phenomenon of non-spherical particles, not displayed by spherical ones.

Chapter 2

Materials and methods

In this chapter, the particles used for the experiments will be presented, with all their characteristics. The measurement of particle density, the used equipment and the experimental set-up will also be described. Moreover, a specific image analysis procedure was developed to analyze the pictures of different mixtures in the drum. The method, that was elaborated with the ImageJ software, will be explained in this chapter. It was developed starting from the analysis of the single particles and it was then applied to analyze binary mixtures of particles of different shape and size in the rotating drum. Some information about the ImageJ software can be found in the Appendix, together with details about the used commands; they could be useful to better understand the procedure that was used.

2.1 Materials

In this paragraph, the spherical and non-spherical particles used for the experiments are described and shown. The non-spherical particles used in this work are 3D printed particles so some information about the 3D printing are reported, too.

2.1.1 *Spherical particles*

Spherical particles of different dimensions were used for the experiments. They are shown in Figure 2.1



Figure 2.1. Three types of spherical particles used in the experimental tests.

The biggest spherical particles were nylon-66 beads with a diameter of 8 mm, while the intermediate sized were plastic particles with a diameter of 6 mm. Their geometrical characteristics are reported in the following table:

Table 2.1. Diameter, projected area and volume of the spherical particles.

d [mm]	A [mm ²]	V [cm ³]
8	50.265	0.268
6	28.274	0.113

Where A is the projected area of a sphere, calculated as:

$$A = \frac{\pi}{4} d^2 \quad (2.1)$$

And V is the volume of a sphere:

$$V = \frac{\pi}{6} d^3 \quad (2.2)$$

The smallest particles were not exactly spherical and they were not all exactly of the same size. They were used since they were available in the laboratory in high quantity. The shape and the mean diameter of these particles were evaluated by scanning a sample of 42 particles on a paper sheet. A picture of the particles (Figure 2.2 (a)) was obtained and the particles could be analysed in ImageJ in order to define their mean size and shape.

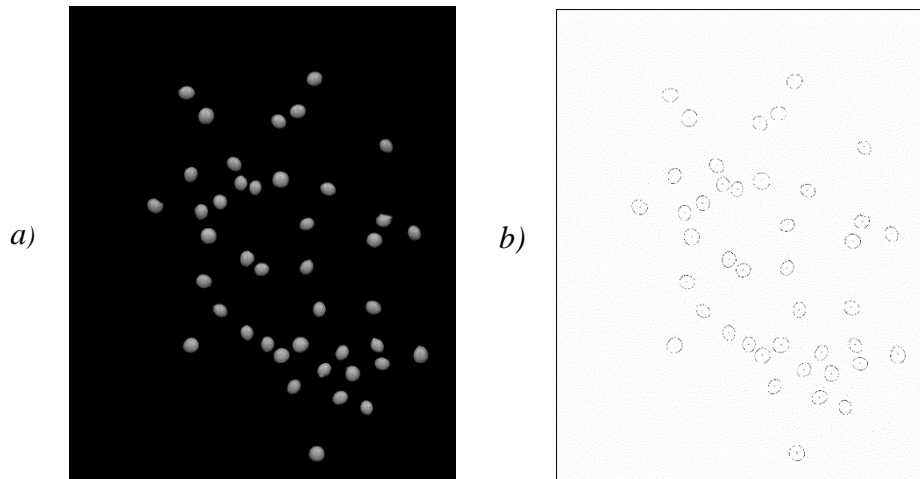


Figure 2.2. a) Scanned picture of the smallest particles; b) outlines of the particles as a result of the analysis.

The results of the analysis are summarized in Table 2.2. The shape of the particles was evaluated in terms of Aspect Ratio.

Table 2.2. Mean diameter and mean aspect ratio of the smallest particles.

d [mm]	AR [-]
3.810	1.176

The mean aspect ratio of the particles was not very different from 1 so these particles could be assumed very similar to spherical ones. The projected area and the volume of the smallest particles are reported in Table 2.3.

Table 2.3. Projected area and volume of the particles with 3.81 mm diameter.

A [mm ²]	V [cm ³]
11.401	0.0290

The density of all the spherical particles was measured experimentally; this will be reported in paragraph 2.1.3.

2.1.2 Ellipsoids

Two types of ellipsoids were considered, which are shown in Figure 2.3 (a).

For the sake of simplicity, in the following the particles with the shorter length will be indicated with the number 1 while the more elongated particles with 2.

Each ellipsoid presents three characteristic geometrical dimensions, which correspond to the three semi-axes of the ellipsoid. In this case, the ellipsoids were designed in such a way to have two semi-axes equal to each other. So, there were two geometric dimensions relevant for each ellipsoid: they were two axes of the ellipsoids, which are indicated as a and b , as reported in the sketch of the particles shown in Figure 2.3. The third axis, c , was equal to b .

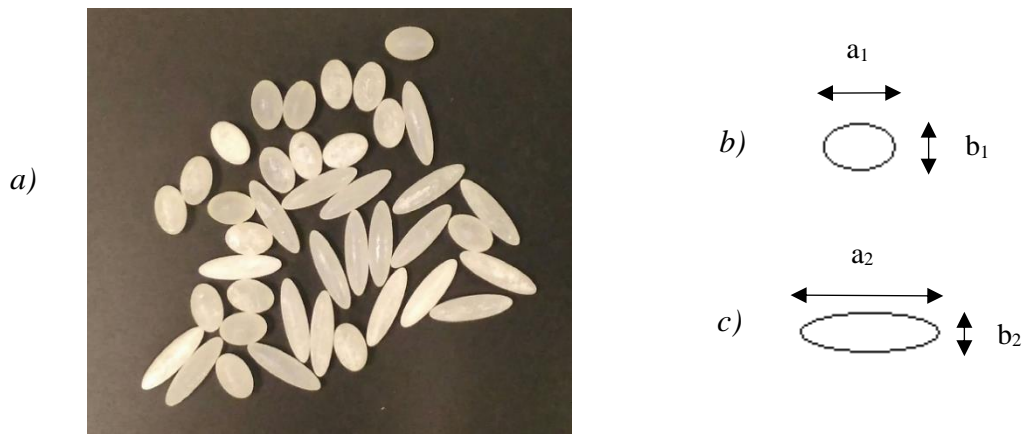


Figure 2.3. a) Types of ellipsoids; b) sketch of ellipsoid 1; c) sketch of ellipsoid 2.

The two types of ellipsoids had different shape and their shape was quantified by the Aspect Ratio, which was defined as the ratio between the larger and the smaller relevant dimension of the particle and so in this case it was the following ratio:

$$AR = \frac{a}{b} \quad (2.3)$$

The aspect ratio is equal to one in the case of spherical particles.

The geometric characteristics of the particles are reported in Table 2.4 in detail:

Table 2.4. Geometrical characteristics of the two types of ellipsoids.

Type	a [mm]	b [mm]	AR [-]	A [mm ²]	V [cm ³]
1	10.48	6.98	1.5	57.452	0.267
2	18.44	5.26	3.5	76.179	0.267

The projected area (A) of the ellipsoids [mm²] was calculated with the following formula:

$$A = \pi \cdot \frac{a}{2} \cdot \frac{b}{2} \quad (2.4)$$

The volume (V) of the particles [cm^3] was calculated as:

$$V = \frac{4}{3} \pi \cdot \frac{a}{2} \cdot \frac{b}{2} \cdot \frac{c}{2} \cdot 10^{-3} \quad (2.5)$$

Where $c=b$ in this case.

As it is displayed in Table 2.4, the two types of ellipsoids were design in order to have the same volume; the volume was also equal to the volume of the spheres with diameter equal to 8 mm, described in the previous paragraph.

Since the particles were not spherical, an equivalent diameter could be defined in order to compare their size with the spherical particles. The particles are three-dimensional particles so the equivalent diameter by volume was used. As the ellipsoids have the same volume of the spheres with 8 mm diameter, their equivalent diameter by volume will be equal to 8 mm. This could be checked by equalling the expression of the volume for the sphere and for the ellipsoids and extracting the value of the equivalent diameter by volume ($d_{eq,v}$).

$$\frac{4}{3} \pi \cdot \frac{a}{2} \cdot \frac{b}{2} \cdot \frac{c}{2} = \frac{\pi}{6} d_{eq,v}^3 \quad (2.6)$$

And so, the equivalent diameter by volume for the ellipsoids was:

$$d_{eq,v} = \sqrt[3]{8 \cdot \frac{a}{2} \cdot \frac{b}{2} \cdot \frac{c}{2}} \quad (2.7)$$

The value of the equivalent diameter resulted to be equal to 7.99 mm for both the ellipsoids.

Furthermore, the ellipsoids were 3D printed, but not all of them were printed with the same 3D printer. The first particles available (100 for each type) were printed by the 3D printer of the mechanical workshop of the University of Surrey. They are made of a special plastic material suitable for 3D printers which is the VisiJet[®] M3 Crystal. It is a translucent material with high durability and stability and with a density of 1.02 g/cm^3 .

When more particles had been needed, they were printed with the *Ultimaker* 3D printer available in the Chemical and Process Engineering Department of the University of Surrey. The material used in this case was the polylactic acid (PLA).

The density of all the particles was experimentally measured and the measurement will be described in the next paragraph.

2.1.3 Density measurement

The density of all the particles used for the experiments was measured with a gas pycnometer. The features of the instrument and the procedure followed for the density measurement will be reported in this paragraph.

2.1.3.1 The gas pycnometer

The Multivolume Pycnometer 1305 was used, which is reported in Figure 2.4.



Figure 2.4. *Multivolume Pycnometer 1305.*

An electrical connection was required for the operation of the instrument, together with the gas supply; nitrogen was used in this case.

The gas pycnometer allowed to measure the skeletal volume of the solid sample by observing the reduction of gas capacity in the sample chamber caused by the presence of the sample.

The pycnometer is provided with a sample chamber, in which the sample is placed, and an expansion volume. The sample chamber is made of stainless steel and it has two holes for the gas inlet and outlet. The volume of the chamber is of about 154 cm³.

2.1.3.2 Density measurement procedure

For each type of particle two measurements of density were done. After the sample was loaded, the sample chamber was charge to a pressure of about 19.5 psig by feeding the gas; this pression was recorded as P_1 . Subsequent expansion in the expansion volume, which was previously at the same temperature and at zero psig, resulted in a second pressure, recorded as P_2 . Application of mass balance equations for the gas permitted easy computation of the sample volume (V_{sample}) since the volume of the empty sample chamber (V_{cell}) and of the expansion chamber (V_{exp}) were known and the pressure drop ratio upon expansion was known. In particular, the volume of the sample was calculated as:

$$V_{sample} = \frac{V_{cell} - V_{exp}}{\left(\frac{P_1}{P_2}\right) - 1} \quad (2.8)$$

The values of V_{cell} and V_{exp} are reported in the following Table:

Table 2.5. Volume of the empty sample cell and of the expansion volume of the pycnometer.

V_{cell} [cm ³]	V_{exp} [cm ³]
8.595	5.763

The mass of the sample (m_{sample}) was evaluated by determining the weight of the cup containing the sample and subtracting the weight of the cup.

Finally, the density of the sample (ρ_{sample}) was calculated as:

$$\rho_{sample} = \frac{m_{sample}}{V_{sample}} \quad (2.9)$$

The procedure was repeated to obtain a second value of density. The final value of density was obtained as a mean of the two measurements.

Table 2.6 reports the recorded values of P_1 and P_2 for each measurement, the mass, the volume and the density of each sample. Also, for each measurement the standard deviation (*STD*) is indicated.

Table 2.6. Gas pycnometer measurement data for each type of particle.

<i>Sample</i>	P_1 [psig]	P_2 [psig]	m [g]	V [cm ³]	ρ [g/cm ³]	<i>mean</i> ρ [g/cm ³]	<i>STD</i> [g/cm ³]
spheres d=8mm	19.527	10.698	1.808	1.612	1.122	1.093	0.029
spheres d=8mm	19.480	10.611	1.808	1.700	1.064		
spheres d=6mm	19.570	10.522	2.211	1.893	1.168	1.194	0.026
spheres d=6mm	19.483	10.534	2.211	1.811	1.221		
particles d=3.81	19.568	10.509	1.997	1.909	1.046	1.060	0.014
particles d=3.81	19.516	10.517	1.997	1.860	1.074		
ellipsoids AR=3.5	19.725	10.918	1.814	1.450	1.251	1.256	0.005
ellipsoids AR=3.5	19.644	10.885	1.807	1.433	1.261		
PLA ellipsoids AR=3.5	19.441	10.798	1.373	1.395	0.984	0.983	0.001
PLA ellipsoids AR=3.5	19.480	10.808	1.387	1.412	0.982		
ellipsoids AR=1.5	19.561	10.397	2.470	2.056	1.201	1.194	0.008
ellipsoids AR=1.5	19.415	10.300	2.470	2.083	1.186		
PLA ellipsoids AR=1.5	19.407	10.383	1.853	1.964	0.944	0.955	0.012
PLA ellipsoids AR=1.5	19.710	10.580	1.853	1.917	0.967		

All the particles have similar densities and so segregation phenomena due to different density are avoided.

The measured density of the spheres with 8 mm diameter is very close to the typical density of the nylon 66 (1.14 g/cm³). The spheres with 6 mm diameter and the particles with mean diameter equal to 3.8 mm have a density very similar to the big spheres, of the order of magnitude of the density of polymeric materials.

The same type of ellipsoids printed with two different 3D printed have a slightly different density. Also, the PLA ellipsoids have a density that is lower than the typical density of the PLA (1.24 g/cm³). This is because the particles were printed with a set *infill density* of the 20%, so they are partially empty inside.

The density of the particles ($\rho_{particle}$), by definition, can be also measured as the following ratio:

$$\rho_{particle} = \frac{m_{particle}}{V_{particle}} \quad (2.10)$$

Where $m_{particle}$ is the mass of one particle [g]; $V_{particle}$ the volume [cm³] of each particle that was reported in the previous tables (see Tables 2.1, 2.3 and 2.4).

The mass of one particle of each type was calculated by weighting a known number of particles and dividing the obtained mass for the number of weighted particles; higher the number of weighted particles was and lower the measurement error. The values of mass, volume and density are reported in the following table:

Table 2.7. Values of mass, volume and density of each type of particle.

<i>Particles</i>	<i>m [g]</i>	<i>V [cm³]</i>	<i>ρ [g/cm³]</i>
spheres d=8mm	0.301	0.268	1.123
spheres d=6mm	0.131	0.113	1.162
particles d=3.81	0.0215	0.029	0.741
ellipsoids AR=3.5	0.313	0.267	1.170
PLA ellipsoids AR=3.5	0.230	0.267	0.861
ellipsoids AR=1.5	0.312	0.267	1.167
PLA ellipsoids AR=1.5	0.232	0.267	0.868

By this measurement, it can be checked that the density of all the particles is very similar and very close to 1 g/cm³. The density of the PLA ellipsoids is found again to be slightly lower than 1 g/cm³, due to the setting defined in the 3D printer.

2.1.4 3D printing

A 3D printer allows to obtain three-dimensional objects through additive manufacturing, starting from a digital file. The object is created on a support plane thanks to a nozzle moving on the plane. In particular, the additive process creates the object by laying down successive layers of material until the object is created. Each of the layers can be seen as a thinly sliced horizontal cross-section of the eventual object.

The starting point is a 3D design of the object to be created. This can be realized with specific software. The 3D design has to be saved in the STL format and it is then uploaded on a slicing software. The slicing is the operation of dividing the 3D design into sections and each one represents a different perspective of the moulded piece. In the slicing software, all the printing parameters and the needed data are set. Finally, when the 3D model is sliced it can be fed to the printer. The printing occurs layer by layer since the printer reads every 2D slice and creates the three-dimensional object.

The software used to realize the 3D design of the particles used in this work is *FreeCAD*, which is an open-source parametric 3D modeller allowing to obtain STL files. By exporting the file, it is possible to save it in the STL format and so it is ready to be printed. One of the 3D printer used to print the non-spherical particle is shown in Figure 2.5.



Figure 2.5. *Ultimaker 3D printer used to print some of the non-spherical particles.*

As said before, in the printer showed above the filling degree of the object to be printed (*infill density*) was set equal to 20% in order to have a fast printing.

2.2 Experimental equipment

In this paragraph, the experimental set-up is described and displayed in detail.

2.2.1 The rotating drum

The experiments presented in this work were conducted by using the rotating drum shown in Figure 2.6.

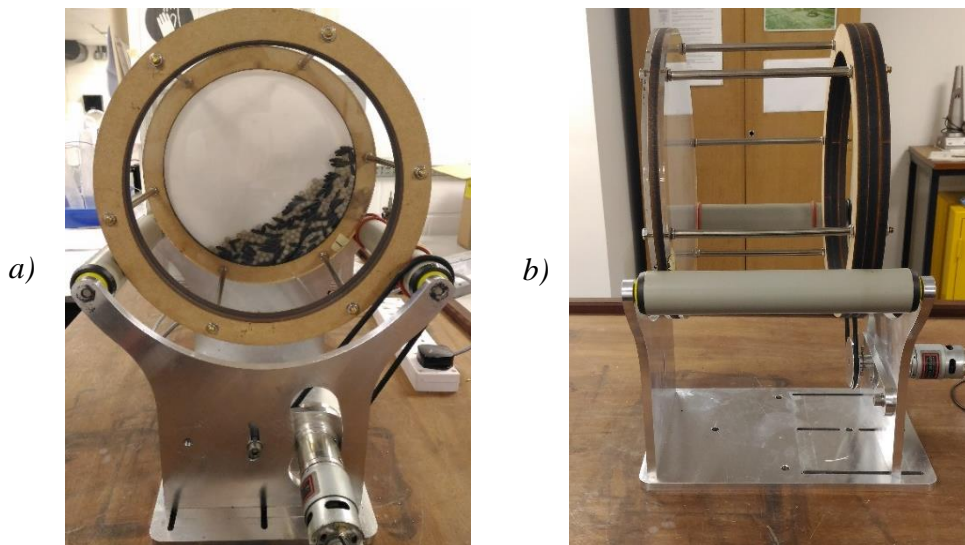


Figure 2.6. a) Front view and b) side view of the rotating drum.

The drum is made of two transparent polycarbonate disks with a diameter of 30 cm and a thickness of 6 mm; between them a wooden spacer is placed, with the same external diameter, an internal diameter of 25 cm and a thickness of about 9.1 mm. The spacer allows to create an internal space of defined thickness which separates the two polycarbonate disks. The internal thickness is covered with a sandpaper layer in order to have enough friction and avoid undesired slippage of the particles. Moreover, to keep the drum in vertical position and allow its rotation, three more wooden spacers are used, at a distance of about 16.3 cm.

This rigid structure can rotate at variable rotational speed thanks to a motor connected to a voltage supplier. Two rollers mounted on a rigid support make the rotation of the drum possible; a pulley transmits the motion to the driving roller, while the second roller is passive and it just keeps the drum in position during the rotation. The rotational speed can be changed by varying the voltage of the motor, with a maximum allowed voltage of 12

V. The structure can be removed from the rollers and by unscrewing the bolts the drum can be easily opened so that the particles can be loaded in the drum.

2.2.2 The recording system

Pictures of the drum were taken by a colour camera and then analysed by the image processing program ImageJ.

To avoid the reflection of the camera and other objects on the front transparent disk, a squared LED panel was used which allowed to have a dominant diffused light illuminating the drum. The LED had a power of 8 W and a colour temperature of 4000 K; it was placed behind the drum and opposite to the camera. A circular sheet of paper, which was attached to the drum between it and the LED, diffused the light properly.

The camera was a Basler ace camera – model acA2000-165uc, with a maximum resolution of 2040×1086 pixels. The focalization and the diaphragm of the camera could be adjusted manually. For each picture, the two parameters were adjusted in order to ensure that the objects to be analysed were properly focalized and that the picture were not too bright. The camera was fixed on a support placed about 28 cm far from the rotating system and connected to a laptop on which the pylon Viewer 64-bit software was installed for the acquisition of the pictures. In the software, some features could be set; they could be saved and reloaded, so that it was not needed to set them each time. The value of the most relevant parameters of the camera are summarized in the following table:

Table 2.8. *Main features set in the pylon Viewer software.*

<i>Balance White Auto</i>	Once
<i>Exposure time [μs]</i>	3000
<i>Acquisition Frame rate [Hz]</i>	200
<i>Width [pixel]</i>	1080
<i>Height [pixel]</i>	1080
<i>OffsetX</i>	576
<i>OffsetY</i>	0

In particular, *Width*, *Height*, *OffsetX* and *OffsetY* of the picture were set up in the *Image Format Control* section of the software.

The *Width* and the *Height* were always set equal to 1080, in order to obtain 1080×1080 squared pictures with a high resolution.

The offset values were defined in order to have the drum exactly at the centre of the lens. Also, the white balance was required before taking pictures or videos of the system and it could be done in the *Image Quality Control*.

Finally, the *Exposure Time* modulated the light entering in the lens of the camera: it was usually set equal to 3000 μs .

Before starting a recording, the frequency of the frames (*fps*) was set in the *Options* menu. A time-based recording was set. It has to be specified that with the set resolution, reported in Table 2.8, 600 frames can be recorded at maximum, due to the maximum size of the video.

The whole experimental set-up is displayed in Figure 2.7.

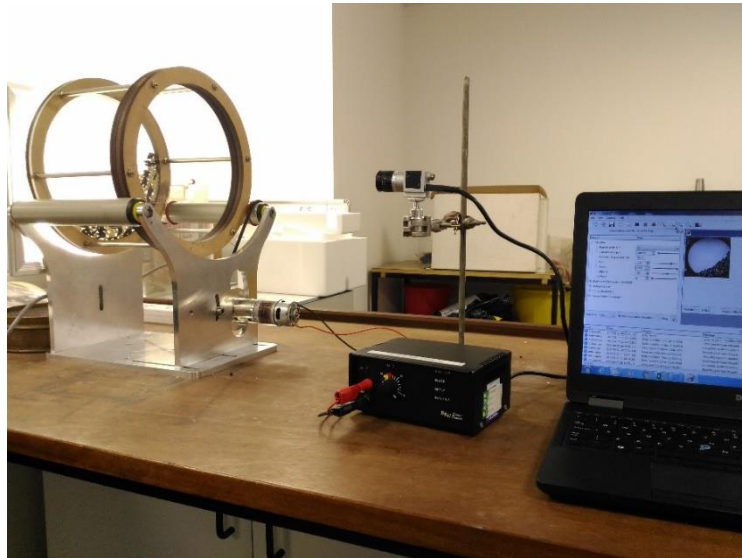


Figure 2.7. *Experimental set-up made of the rotating drum, the colour camera and the laptop for the acquisition of the pictures.*

2.2.3 Velocity calculation

The rotational velocity of the drum was changed by changing the voltage of the motor. On the front of the drum a marker was placed and the following procedure was used to evaluate the rotational speed:

1. The rotation of the drum was started at a given voltage.
2. The recording of the rotating drum was started with $\text{fps}=0.2$ s.
3. A given position of the marker was assumed as reference and the frame at which the marker was at the reference position was recorded as f_i .

4. After one rotation, the frame at which the marker was again at the reference position was recorded as f_2 .
5. The rotational velocity [rpm] was evaluated as:

$$\omega = \left(\frac{1}{(f_2 - f_1) \cdot fps} \right) \cdot 60 \quad (2.11)$$

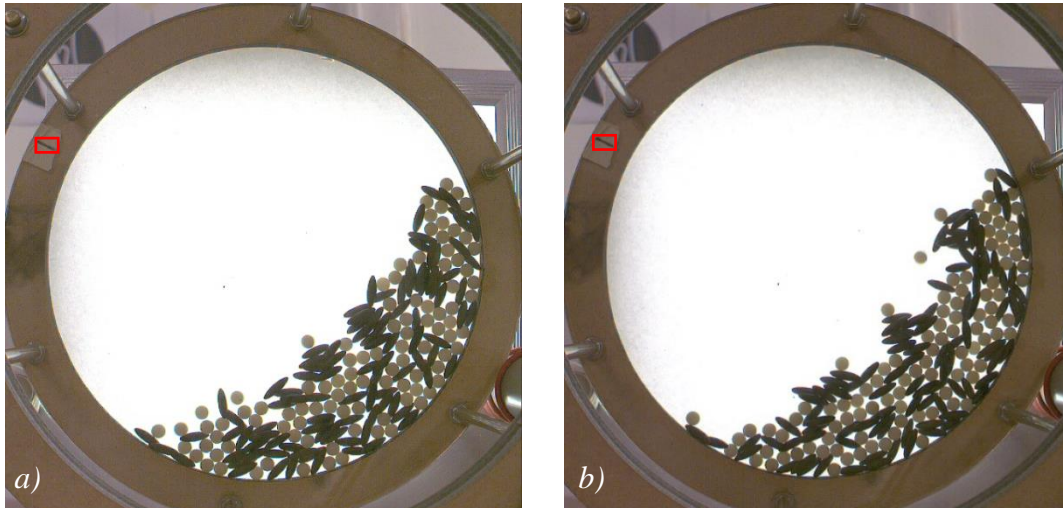


Figure 2.8. a) Reference frame f_1 ; b) frame f_2 after one rotation of the drum.

The rotational speed was evaluated for different voltages; the trend of the rotational velocity as a function of the voltage of the motor is reported in Figure 2.9.

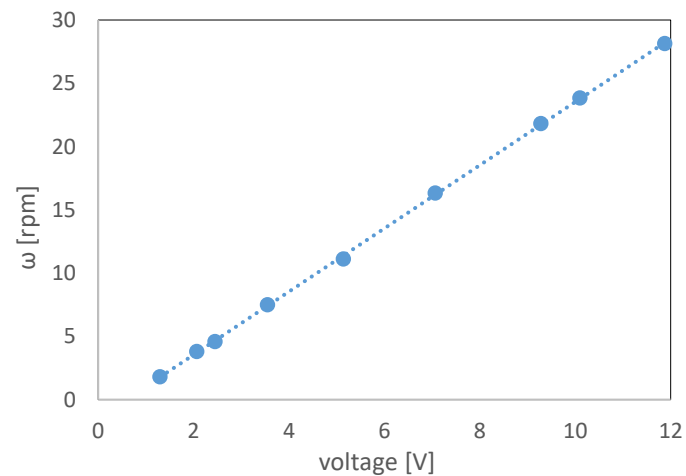


Figure 2.9. Rotational speed of the drum vs. the voltage of the motor.

The plot shows that the speed of the drum changed with the voltage in a linear way.

2.3 Experimental plan

The experiments reported in this work concern segregation and mixing phenomena of particles of different shape and size. The main attention was focused on mixtures of particles with different shapes, since segregation phenomena due to different size had been widely investigated and many studies exist related to it.

2.3.1 Mixtures of particles of different shapes

The particles that were considered to investigate segregation phenomena due to different shape are the ones described in the previous chapter (see § 2.1.1 and § 2.1.2). Three mixtures were considered, with two different initial segregated configurations.

The experimental tests are summarized in the following table.

Table 2.9. *Experimental tests performed with differently shaped particles.*

<i>AR 1 [-]</i>	<i>AR 2 [-]</i>	<i>ω [rpm]</i>	<i>ϕ [-]</i>	<i>initial configuration</i>	<i>time [min]</i>	<i>repetitions</i>
1	1.5	4.22	25%	E/S	30	3
1	1.5	4.22	25%	S/E	30	1
1	1.5	4.22	47%	E/S	30	3
1	1.5	4.22	47%	S/E	30	1
1	1.5	11.51	25%	E/S	30	3
1	1.5	11.51	47%	E/S	30	3
1	1.5	4.22	25%	E/S	2	1
1	3.5	4.22	25%	E/S	30	3
1	3.5	4.22	25%	S/E	30	1
1	3.5	4.22	47%	E/S	30	3
1	3.5	4.22	47%	S/E	30	1
1	3.5	11.51	25%	E/S	30	3
1	3.5	11.51	47%	E/S	30	3
1	3.5	4.22	25%	E/S	2	1
1.5	3.5	4.22	25%	E ₂ /E ₁	30	3
1.5	3.5	4.22	25%	E ₁ /E ₂	30	1
1.5	3.5	4.22	47%	E ₂ /E ₁	30	3
1.5	3.5	4.22	47%	E ₁ /E ₂	30	1
1.5	3.5	4.22	25%	E ₂ /E ₁	2	1

AR 1 and AR 2 indicate the aspect ratios of the particles in the binary mixture. It is reminded that the spheres (AR=1) and the two types of ellipsoids (AR=1.5 and AR=3.5) have the same volume.

The E/S initial configuration indicates a segregated configuration with ellipsoids above spheres below (this was assumed as basis configuration); the S/E configuration is the inverted initial configuration with spheres above and ellipsoids below. For the mixtures of ellipsoids, E_2 indicates the ellipsoids with $AR=3.5$, while E_1 the ellipsoids with $AR=1.5$.

All the experiments were performed with binary mixtures with a composition of 50% and 50% on a number basis, so with an equal number of particles of the two types.

The filling level (φ) of the 25% was obtained with a total number of particles equal to 200 (100 particles of one type and 100 of the other type); with 320 total particles (160 of each types) the filling level of the drum was equal to 47%.

Since recording the system for 30 minutes does not allow to set a low fps, some tests were performed for two minutes: in this case it was possible to set a $\text{fps}=0.2$ s and so to better observe the system and the phenomena occurring.

2.3.2 Mixtures of particles of different sizes

Some experiments with particles with the same shape but with different size were performed. The particles were described in paragraph 2.1.2.

Table 2.10. *Experimental tests performed with differently sized particles.*

<i>Size 1 [mm]</i>	<i>Size 2 [mm]</i>	<i>ω [rpm]</i>	<i>φ [-]</i>	<i>initial configuration</i>	<i>time [min]</i>	<i>repetitions</i>
3.81	8	4.22	24.734%	S1/S2	2	1
6	8	4.22	24.915%	S1/S2	2	1

The number of particles was defined in order to have binary mixtures with a composition of 50% on a volume base and a filling level as equal as possible to 25%. The volume occupied by the particles of a certain dimension was calculated as the product between the volume of one particles and the number of particles. The initial configuration was a segregated one, with the bigger spheres placed below and the smaller ones above (S1/S2). One test was performed for each mixture. Since size segregation phenomena are known to occur fast, the drum was rotated for just two minutes.

2.4 Particles analysis

Firstly, the particles described in paragraph 2.1.2 were considered for the image analysis. They were not immediately placed in the drum, but simply on a black cardboard and some pictures were taken. The pictures were then analysed with ImageJ in order to obtain the position and the orientation of each particle. An example of the analysed pictures is reported in Figure 2.10.

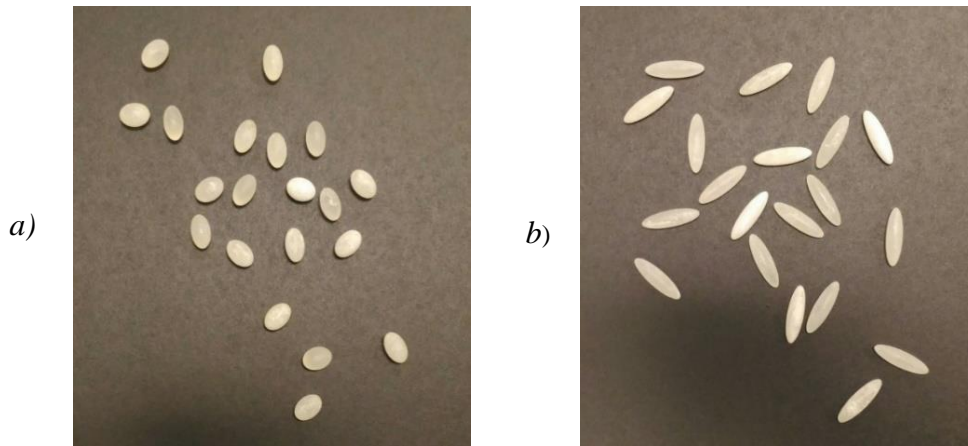


Figure 2.10. a) Ellipsoids of type 1; b) ellipsoids of type2.

To analyse the particles the following operations were done:

1. First the picture was converted into an 8-bit image, as the *Threshold* operation works only with grayscale images.
2. Then a proper threshold was set to separate the particles from the background.
3. Finally, the results for each particle were obtained with the *Analyze Particle* command. Also, the *Outlines* of the particles could be obtained.

The procedure followed to obtain the results is reported in the following code:

```
// ELLIPSOIDS
selectWindow("Image1.jpg");
run("8-bit");
setAutoThreshold("Default dark");
//run("Threshold...");
//setThreshold(157, 255);
setOption("BlackBackground", false);
```

```

run("Convert to Mask");
run("Close");
run("Analyze Particles...", "size=100-Infinity
show=Outlines display");
String.copyResults();

```

In Figure 2.11 the outlines obtained for the two pictures reported above are shown.

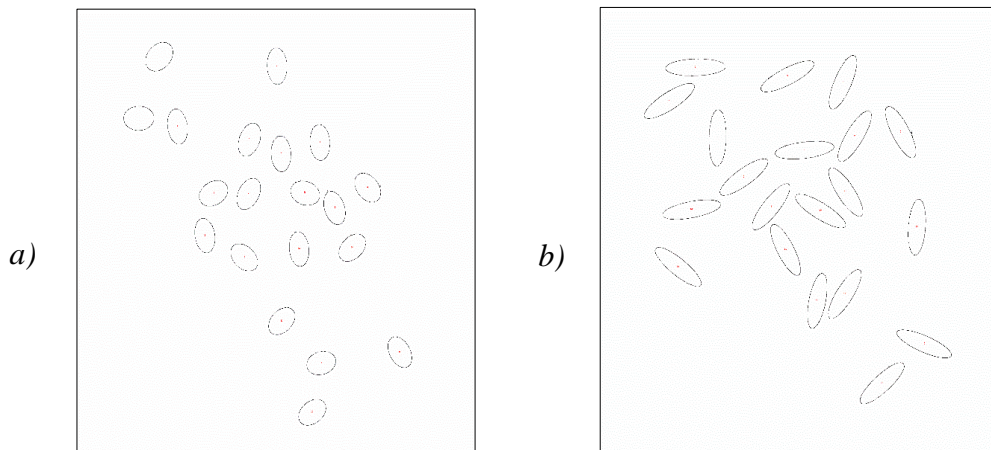


Figure 2.11. a) Outlines of the ellipsoids of type 1; b) outlines of the ellipsoids of type 2.

Table 2.11 contains an example of the more significant results obtained for five particles of the type 1.

Table 2.11. More significant results for the ellipsoids of type 1.

	<i>Area</i> [pixel ²]	<i>XM</i> [pixel]	<i>YM</i> [pixel]	<i>Circ.</i> [-]	<i>Feret</i> [pixel]	<i>FeretAngle</i> [degrees]	<i>AR</i> [-]	<i>Round.</i> [-]
1	12111	402.927	199.043	0.849	147.411	36.170	1.390	0.719
2	11624	980.721	238.318	0.826	153.395	94.112	1.575	0.635
3	11842	302.74	456.526	0.835	149.272	176.543	1.474	0.678
4	11303	492.605	491.349	0.833	150.233	101.908	1.543	0.648
5	11354	845.627	546.189	0.816	149.402	64.636	1.512	0.661

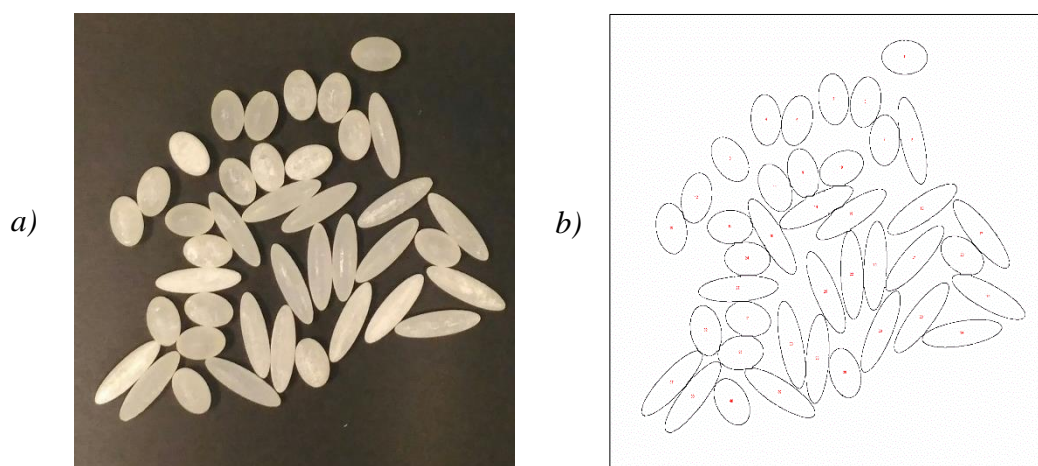
In Table 2.12 the results for the particles of type 2 are shown.

Table 2.12. More significant results for the ellipsoids of type 2.

	Area [pixel ²]	XM [pixel]	YM [pixel]	Circ. [-]	Feret [pixel]	FeretAngle [degrees]	AR [-]	Round. [-]
1	13563	983.564	320.828	0.505	247.348	68.414	3.527	0.284
2	13781	386.346	257.208	0.544	243.463	3.532	3.381	0.296
3	13499	758.998	295.605	0.526	243.417	28.46	3.442	0.291
4	13791	280.208	400.826	0.552	243.249	34.278	3.345	0.299
5	13657	1217.299	533.695	0.489	242.012	115.189	3.364	0.297

The area of each particle was obtained together with the coordinates of the centre of mass, indicated as *XM* and *YM*. The Feret's diameter (*Feret*) was also evaluated and the angle of the Feret's diameter was displayed as *Feret Angle*. The Aspect Ratio (*AR*) defined the shape of the particles; the roundness (*Round.*) is the inverse of the Aspect Ratio. Finally, the circularity (*Circ.*) is defined as $4\pi \cdot \text{Area} / (\text{Perimeter})^2$ and it is a dimensionless parameter equal to 1 for a perfect circle; as it approaches 0 it indicates a more elongated shape: so, the circularity could give information about the particles shape as well. It has to be noted that the values of area, centre of mass and Feret's diameter are expressed in pixels, since no units were defined to calibrate the picture.

A similar procedure was repeated in the case of a mixture of the two types of particles. In the case of touching particles, the *Erode* command and the *Watershed* operation were required to separate them. An example is reported in the following pictures; also, the code is reported.

**Figure 2.12.** a) Mixture of two types of ellipsoids; b) outlines obtained as a result.

```
// MIXTURE
selectWindow("Image2.jpg");
run("8-bit");
setAutoThreshold("Default dark");
//run("Threshold...");
//setThreshold(119, 255);
run("Convert to Mask");
run("Erode");
run("Watershed");
run("Analyze Particles...", "size=100-Infinity
show=Outlines display");
String.copyResults();
```

Successively, to have a contrast between the two type of particles it was decided to paint one type of them with a different colour. This allowed to repeat the threshold twice, once for the light particles and once for the darker particles and so better identify them when touching each other. So, the particles of type 2 were darkened with a black paint. Some pictures of the black particle were taken placing them simply on a light desk. The outlines of the particles are shown in Figure 2.13.

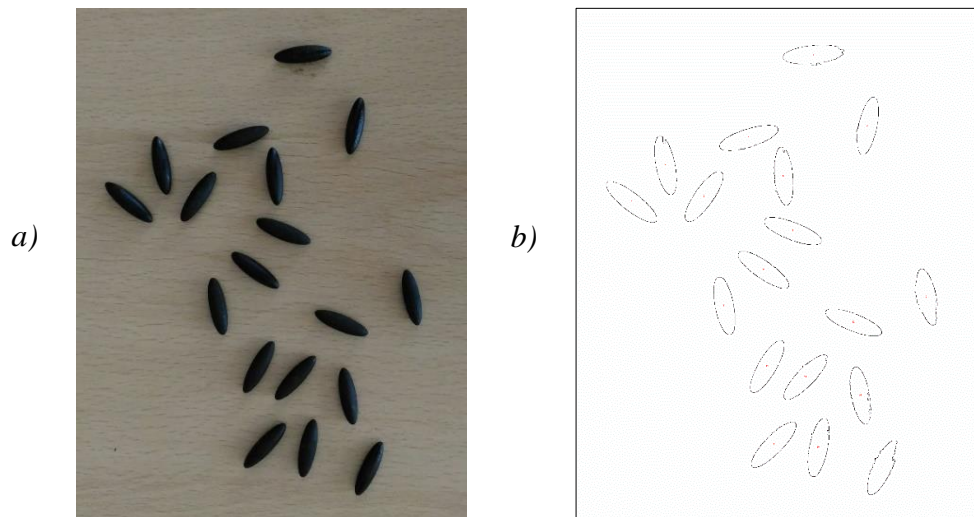


Figure 2.13. a) Ellipsoids of type 2, darken with a black paint; b) outlines of the dark particles.

Some problems for the image analysis appeared considering a mixture of light and dark particles. The particles were placed on a green surface in order to have a high contrast between the background and the objects.

For the light particles, it was possible to set a proper threshold and analyse them, obtaining the results for each particle.

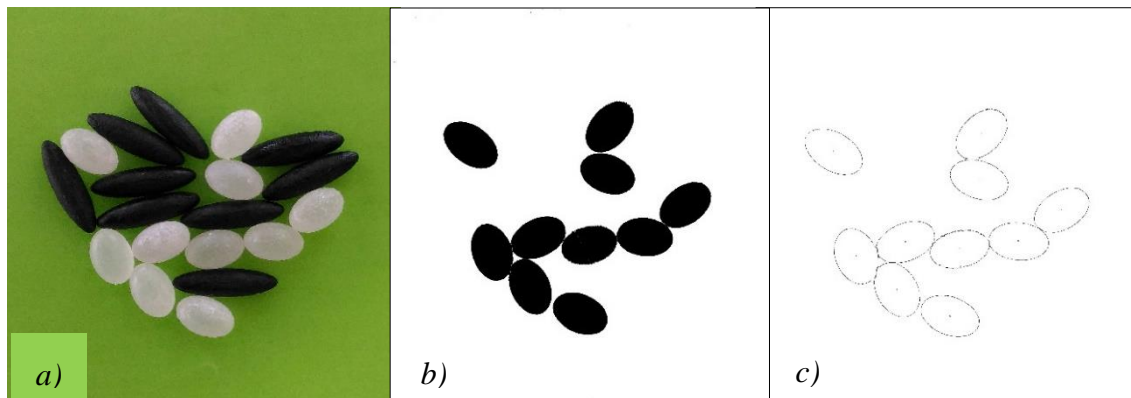


Figure 2.14. a) Original picture; b) threshold of the light particles; c) outlines of the light particles.

For the black particles, instead, it was not possible to set a proper threshold, and the results could not be obtained, as it can be seen in the following images.

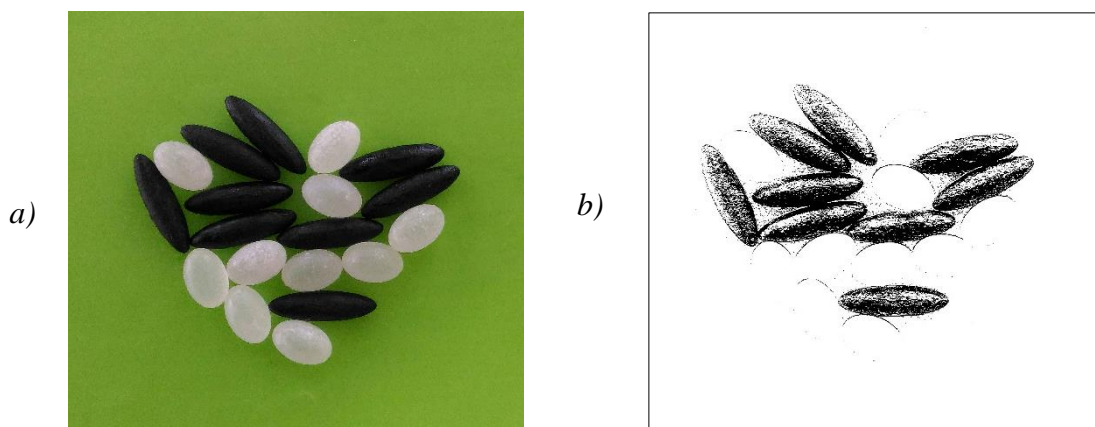


Figure 2.15. a) Original picture; b) threshold of the dark particles.

The difficulties mainly originated from the light of the environment and from the shadows and reflection on the black particles. To solve the problem, the use of an intense and diffusive light was needed to enlighten the particles and remove any reflection. To get the proper lighting a LED panel was used, able to ensure an intense light that was diffused

by the use of a paper sheet. The optimization of the light was realized directly on the drum, where the particles were put.

2.5 Drum analysis

The particles were afterwards placed in the drum. The drum was not already mounted on the rollers that allowed to rotate it, but it was simply kept in vertical position. Moreover, also spheres with diameter of 8 mm (described at § 2.1.1) were added together with the ellipsoids. The drum was illuminated by the LED, placed very close to the drum and pictures were taken by the colour camera. In particular, mixtures of spheres and ellipsoids were considered and, the ImageJ program was used to identify the different types of particles in the drum.

2.5.1 Binary mixtures of spheres and ellipsoids with $AR=1.5$

Spheres and ellipsoids with Aspect Ratio equal to 1.5 were considered in the drum and analysed, taking into account mixtures with different composition. Some pictures are reported in Figure 2.16.

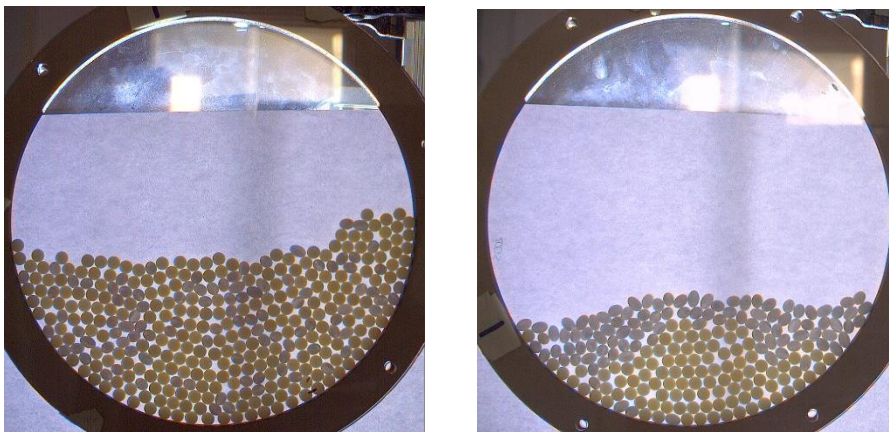


Figure 2.16. Binary mixtures made of spheres and ellipsoids with $AR=1.5$.

The procedure followed in ImageJ was equal to the one described in the previous paragraph. The two types of particles had both a light colour, so the *Threshold* operation was done once only. The ImageJ results were obtained for both the spheres and the ellipsoids. The *Outlines* are displayed in Figure 2.17.

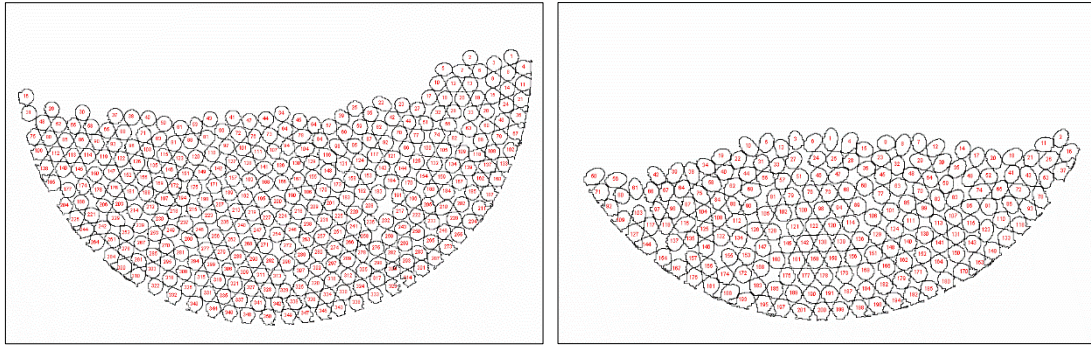


Figure 2.17. Outlines for the binary mixtures of spheres and ellipsoids with $AR=1.5$ of Figure 2.16.

It was possible to distinguish the spheres from the ellipsoids due to their different shape: the Aspect Ratio was the parameter used for this aim. The values of the aspect ratio for some particles of the two types are reported in Table 2.13. They are obtained from the analysis of a mixture of spheres and ellipsoids of type 1, as the ones reported in Figure 2.16.

Table 2.13. Values of Aspect Ratio obtained from image analysis.

<i>AR [-]</i>	
Spheres	Ellipsoids
1.027	1.314
1.063	1.384
1.017	1.471
1.057	1.561
1.010	1.543

The value of the aspect ratio was very close to 1 for the spheres; for the ellipsoid, instead, the value was higher, close to 1.5.

The identification of the two types of particles through the aspect ratio was more difficult for the particles at the border of the drum; in some case, in fact, the ellipsoids were erroneously identified as spheres. Also, the presence of the border of the drum complicated the *Watershed* operation.

2.5.2 Mixtures with ellipsoids with $AR=3.5$

Also, mixtures with elongated particles with aspect ratio equal to 3.5 were considered. An example is reported in Figure 2.18.

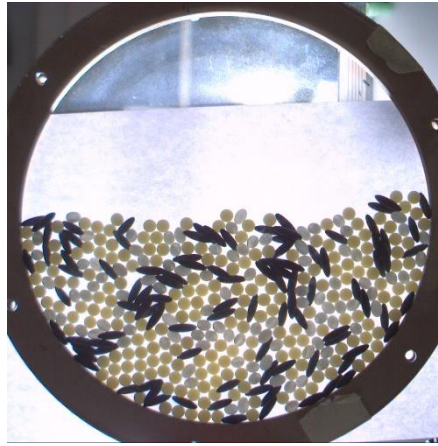


Figure 2.18. Ternary mixture of spheres, ellipsoids with $AR=1.5$ and ellipsoids with $AR=3.5$.

In the case of those mixtures, the correct identification of the black particles following the procedure used so far was not suitable. Problems arose from the possibility for these particles to overlap each other, being not individually identifiable. Moreover, the *Watershed* operation very often led to an oversegmentation, as it is shown in the following picture:

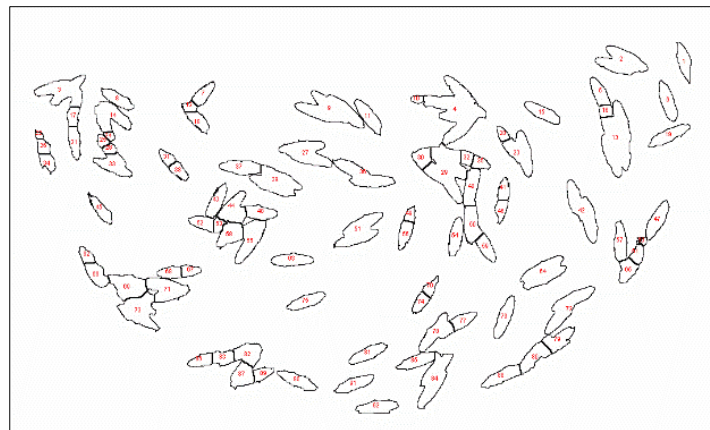


Figure 2.19. Outlines of the black particles of Figure 2.18 obtained with the *Watershed* operation.

As it can be seen in Figure 3.10, in some cases two or more particles were identified together. However, the most problematic issue was the oversegmentation of the particles:

some particles instead of being identified as one were cut in two or more pieces by the *Watershed*. The reason of the oversegmentation was found in the algorithm that is at the basis of the *Watershed* operation (see Appendix A).

To solve the problem and better identify the black particles, different attempts were made. Firstly, the black particles were bleached in order to have them in their original light colour. However, the change in colour did not solve the oversegmentation problem. Therefore, other ImageJ plugins were taken into account, looking for a plugin able to properly identify overlapping and touching objects. The *Graylevel Watershed*, the *Morphological Segmentation* and the *Distance Transform Watershed* plugins were tried but without significant improvements. The best solution was found in an ImageJ plugin called *Adjustable Watershed* in which the *tolerance* can be set: higher the tolerance and lower the segmentation of the analysed objects. With this plugin was not possible to separate all the ellipsoids and identify them individually, but it was possible to effectively reduce the oversegmentation. The *Outlines* obtained for the black particles of Figure 2.18, with the *Adjustable Watershed* are reported in Figure 2.20.

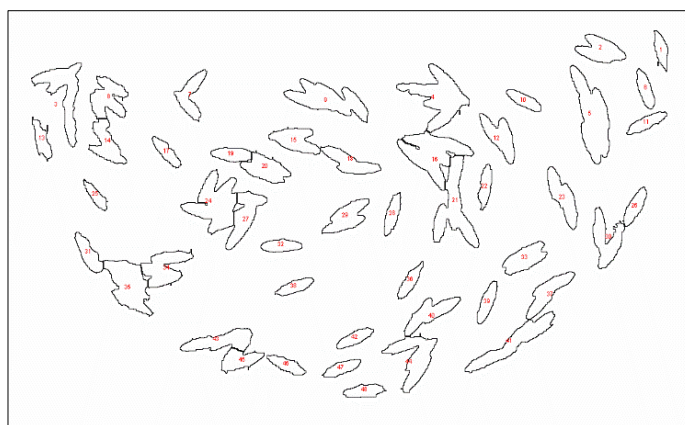


Figure 2.20. *Outlines of the black particles of Figure 2.18 obtained with the Adjustable Watershed with tolerance=4.*

As it can be seen from Figure 2.20, there is a clear difference between the *Outlines* obtained in this case and the ones obtained with the *Watershed*. Even if also with the *Adjustable Watershed* some particles are erroneously cut, the segmentation is significantly reduced and the result is better than the one reported in Figure 2.19.

2.6 Image analysis procedure

Starting from the preliminary procedure developed and based on the considerations reported previously (§ 2.5), a method of analysis was formulated and applied to the binary mixtures mentioned in paragraph 2.3. The image analysis procedure allowed to calculate the radial distance of the particles in the drum.

2.6.1 Procedure

The image analysis procedure is reported in the following.

1. The starting point of the analysis was a given colour picture of the drum of the dimensions of 1080×1080 pixels (an example is represented by Figure 2.21(a)).
2. The sharpness of the picture was increased with the *Sharpen* option and the brightness adjusted at the best value by adjusting *Brightness/Contrast*.
3. To obtain a grayscale image the *Split Channels* command was run. Among the three black and white images obtained, the green component of the original picture was selected, as it was the best one in terms of sharpness and definition.
4. To isolate the part of the image of interest, the circular front part of the drum was delineated with the *makeOval* command and then cut and paste in a new blank picture of the same dimension of the circle. An example is reported in Figure 2.21.

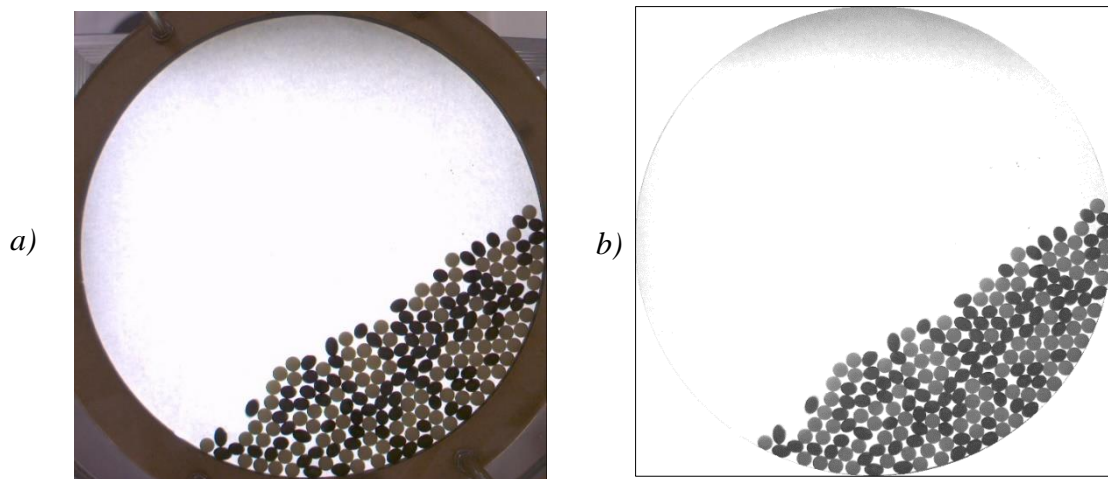


Figure 2.21. a) Example of original colour image; b) example of the circle cut from the original picture obtained after converting the picture to a grayscale one.

5. As the circular drum image was inscribed in a squared picture, the centre of the drum was assumed to be the centre of the squared picture; the coordinates of the centre of the drum were indicated as x_c and y_c .
6. Since different types of particles in the drum were always of two different colours, the *Threshold* operation was run twice, once for the light particles and once for the black particles. An example of the Threshold operation applied to the dark and light particles is shown in Figure 2.22

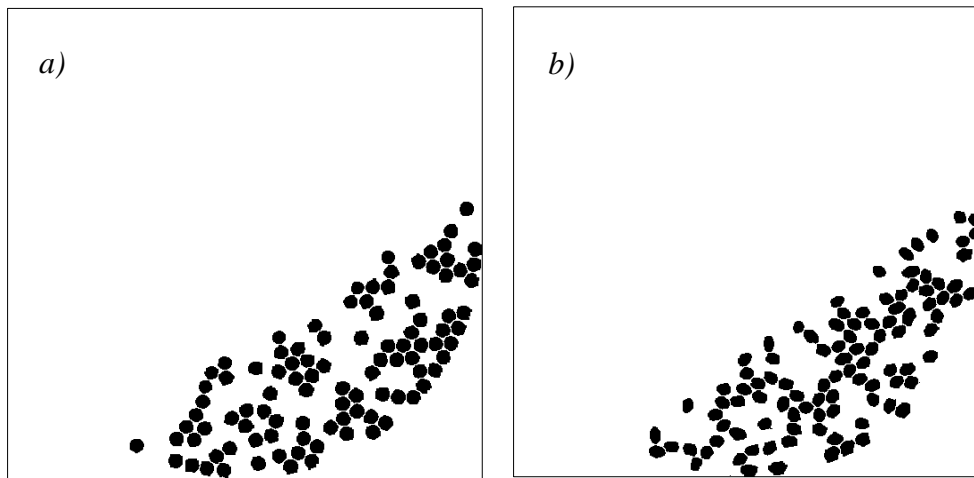


Figure 2.22. Threshold operation applied to a) light particles and b) dark particles; the original picture is Figure 2.21(a).

7. The successive operations have to be distinguished between binary mixtures of spheres and ellipsoids with AR=1.5 and mixtures with ellipsoids with AR=3.5, since the procedure was slightly different in the two cases.

7.1 In the case of mixtures of spheres and ellipsoids with AR=1.5, the *Watershed* operation was run for both types of particles on the two thresholded images and the results for the spheres and the ellipsoids were obtained. In particular, from the coordinates of the centre of mass of each particle ($x_{m,i}$ and $y_{m,i}$) it was possible to calculate the radial distance (d_i) from the centre of the drum of each particle. It was calculated as:

$$d_i = \sqrt{(x_c - x_{m,i})^2 + (y_c - y_{m,i})^2} \quad (2.12)$$

The mean value of distance (d_m) for the spheres and for the ellipsoids was then calculated according to the following formula:

$$d_m = \frac{\sum_{i=1}^N d_i}{N} \quad (2.13)$$

Where N is the total number of each type of particle.

7.2 In the case of mixtures of spheres and ellipsoids with AR=3.5 the procedure was different. For the spheres, the same was done as described at the previous point and the mean distance of the spheres was obtained according to formula (2.13). For the ellipsoids, instead, the *Adjustable Watershed* was used and in some cases more particles were identified as one single particle; of each block of particles identified by the *Adjustable Watershed* the coordinates $x_{m,i}$ and $y_{m,i}$ and the Area (A_i) were defined. Considering that the ellipsoids with AR=3.5 were not exactly and individually identifiable, only one value of the two coordinates of their centre of mass (x_m and y_m) was calculated, by weighting the values on the area of each identified particle, or block of particles:

$$x_m = \frac{\sum_{i=1}^N x_{m,i} A_i}{\sum_{i=1}^N A_i} \quad (2.14), \quad y_m = \frac{\sum_{i=1}^N y_{m,i} A_i}{\sum_{i=1}^N A_i} \quad (2.15)$$

From these values, a value of distance from the centre of drum representative of all the ellipsoids was calculated from formula (2.12).

8. Given the values of the mean distance of the two types of particles in the mixture, the mean radial distance of all the particles from the centre of the drum (d_c) was calculated as:

$$d_c = \frac{d_{m,spheres} + d_{m,ellipsoids}}{2} \quad (2.16)$$

9. Also, the coordinates of the barycentre of the granular bed were calculated.

9.1 In the case of mixtures of spheres and ellipsoids with AR=1.5, the coordinates of the barycentre of the spheres ($x_{b,spheres}$, $y_{b,spheres}$) were calculated as the mean of the $x_{m,i}$ and $y_{m,i}$ of all the spheres. Equally, for

the ellipsoids, $x_{b,ellipsoids}$ and $y_{b,ellipsoids}$ were evaluated as the mean of all $x_{m,i}$ and $y_{m,i}$ of all the ellipsoids. The coordinates of the barycentre of the granular bed then were:

$$x_b = \frac{x_{b,spheres} + x_{b,ellipsoids}}{2} \quad (2.17)$$

$$y_b = \frac{y_{b,spheres} + y_{b,ellipsoids}}{2} \quad (2.18)$$

9.2 In the case of mixtures of spheres and ellipsoids with AR=3.5, the barycentre of the spheres was calculated as the mean of the $x_{m,i}$ and $y_{m,i}$ of all the spheres. For the ellipsoids, instead, the values of x_m and y_m calculated by formulas (2.12) and (2.13) were also assumed to be the values of the coordinates of the barycentre of the ellipsoids. And so, the coordinates of the barycentre of the granular bed were:

$$x_b = \frac{x_{b,spheres} + x_{m,ellipsoids}}{2} \quad (2.19)$$

$$y_b = \frac{y_{b,spheres} + y_{m,ellipsoids}}{2} \quad (2.20)$$

10. The values of distance calculated above from the ImageJ results were expressed in pixels. They needed to be converted in millimetres and referred to the drum dimensions. To define the conversion factor (k), it was considered that the side (l) of the square in which the circular front section of the drum was inscribed had to be equal to the diameter (D) of the drum. So, the conversion factor was defined as:

$$k = \frac{D [mm]}{l [pixels]} \quad (2.21)$$

The procedure described above was applied also to the mixtures made of particles of different sizes, mentioned at § 2.3.2. It has to be specified that the particles with 3.81 mm mean diameter were not detectable with the developed procedure, since they were so

small to form more layers in the drum. For the mixture of differently shaped particles the distance of all the particles from the centre of the drum (d_c) was calculated as the distance of the barycentre of the granular bed from the centre of the drum.

2.6.2 Filling level evaluation

The filling level (φ) of the drum was evaluated from pictures of the front circular drum with the mixture in its initial segregated configuration. Given the circular front picture of the drum, to evaluate the filling level, the following procedure was used.

1. By a proper threshold, the total area of the drum (A_{tot}) was evaluated.
2. By a proper threshold, the area of all the particles ($A_{particles}$) was calculated, including all the voids between particles.
3. By subtracting the area of all the particles from the total area of the drum, the void area of the drum (A_{void}) was obtained.
4. Finally, the filling level (%) was:

$$\varphi = \frac{A_{tot} - A_{void}}{A_{tot}} \cdot 100 \quad (2.22)$$

2.6.3 Angle evaluation

Three angles were evaluated for the binary mixtures considered in the drum:

1. The Maximum Angle of Stability (α_{max}), which is the maximum angle reached by the granular bed before an avalanche occurs.
2. The Angle of Repose (β) that is the angle formed by the granular bed, after the avalanche ends and before the granular bed starts to raise up again.
3. The Dynamic Angle of Repose (β_d), which is the angle of the granular surface during the motion.

From literature, (Cheng, 2016) it was found that the Dynamic Angle of Repose can be expressed as the mean of the other two angles:

$$\beta_d = \frac{(\alpha_{max} + \beta)}{2} \quad (2.23)$$

The angles give information about the particles behaviour in the drum: a higher value of the angles indicates the tendency to form more stable structures.

The pictures from which the angles were evaluated were taken from videos of the rotating drum that were recorded with low frequency of the frames (fps= 0.2 s) and high exposure time (equal to 35000 μ s); the high exposure time allowed to highlight the particles in motion in the active layer.

The three angles could be evaluated following two different methods:

- *Method 1*

The angles could be evaluated manually through the *Angle Tool* available in ImageJ.

In particular, given a picture of the drum, two consecutive lines were drawn: the first one was exactly horizontal, the second one fitted the particles surface. The *Angle Tool* automatically estimated the angle between the two lines.

An example is reported in Figure 2.23 for the evaluation of two angles.

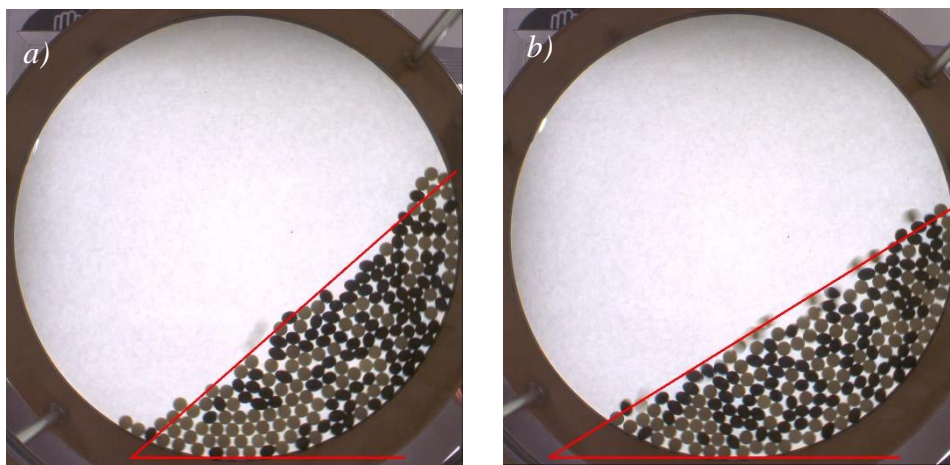


Figure 2.23. Evaluation of a) the Maximum Angle of Stability and b) the Angle of Repose with the Angle Tool of ImageJ (Method 1).

Method 1 gave a correct estimation of the angle. The fitting line, however, was drawn manually so the method could be not exactly precise. Moreover, in some case the straight line did not fit the surface of the particles at the best, especially when the surface is not exactly flat.

- *Method 2*

A more precise estimation could be obtained by calculating the angle that the centre of mass of the particles forms with respect to a vertical line passing through the centre of the drum.

For the calculation, first a proper *Threshold* was set in order to identify all the particles as a single object. Then, by the *Analyze Particles* command, the coordinates of the centre of mass of all the particles (x_m and y_m) were obtained. The angle α [degrees] was then evaluated as:

$$\alpha = \arctan\left(\frac{x_m - x_c}{y_m - y_c}\right) \cdot \frac{180}{\pi} \quad (2.24)$$

Where x_c and y_c are the coordinates of the centre of the drum.

An example is reported in Figure 2.24.

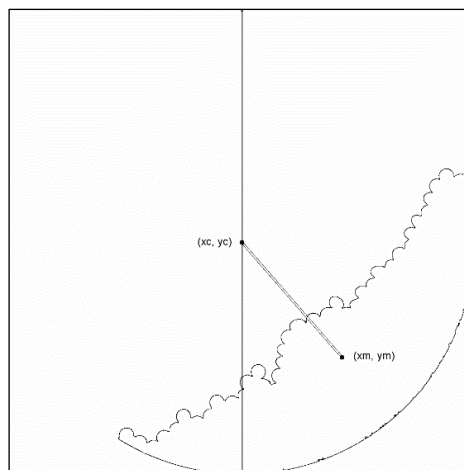


Figure 2.24. Evaluation of the angle formed by the particles surface with Method 2.

Assuming that the fitting line drawn with Method 1 is perpendicular to the segment connecting the centre of the drum and the centre of the particles, it can be demonstrated that the two angles calculated with Method 1 and Method 2 are the same angle. So, Method 2 could be used to check how correct is the estimation made with Method 1.

Chapter 3

Results and discussion

In this chapter, the results of the experimental tests presented previously (§ 2.3) will be exposed and discussed. The results are divided into three main paragraphs. In the first one the results for mixtures of particles with different shapes are presented. The second paragraph reports the results obtained for mixtures of particles with different sizes. Finally, the calculation of the Maximum Angle of Stability, the Angle of Repose and the Dynamic Angle of Repose will be presented, in the third paragraph of the chapter. All the results were obtained following the procedure described in Chapter 2 (§ 2.6).

3.1 Mixtures of particles of different shapes

In this paragraph, the results related to different shaped particles will be reported. Different mixtures have been considered, but also different filling levels and rotational speeds of the drum.

3.1.1 Spheres and ellipsoids $AR=1.5$, $\omega=4.22$ rpm, $\varphi=25\%$

Four tests of 30 minutes were performed with the binary mixture made of spheres and ellipsoids with $AR=1.5$, at the conditions reported in Table 3.1.

Table 3.1. Conditions of the tests with spheres and ellipsoids with $AR=1.5$ at lower filling level.

<i>AR 1</i> [-]	<i>AR 2</i> [-]	<i>ω</i> [rpm]	<i>φ</i> [-]	<i>initial configuration</i>	<i>time</i> [min]	<i>repetitions</i>
1	1.5	4.22	25%	E/S	30	3
1	1.5	4.22	25%	S/E	30	1
1	1.5	4.22	25%	S/E	2	1

Some pictures of the system with the E/S initial configuration are reported in Figure 3.1.

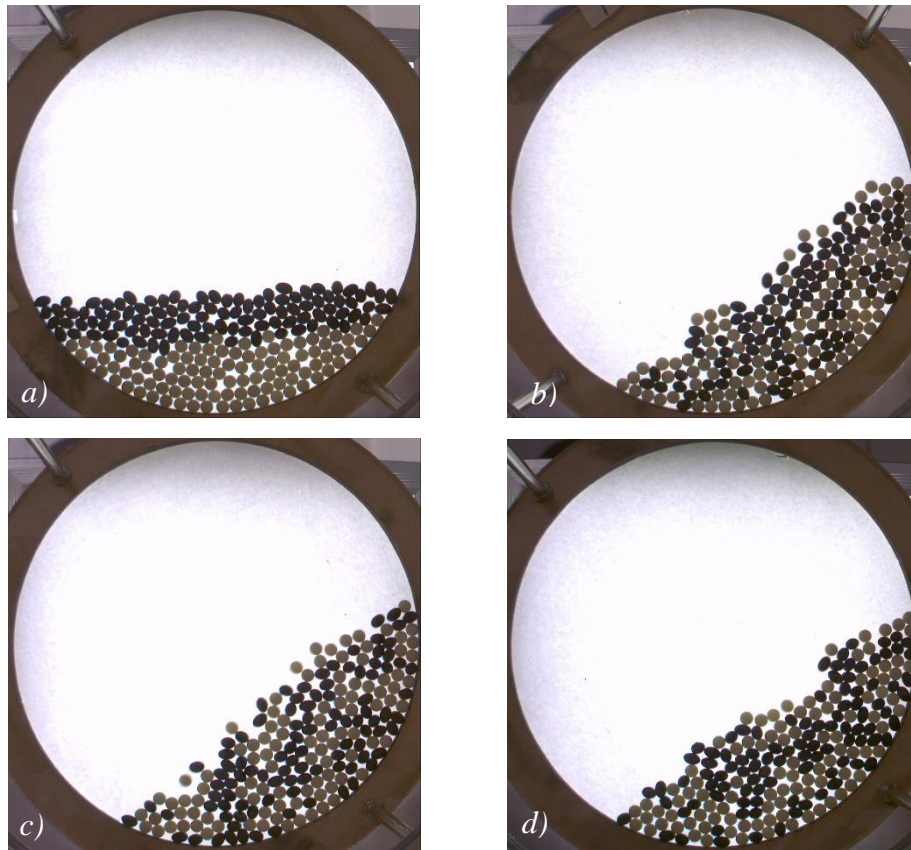


Figure 3.1. Drum at a) $t=0$; b) $t=5$ min; c) $t=15$ min; d) $t=30$ min (test 3), ($\omega=4.22$ rpm; $\varphi=25\%$; the initial configuration was the E/S one).

The radial distance (d_m) of the two types of particles was calculated according to formula (2.13), at different time instants and plotted versus time. The trend is reported in Figure 3.2.

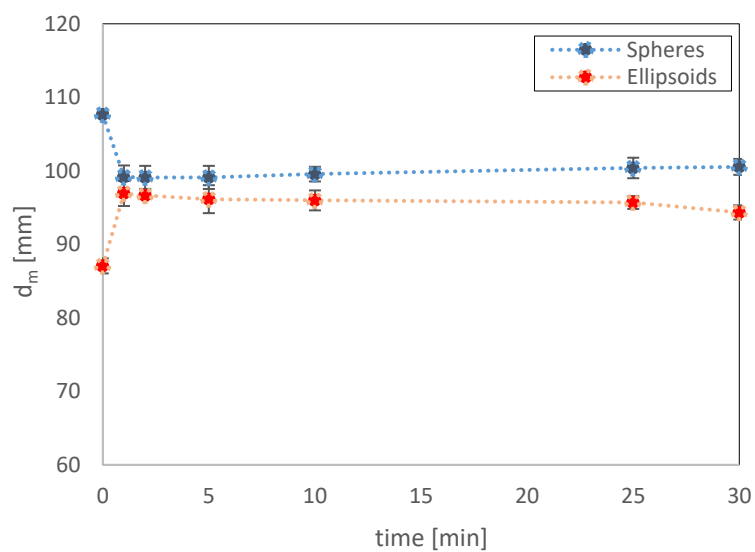


Figure 3.2. Trend of the radial distance vs. time for the mixture of spheres and ellipsoids with $AR=1$; the graph was obtained by averaging the values of distance of the three tests ($\omega=4.22$ rpm; $\varphi=25\%$; the initial configuration was the E/S one).

As it can be seen from Figure 3.2, the radial distance varies from the initial value and for both the spheres and the ellipsoids settles to a steady value. A steady state is reached and kept in time and no other phenomena occur during the time in which the system is observed. The mean radial distance of the two type of particles settles to very similar values; this can suggest that the two types of particles mix in the drum. However, a deeper analysis can be carried out considering the distribution of the radial distance of the spheres and ellipsoids. The radial distance from the centre of the drum (d) was divided in classes of 10 mm and the number of particles (N) in each class was defined. To obtain the distribution, N was normalized on the radial distance and N/d was plotted versus d . In the case of completely mixed particles N/d should be constant and equal for the two types of particles in each class.

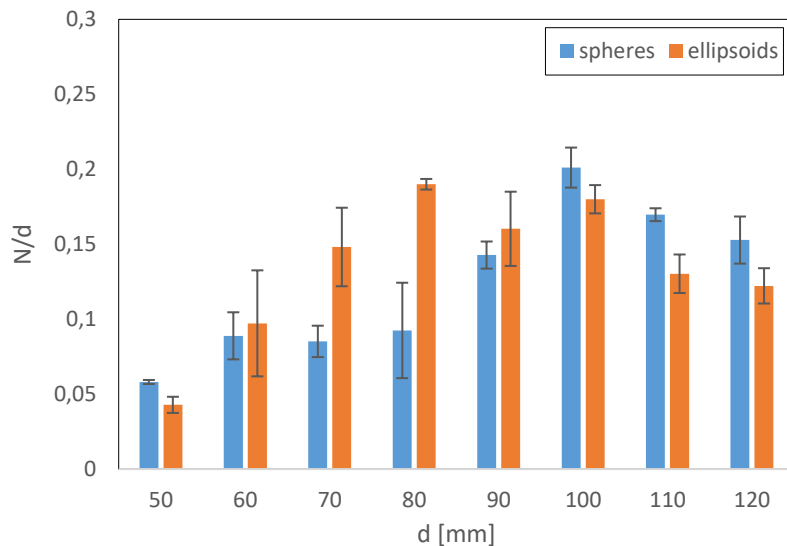


Figure 3.3. Distribution of the radial distance of the two types of particles, obtained as the average of the distributions of the three tests. The histogram refers to the values of radial distance obtained at $t=30$ min ($\omega=4.22$ rpm; $\varphi=25\%$; the initial configuration was the E/S one).

The peak of the distribution of the ellipsoids is found at lower distance than the peak of the distribution of the spheres. Moreover, at lower distance, the number of ellipsoids is higher than the number of spheres, especially for distances between 70 and 90 mm; at higher distance and so closer to the drum wall, instead, the number of spheres is higher than the number of ellipsoids. So, the distribution shows that the two types of particles are mainly found in two different regions of the system: the ellipsoids at the centre at the spheres at the borders of the granular bed.

Also, the *number composition (%)* of the spheres in each class was obtained by dividing the number of spheres by the total number of particles in that class and multiplying by 100. The trend of the composition versus d is shown in Figure 3.4.

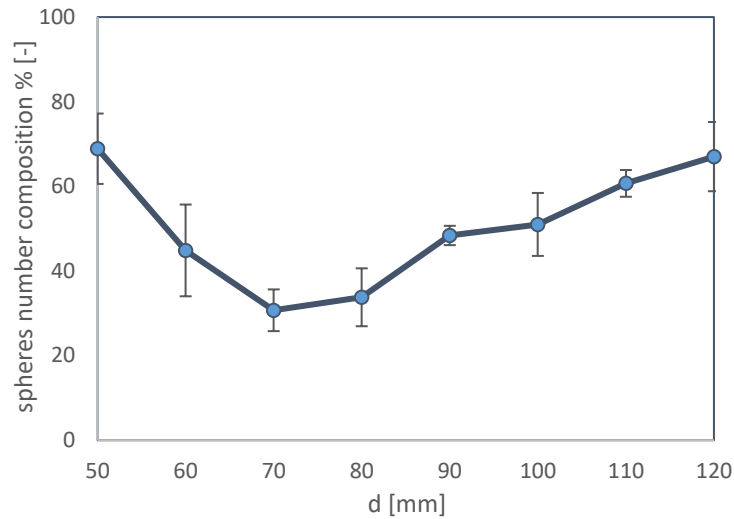


Figure 3.4. Trend of the number composition of the spheres vs. the radial distance, obtained as the average of the composition curves of the three tests ($\omega=4.22$ rpm; $\phi=25\%$; the initial configuration was the E/S one).

The composition of the spheres decreases at intermediate distances and then increases at higher distance from the centre of the drum. It means that the spheres are found in high number at the borders while the ellipsoids settle at a preferential distance at the centre of the granular bed; the two types of particles do not mix homogeneously and so segregation occurs.

To verify whether the initial configuration of the particles could affect the system, one test was performed with the same mixture but with the inverted initial configuration, as shown in Figure 3.5.

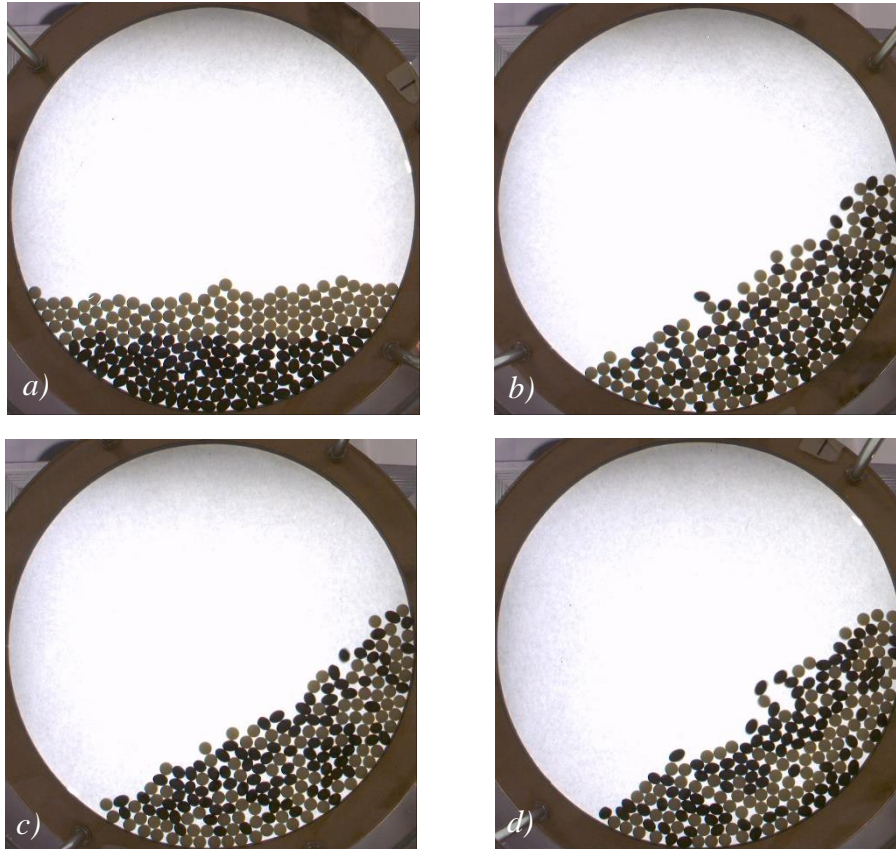


Figure 3.5. Drum at a) $t=0$; b) $t=5$ min; c) $t=15$ min; d) $t=30$ min, ($\omega=4.22$ rpm; $\varphi=25\%$; the initial configuration was the S/E one).

The trend of the radial distance was found to be the same of the other configuration, as reported in Figure 3.6.

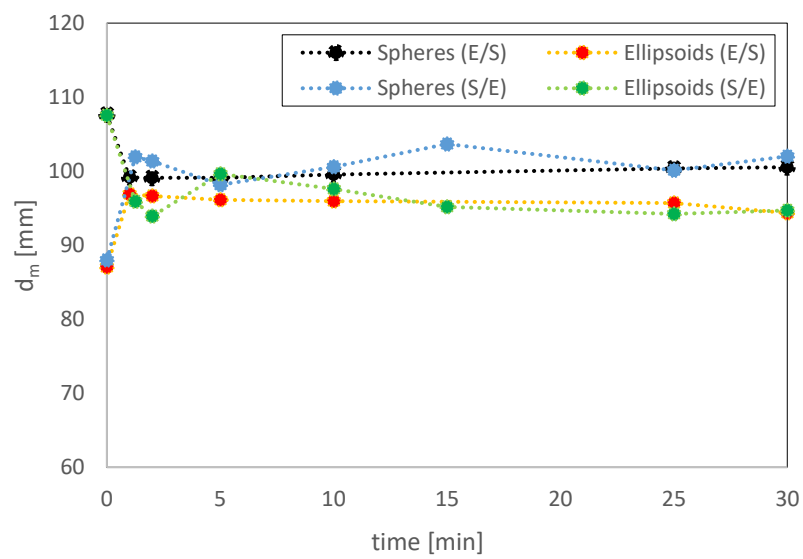


Figure 3.6. Trend of the radial distance vs time for the two initial configurations ($\omega=4.22$ rpm; $\varphi=25\%$).

Even if it is more oscillating, the trend of the radial distance of the two types of particles is the same of the previous case and it stabilizes to steady values that are equal to the ones obtained with E/S initial configuration. The radial distance of the two types of particles settles to the same steady value, independently from the initial configuration of the system, that so does not affect the final configuration reached in the drum.

The distribution of the particles at the final time is reported in Figure 3.7.

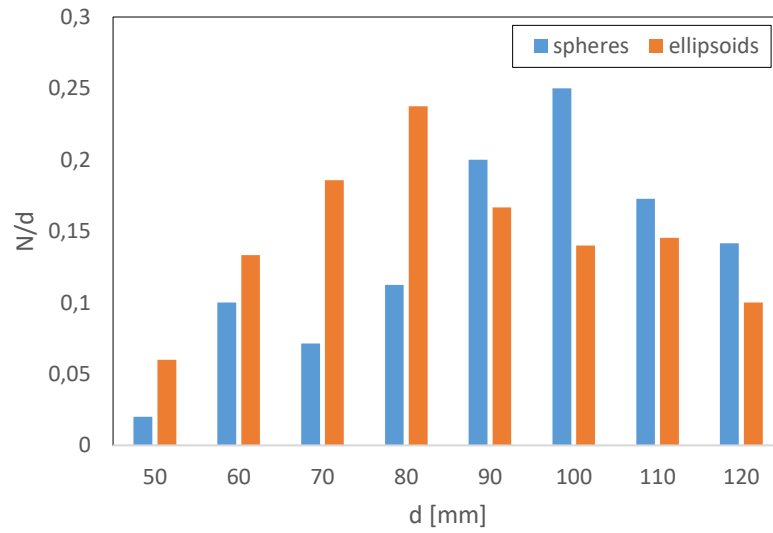


Figure 3.7. Distribution of the radial distance of the two types of particles. The histogram refers to the values of radial distance obtained at $t=30$ min ($\omega=4.22$ rpm; $\varphi=25\%$; the initial configuration of the particles was the S/E one).

The distribution is very similar to the one obtained for the tests with different initial configuration (Figure 3.3). At lower distance, the number of ellipsoids is higher than the number of spheres, while the spheres are present in higher number at larger distances.

The initial configuration of the particles represents, in fact, the way in which the particles are loaded in the drum; so, it is found that loading one type of particles before the other one does not affect the final configuration reached by a mixture of spheres and ellipsoids with an aspect ratio equal to 1.5 and with the same volume.

Furthermore, as it can be seen from Figures 3.2 and 3.6, the achievement of the final steady state occurs quite fast: after one minute, in fact, the value of distance is the final one, or very close to it. To better understand how fast the transition to the final steady

value is, the drum was rotated for a shorter time (2 minutes); it was so possible to record the system with higher fps and better observe the phenomenon.

The radial distance plotted versus time is reported in Figure 3.8.

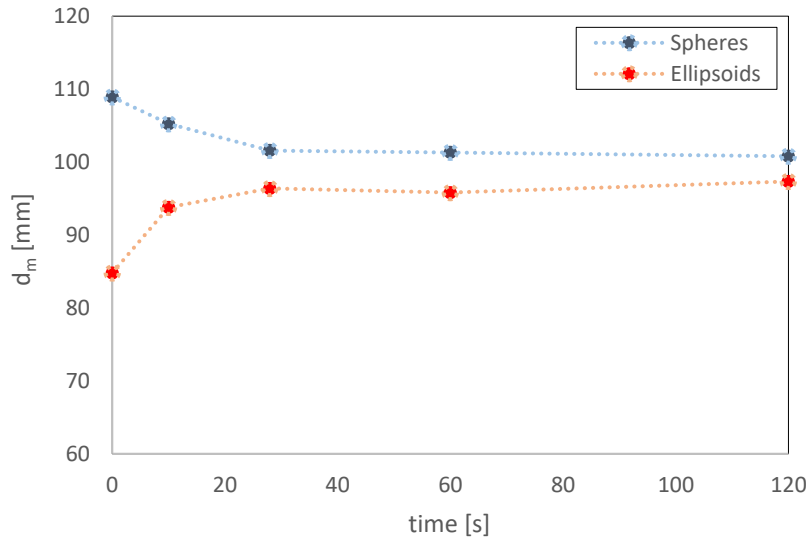


Figure 3.8. Trend of the radial distance vs. time for the 2 minutes test performed with the mixture of spheres and ellipsoids with $AR=1.5$ ($\omega=4.22$ rpm; $\varphi=25\%$).

After 30 seconds, the radial distance reaches the steady state value, so the transition to the final state is very fast.

3.1.2 Spheres and ellipsoids $AR=3.5$, $\omega=4.22$ rpm, $\varphi=25\%$

The tests with the binary mixture of spheres and ellipsoids with $AR=3.5$ were run at the conditions specified in Table 3.2.

Table 3.2. Conditions of the tests with spheres and ellipsoids with $AR=3.5$ at lower filling level.

$AR 1$ [-]	$AR 2$ [-]	ω [rpm]	φ [-]	initial configuration	time [min]	repetitions
1	3.5	4.22	25%	E/S	30	3
1	3.5	4.22	25%	S/E	30	1
1	3.5	4.22	25%	S/E	2	1

As in the previous case, three tests were run with the E/S initial configuration, as shown in Figure 3.9.

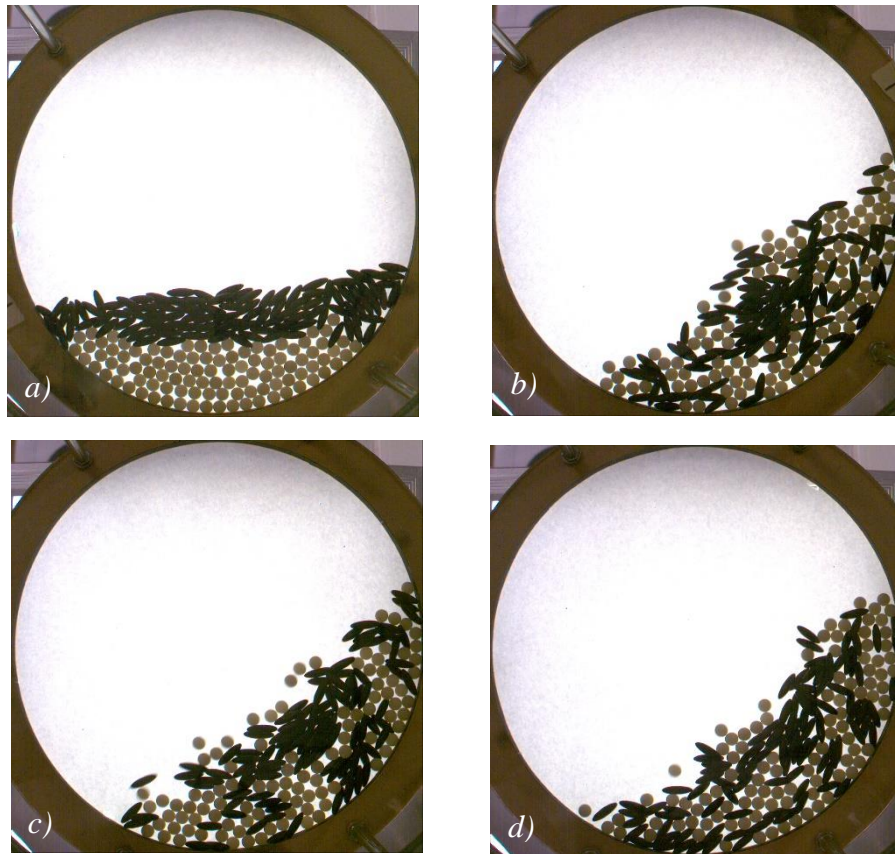


Figure 3.9. Drum at a) $t=0$; b) $t=5$ min; c) $t=20$ min; d) $t=30$ min (test 1), ($\omega=4.22$ rpm; $\phi=25\%$; the initial configuration was the E/S one).

In this case, the ellipsoids were found to evidently accumulate at the centre of the granular bed, as displayed in the pictures of Figure 3.9. The accumulation of the non-spherical particles is shown also by plotting the coordinates of the centre of mass of the spherical particles. The elongated particles were not exactly identifiable and so the coordinates of the centre of mass were not defined for each particle and could not be plotted; however, it was possible for the spherical particles, as reported in Figure 3.10.

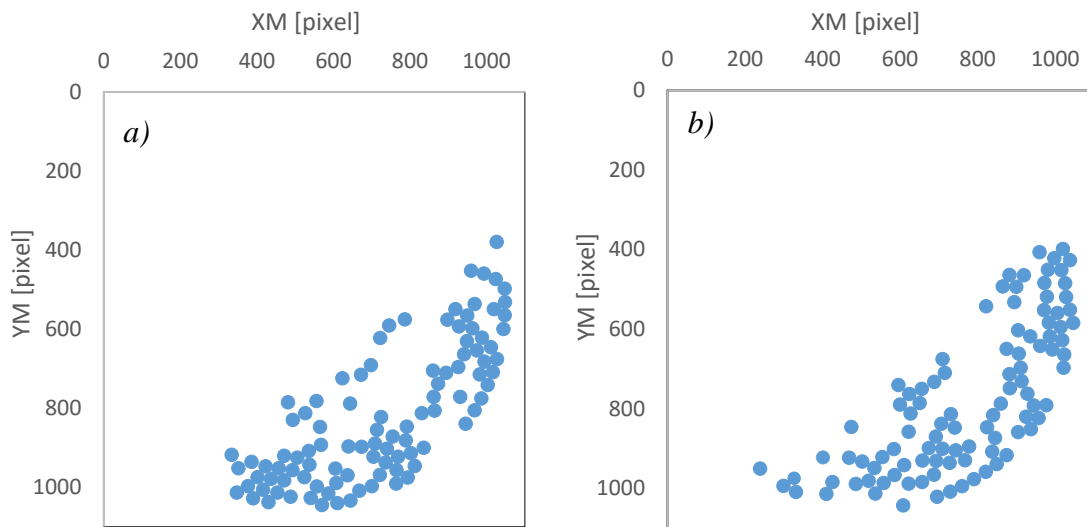


Figure 3.10. Coordinates of the centre of mass for the spherical particles at a) $t=10$ min; b) $t=30$ min (test 1).

The blank space between the plotted centres of mass of the spheres is the space occupied by the ellipsoids and by the voids between the particles. The more elongated particles clearly accumulate at the centre of the granular bed.

The radial distance of the particles was plotted in time and it is shown in Figure 3.11.

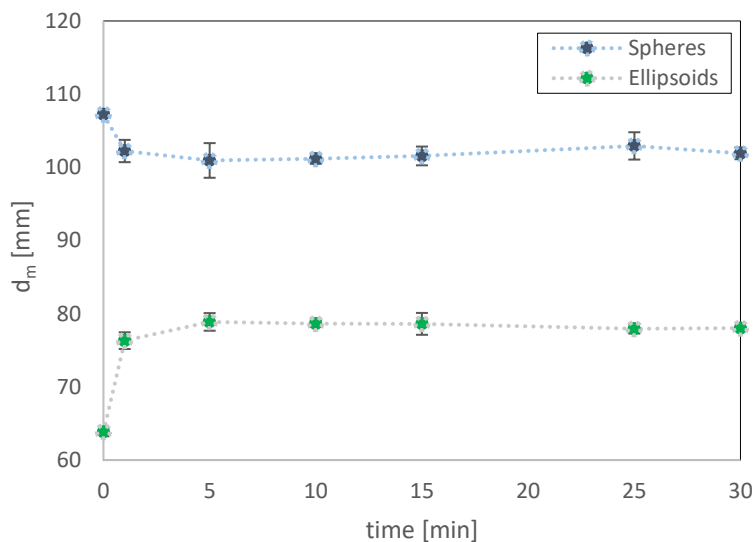


Figure 3.11. Trend of the radial distance vs. time for the E/S configuration for the mixture of spheres and ellipsoids with $AR=3.5$; the graph was obtained by averaging the values of distance of the three tests ($\omega=4.22$ rpm; filling level= 25%; the initial configuration was the E/S one).

Also in this case, the radial distance stabilizes to a steady value and so the system reaches a stable configuration. Moreover, the radial distance of the spheres and of the ellipsoids

settles to different values, meaning that particles does not mix completely and some level of segregation occurs.

The accumulation of the elongated particles at the centre of the granular bed is shown also by the trend of the distance of the two types of particles from the barycentre of the granular bed.

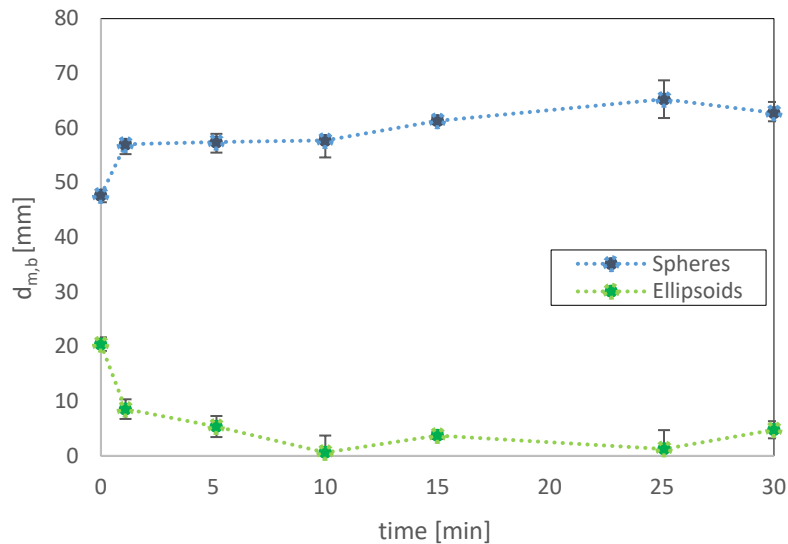


Figure 3.12. Distance from the barycentre of the bed vs. time for the spheres and the ellipsoids with AR 3.5 ($\omega=4.22$ rpm; $\varphi=25\%$; the initial configuration was the E/S one),

The distance of the ellipsoids from the barycentre of the bed settles to very low values, indicating that the non-spherical particles are on average at the centre of the granular bed. The normalized distribution of the radial distance could be obtained only for the spherical particles, since the elongated ones were not individually identifiable.

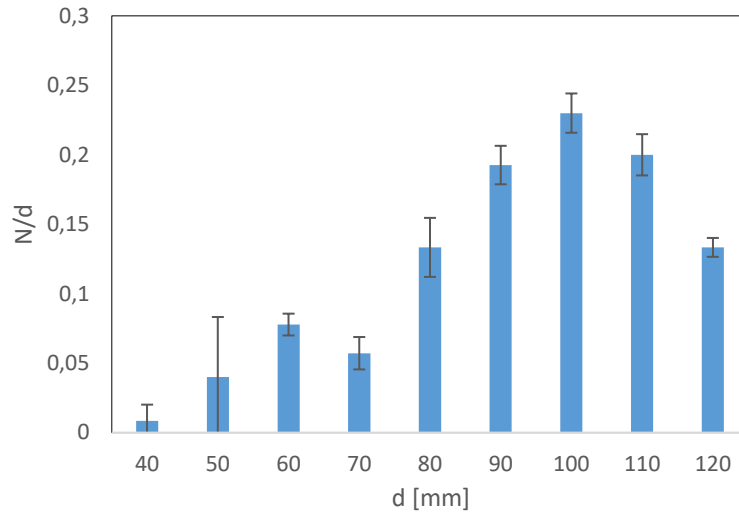


Figure 3.13. Distribution of the radial distance of the spheres, obtained as the average of the distributions of the three tests. The histogram refers to the values of radial distance obtained at $t=30$ min ($\omega=4.22$ rpm; filling level= 25%; the initial configuration was the E/S one).

The distribution shows that the number of spheres at distance lower than 80 mm is very low, since in this region of the granular bed the ellipsoids accumulate. The spheres are, instead, present in higher number at larger distances.

To evaluate how fast the system is in reaching the steady configuration, the drum was rotated for two minutes and the radial distance was plotted in time.

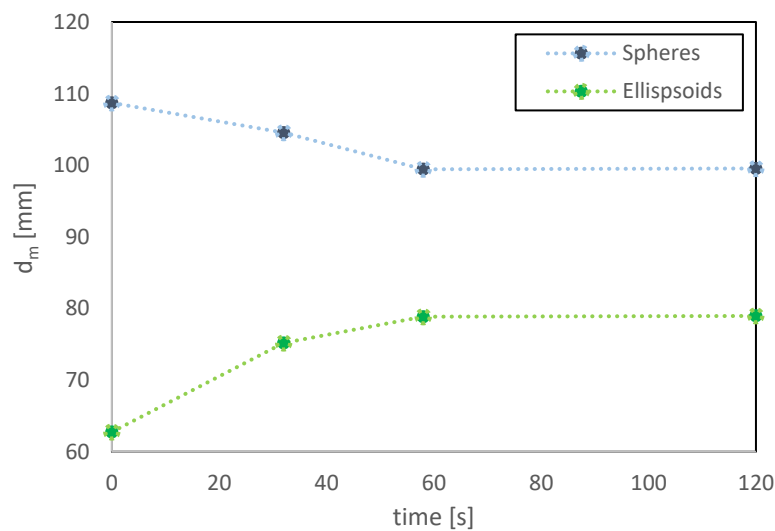


Figure 3.14. Trend of the radial distance vs. time for the 2 minutes test performed with the mixture of spheres and ellipsoids with $AR=3.5$ ($\omega=4.22$ rpm; filling level= 25%).

After one minute, the radial distance reaches its steady value; so, the transition to the final configuration occurs quite fast. It has to be noted, however, that the transition is slower than the mixtures of spheres and ellipsoids with aspect ratio equal to 1.5. It takes more time for the binary mixture of spheres and more elongated particles to reach the steady configuration.

Figure 3.15 shows some pictures of the drum, starting with S/E initial configuration.

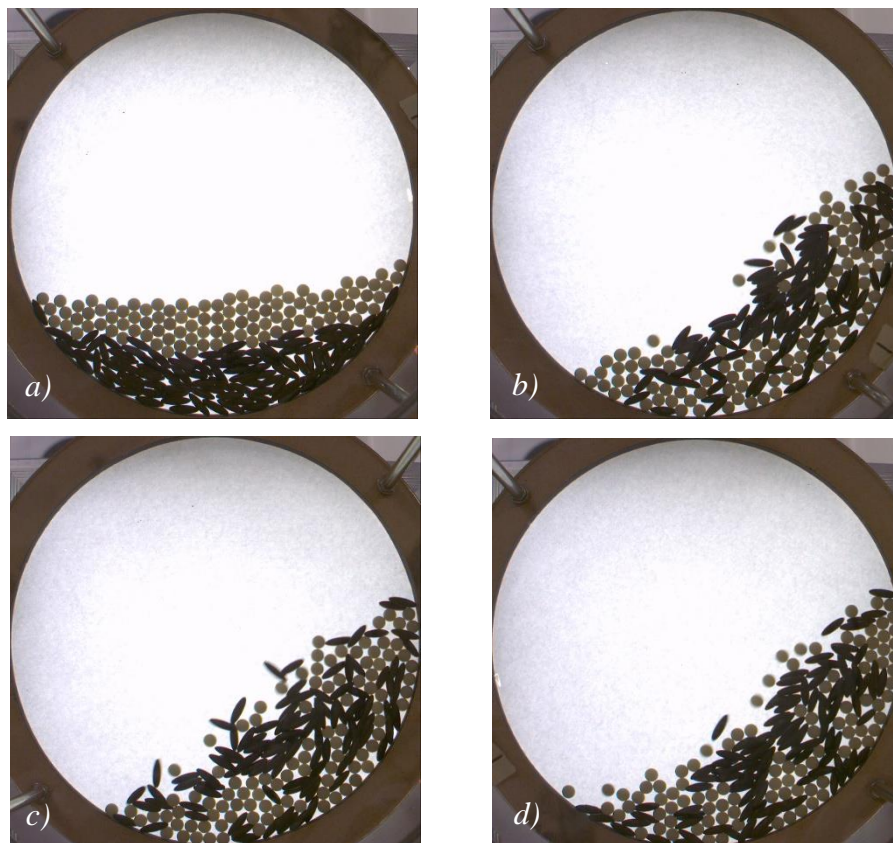


Figure 3.15. Drum at a) $t=0$; b) $t=5$ min; c) $t=20$ min; d) $t=30$ min ($\omega=4.22$ rpm; $\phi=25\%$; the initial configuration was the S/E one).

Also with a different initial configuration the more elongated particles accumulate at the centre of the granular bed and at lower distance from the centre of the drum.

The trend of the radial distance for the inverted configuration is reported in Figure 3.16.

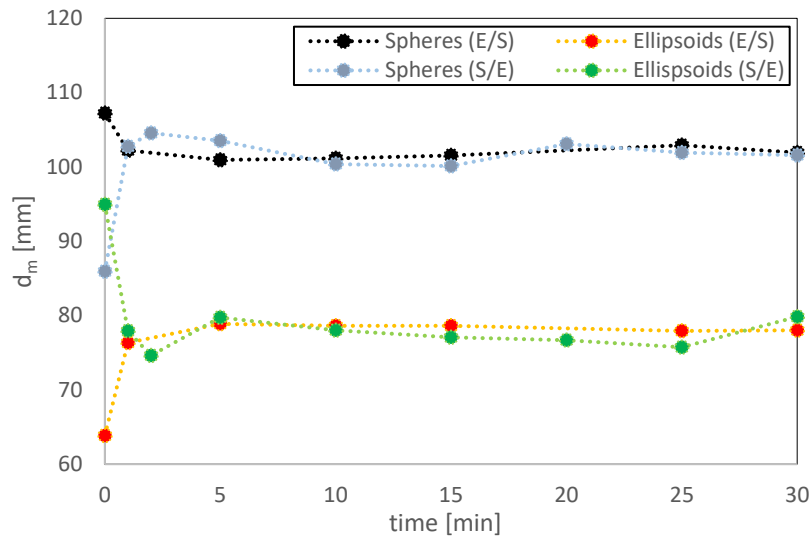


Figure 3.16. Trend of the radial distance vs time for the two initial configurations. ($\omega=4.22$ rpm; $\varphi=25\%$)

Also for the binary mixture of spheres and more elongated ellipsoids it is found that the initial configuration of the particles does not affect the final state of the system, since the radial distance of the two types of particles settle to the same values, as shown in Figure 3.16. At the final time, the distribution of the distance of the spherical particles was obtained, showing that they are mainly found close to the drum wall.

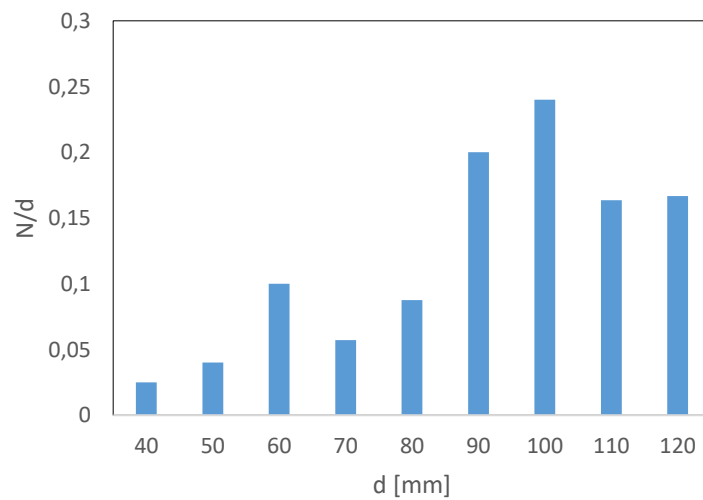


Figure 3.17. Distribution of the radial distance of the spheres. The histogram refers to the values of radial distance obtained at $t=30$ min ($\omega=4.22$ rpm; $\varphi=25\%$; the initial configuration was the S/E one).

3.1.3 Spheres and ellipsoids $AR=1.5$, $\omega=4.22$ rpm, $\phi=47\%$

In order to evaluate the effect of the filling level of the drum, four tests were performed at the same conditions of speed but with higher filling level. The tests conditions are reported in Table 3.3.

Table 3.3. Conditions of the tests with spheres and ellipsoids with $AR=1.5$ at higher filling level.

$AR 1$ [-]	$AR 2$ [-]	ω [rpm]	ϕ [-]	initial configuration	time [min]	repetitions
1	1.5	4.22	47%	E/S	30	3
1	1.5	4.22	47%	S/E	30	1

Figure 3.18 shows some images of the drum, at higher filling level; three tests were performed with the E/S initial configuration.

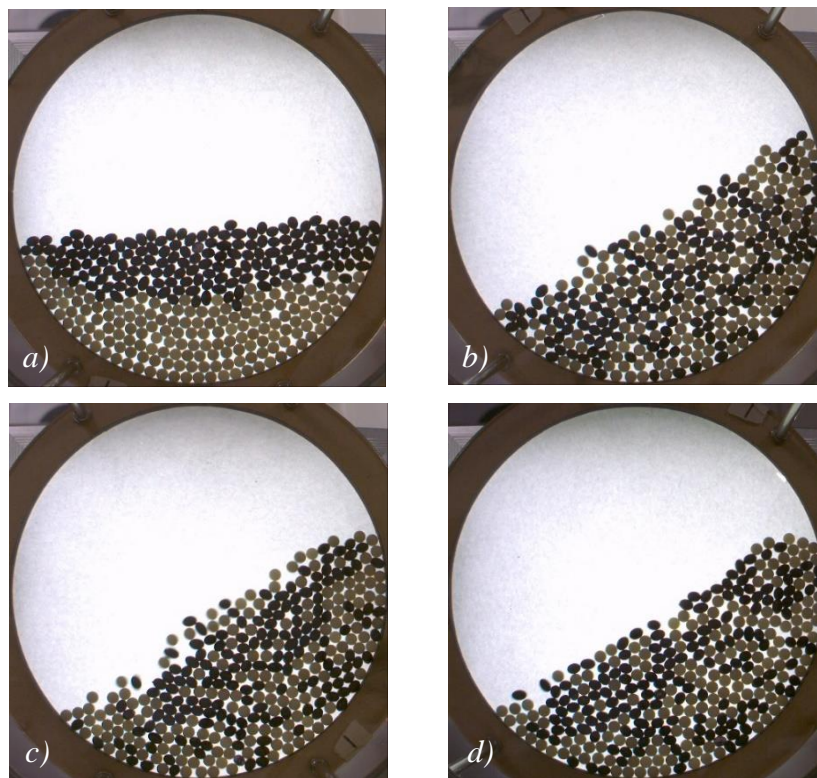


Figure 3.18. Drum at a) $t=0$; b) $t=5$ min; c) $t=15$ min; d) $t=30$ min, ($\omega=4.22$ rpm; $\phi=25\%$; the initial configuration was the E/S one).

The radial distance versus time is displayed in Figure 3.19.

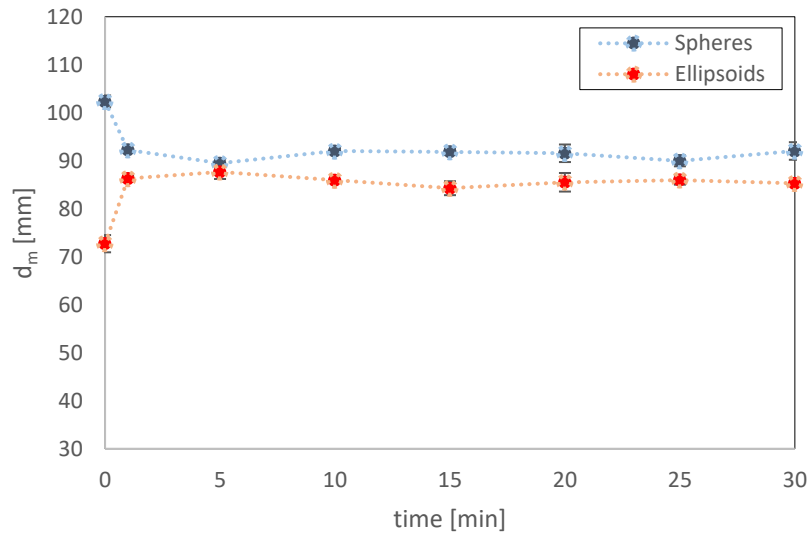


Figure 3.19. Trend of the radial distance vs. time for the E/S configuration for the mixture of spheres and ellipsoids with $AR=1.5$; the graph was obtained by averaging the values of distance of the three tests ($\omega=4.22$ rpm; $\varphi=47\%$; the initial configuration was the E/S one).

The trend of the radial distance of the two types of particles is the same of the one found at lower filling level, but moved to lower values, since the filling level is higher.

The distribution of the spheres and of the ellipsoids at higher filling level is reported in Figure 3.20.

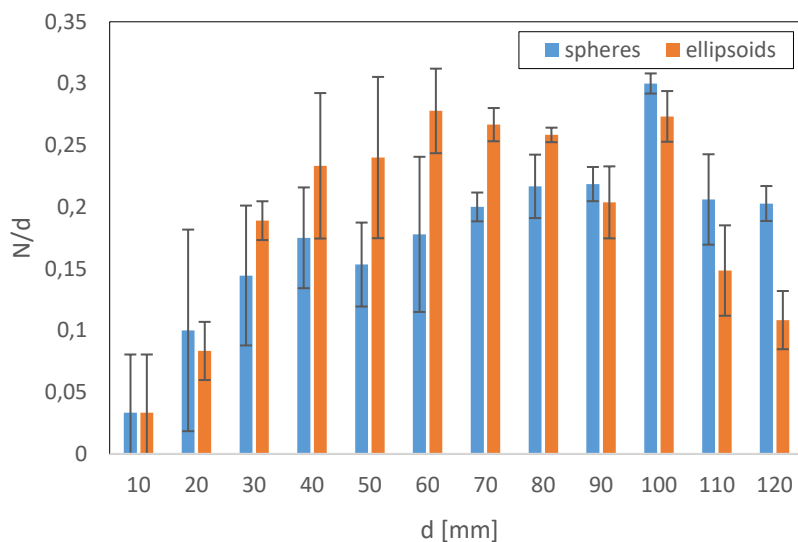


Figure 3.20. Distribution of the radial distance of the two types of particles, obtained as the average of the distributions of the three tests. The histogram refers to the values of radial distance obtained at $t=30$ min ($\omega=4.22$ rpm; $\varphi=47\%$; the initial configuration was the E/S one).

At intermediate distances, a higher number of ellipsoids is found, while close to the wall the number of spheres is larger than the number of ellipsoids.

The number composition of the spheres is reported in Figure 3.21.

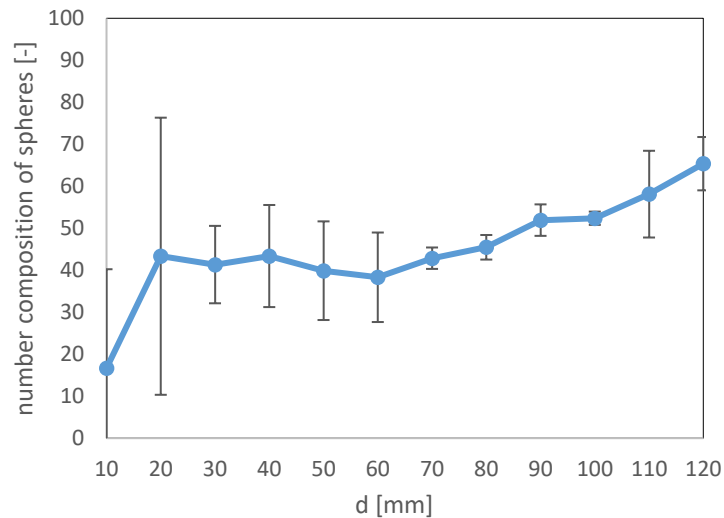


Figure 3.21. Trend of the number composition of the spheres versus the radial distance, obtained as the average of the composition curve of the three tests ($\omega=4.22$ rpm; $\phi=47\%$; the initial configuration was the E/S one).

The composition of spheres is lower than the 50% for radial distance lower than 60 mm, meaning that at intermediate distances the number of ellipsoids is higher than the number of spherical particles. At distances larger than 90 mm, instead, the composition of spheres increases, indicating that the spherical particles tend mainly to settle close to the drum wall and so the mixture does not mix uniformly.

Also at higher filling level, the effect of the initial configuration of the particles was investigated, running one test with the S/E initial configuration. The binary mixture is displayed in Figure 3.22 at different time instants.

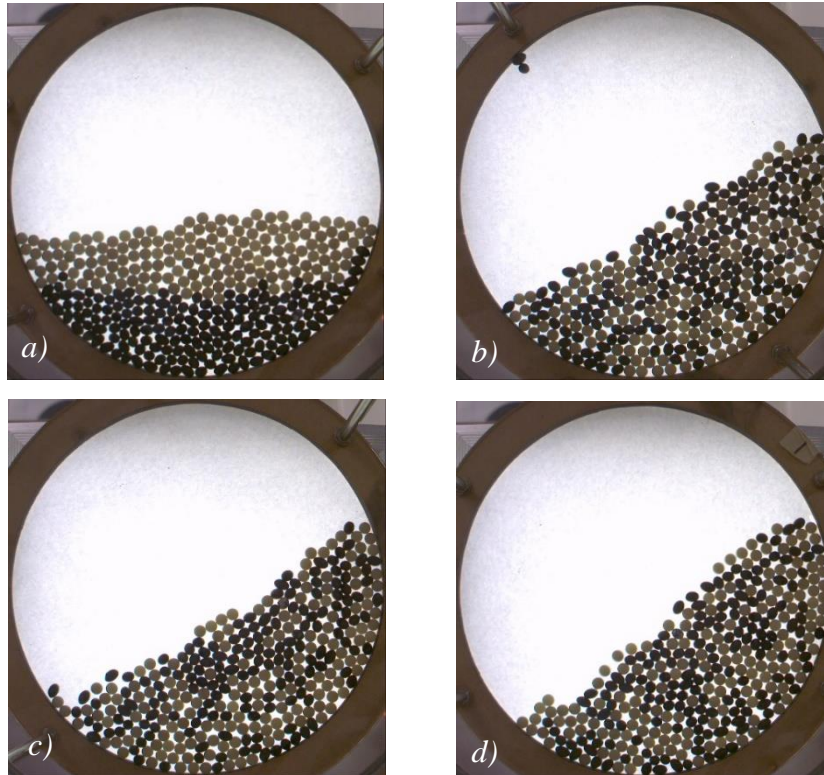


Figure 3.22. Drum at a) $t=0$; b) $t=5$ min; c) $t=15$ min; d) $t=30$ min (test 1). ($\omega=4.22$ rpm; $\phi=47\%$; the initial configuration was the S/E one).

The distribution of the radial distance, obtained at the final time is illustrated in Figure 3.23.

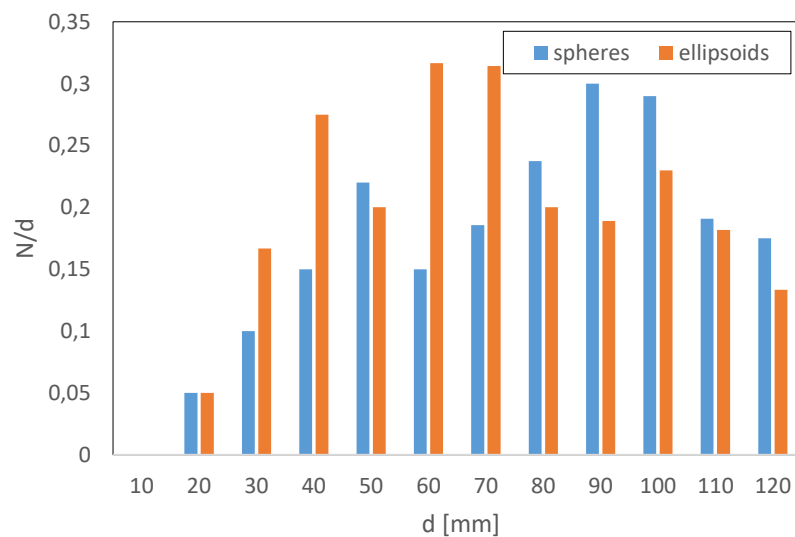


Figure 3.23. Distribution of the radial distance of the two types of particles; the initial configuration of the particles was the S/E one. The histogram refers to the values of radial distance obtained at $t=30$ min ($\omega=4.22$ rpm; $\phi=47\%$; the initial configuration was the S/E one).

The distribution shows again that the ellipsoids are mainly found at the centre of the granular bed, while the spheres are mainly at higher distances.

The comparison of the two trends of the radial distance, depending on the initial configuration is shown in Figure 3.24.

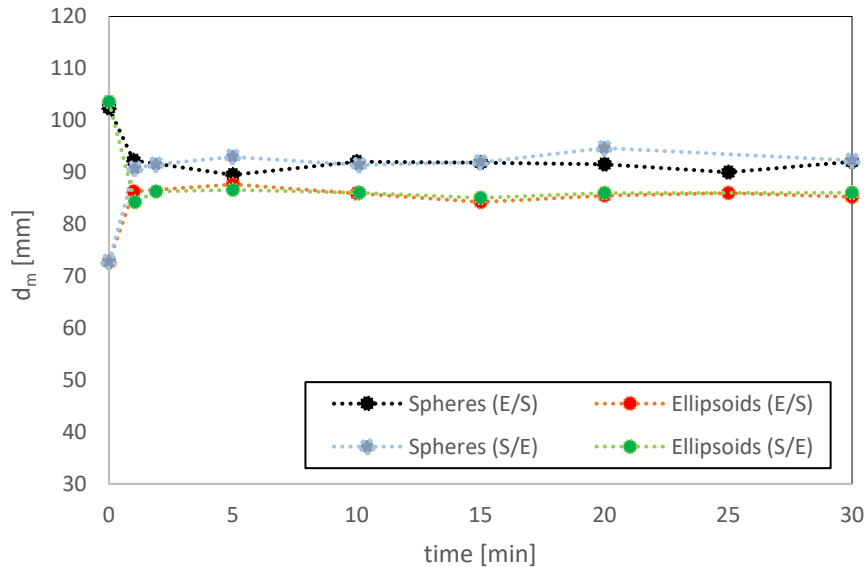


Figure 3.24. Trend of the radial distance vs time for the two initial configurations.

From Figure 3.24 it can be concluded that that the initial configuration does not affect the system, neither at higher filling level of the drum.

3.1.4 Spheres and ellipsoids $AR=3.5$, $\omega=4.22$ rpm, $\phi=47\%$

At higher filling level of the drum, also the binary mixture of spheres and ellipsoids with aspect ratio equal to 3.5 was considered, as reported in Table 3.4.

Table 3.4. Conditions of the tests with spheres and ellipsoids with $AR=3.5$ at higher filling level.

$AR 1$ [-]	$AR 2$ [-]	ω [rpm]	ϕ [-]	initial configuration	time [min]	repetitions
1	3.5	4.22	47%	E/S	30	3
1	3.5	4.22	47%	S/E	30	1

The rotating drum at different time instants is shown in Figure 3.25.

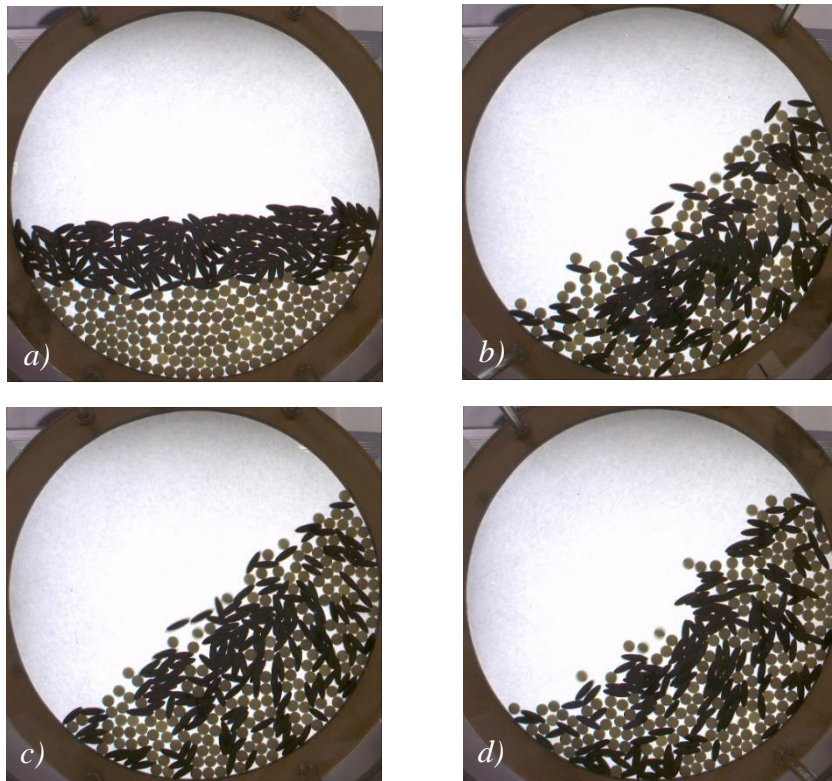


Figure 3.25. Drum at a) $t=0$; b) $t=5$ min; c) $t=20$ min; d) $t=30$ min (test 2). ($\omega=4.22$ rpm; $\phi=47\%$; the initial configuration was the S/E one).

As for lower filling level, an accumulation of the more elongated particles at the centre of the solid bed is clearly observed; it is displayed also by plotting the coordinates of the centre of mass of the spherical particles:

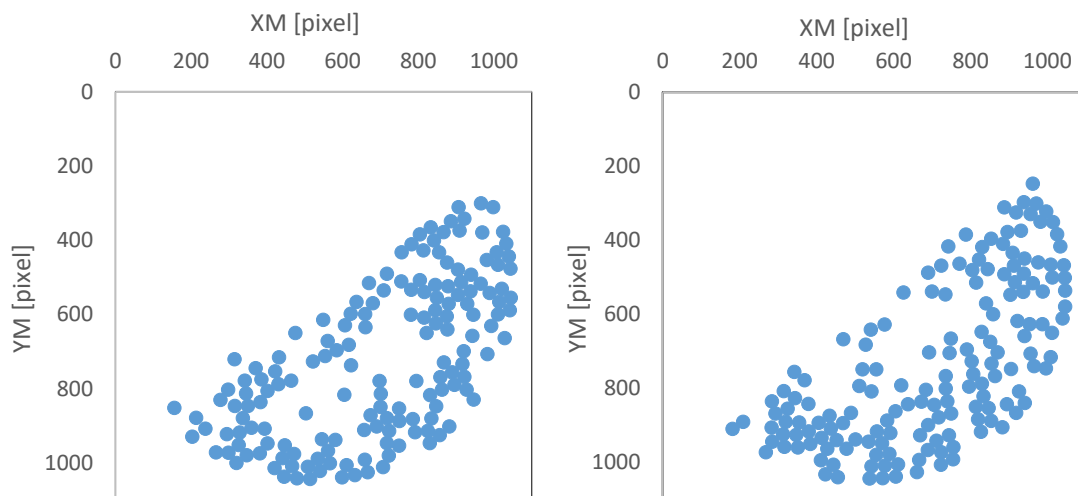


Figure 3.26. Coordinates of the centre of mass for the spherical particles at a) $t=5$ min; b) $t=20$ min (test 2).

The trend of the radial distance versus time was found to be equal to the trend at lower filling level, but shifted at lower values.

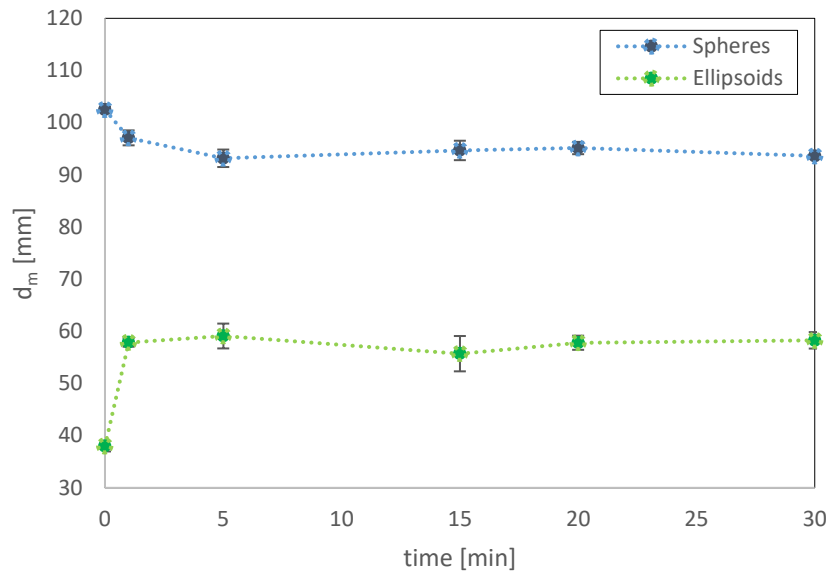


Figure 3.27. Trend of the radial distance vs. time for the mixture of spheres and ellipsoids with $AR=3.5$; ($\omega=4.22$ rpm; $\varphi=47\%$; the initial configuration was the E/S one); the graph was obtained by averaging the values of distance of the three tests.

Moreover, the distance of the spheres and the ellipsoids from the barycentre of the bed shows that the more elongated particles settle at the centre of the granular bed.

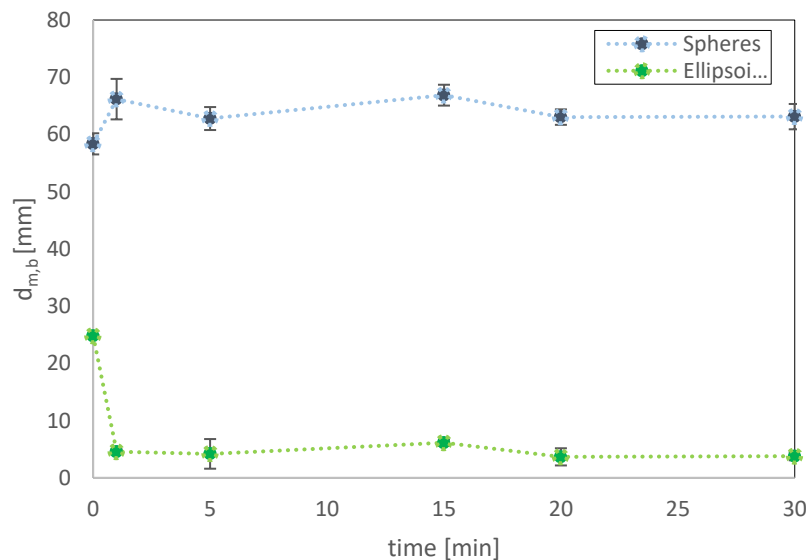


Figure 3.28. Distance from the barycentre of the bed vs. time for the spheres and the ellipsoids with $AR 3.5$ ($\omega=4.22$ rpm; $\varphi=47\%$; the initial configuration was the E/S one),

As it is shown, in fact, the distance of the more elongated particles from the barycentre of the grains is very low, indicating their tendency to settle at the centre.

The same is shown by the distribution of the distance of the spheres.

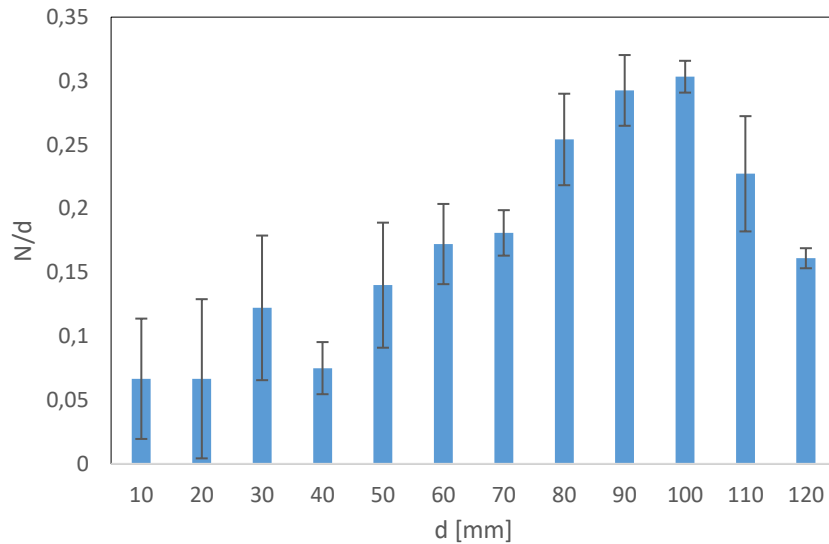


Figure 3.29. Distribution of the radial distance of the spheres, obtained as the average of the distributions of the three tests. The histogram refers to the values of radial distance obtained at $t=30$ min ($\omega=4.22$ rpm; $\varphi=47\%$; the initial configuration was the E/S one).

At distance from the centre of the drum lower than 70 mm, the number of spherical particles is very low, since there is an accumulation of the other type of particles. So, the behaviour of the binary mixture of spheres and elongated particles is found to be the same at the two different filling levels.

Also, the inverted configuration S/E was considered (Figure 3.30).

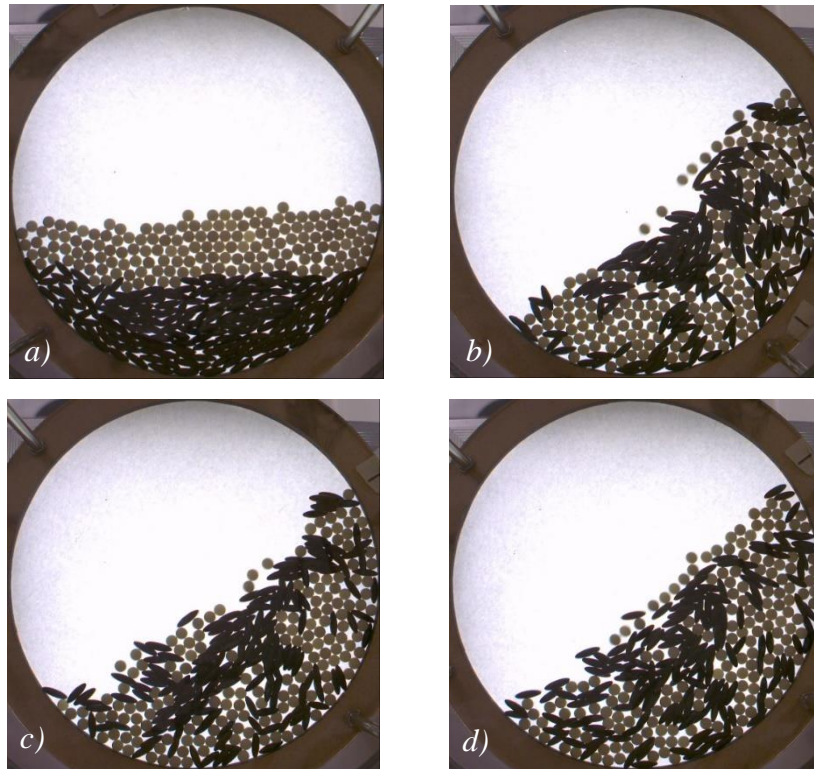


Figure 3.30. Drum at a) $t=0$; b) $t=5$ min; c) $t=20$ min; d) $t=30$ min. ($\omega=4.22$ rpm; $\phi=47\%$; the initial configuration was the S/E one).

The trend of the radial distance is illustrated in Figure 3.31, compared with the one obtained for the S/E initial configuration.

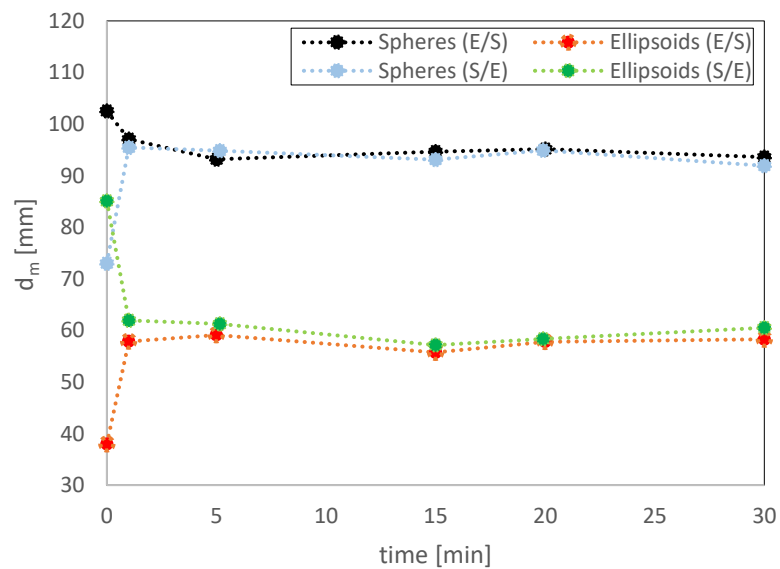


Figure 3.31. Trend of the radial distance vs time for the two initial configurations ($\omega=4.22$ rpm; $\phi=47\%$).

The graph of Figure 3.31 shows that the initial configuration again does not affect the final state of the system. Also in this case, in fact, the more elongated particles accumulate at lower distance from the centre of the drum; this is shown by the distribution of the spherical particles, too (Figure 3.32)

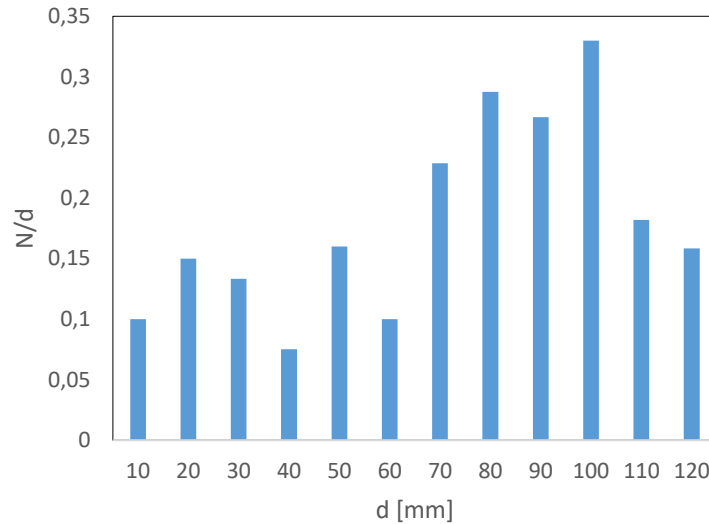


Figure 3.32. Distribution of the radial distance of spheres, with the S/E initial configuration. The histogram refers to the values of radial distance obtained at $t=30$ min.

3.1.5 Mixtures of ellipsoids (AR=1.5 and AR=3.5)

Also, binary mixtures made of the two types of ellipsoids (AR=1.5 and AR=3.5) were taken into account at the same filling levels of the previous experimental tests and at the lower rotational speed.

The experimental conditions are reported in Table 3.5.

Table 3.5. Conditions of the tests with ellipsoids with AR=1.5 and AR=3.5.

AR 1 [-]	AR 2 [-]	ω [rpm]	ϕ [-]	initial configuration	time [min]	repetitions
1.5	3.5	4.22	25%	E ₂ /E ₁	30	3
1.5	3.5	4.22	25%	E ₁ /E ₂	30	1
1.5	3.5	4.22	25%	E ₂ /E ₁	2	1
1.5	3.5	4.22	47%	E ₂ /E ₁	30	3
1.5	3.5	4.22	47%	E ₁ /E ₂	30	1

Some pictures of the mixture in the drum at lower filling level are shown in Figure 3.33.

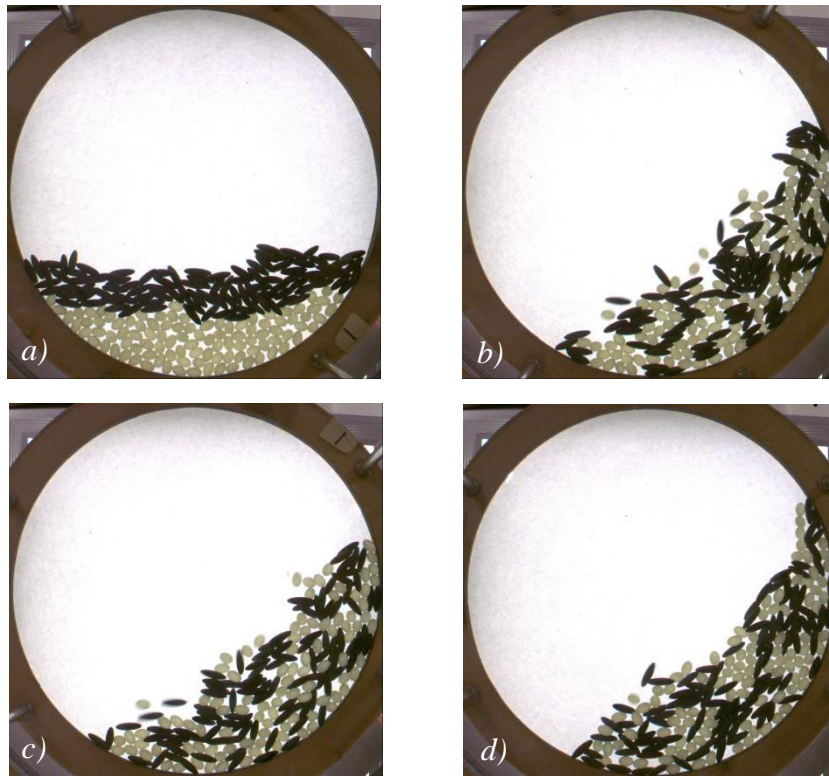


Figure 3.33. Drum at a) $t=0$; b) $t=10\text{min}$; c) $t=25\text{ min}$; d) $t=30\text{ min}$ (test 3), ($\omega=4.22\text{ rpm}$; $\varphi=25\%$; the initial configuration was the E2/E1 one).

The trend of the radial distance of the two types of particles versus time is displayed in Figure 3.34.

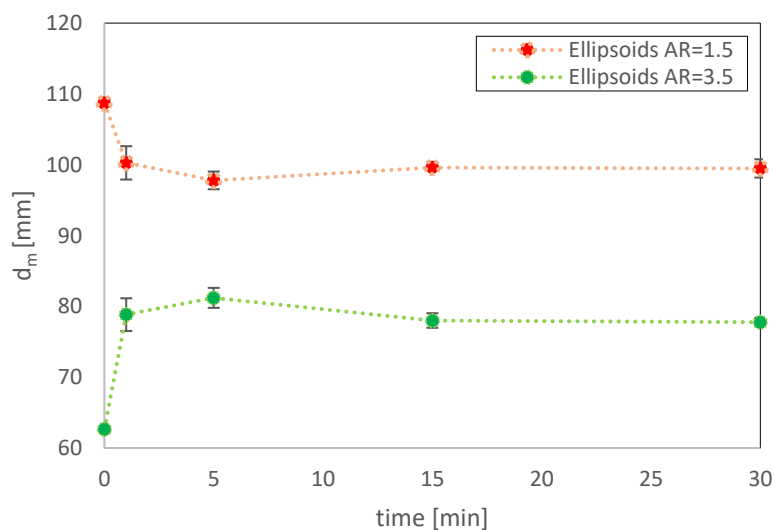


Figure 3.34. Trend of the radial distance vs. time for the mixture of ellipsoids ($AR=1.5$ and $AR=3.5$); the graph was obtained by averaging the values of distance of the three tests ($\omega=4.22\text{ rpm}$; $\varphi=47\%$; the initial configuration was the E2/E1 one).

As in the previous cases, the binary mixture reaches a steady state and settles to a stable condition.

It has to be considered that, also in this case, the more elongated particles were not individually identifiable and so the distance distribution was defined only for the ellipsoids with $AR=1.5$; it is shown in Figure 3.35.

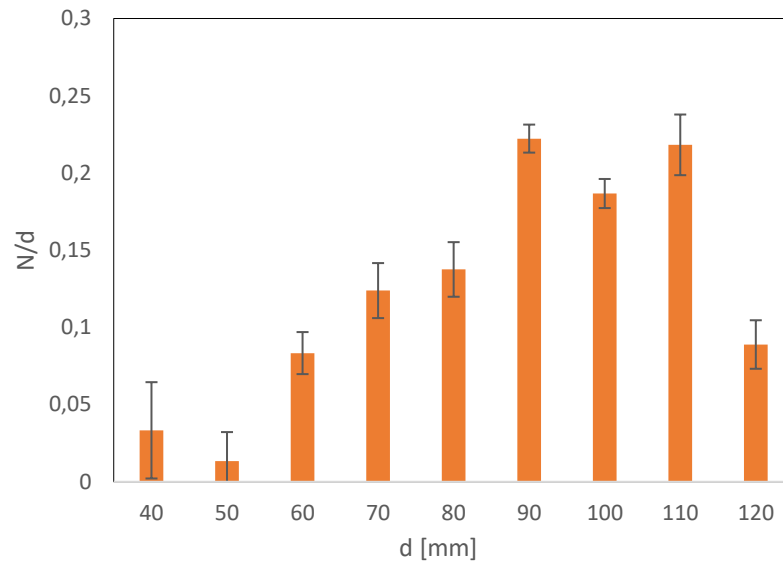


Figure 3.35. Distribution of the radial distance of the ellipsoids with $AR=1.5$, obtained as the average of the distributions of the three tests. The histogram refers to the values of radial distance obtained at $t=30$ min ($\omega=4.22$ rpm; $\varphi=25\%$; the initial configuration was the E2/E1 one).

The ellipsoids with $AR=1.5$ behave like the spheres in the previously considered mixtures. At lower distance, the more elongated particles are present in higher number, while the particles with lower aspect ratio are distributed in higher number close to the walls. So, also the two types of ellipsoids do not mix homogeneously and some level of segregation is observed.

The inverted configuration was also considered; some images are reported in Figure 3.36.

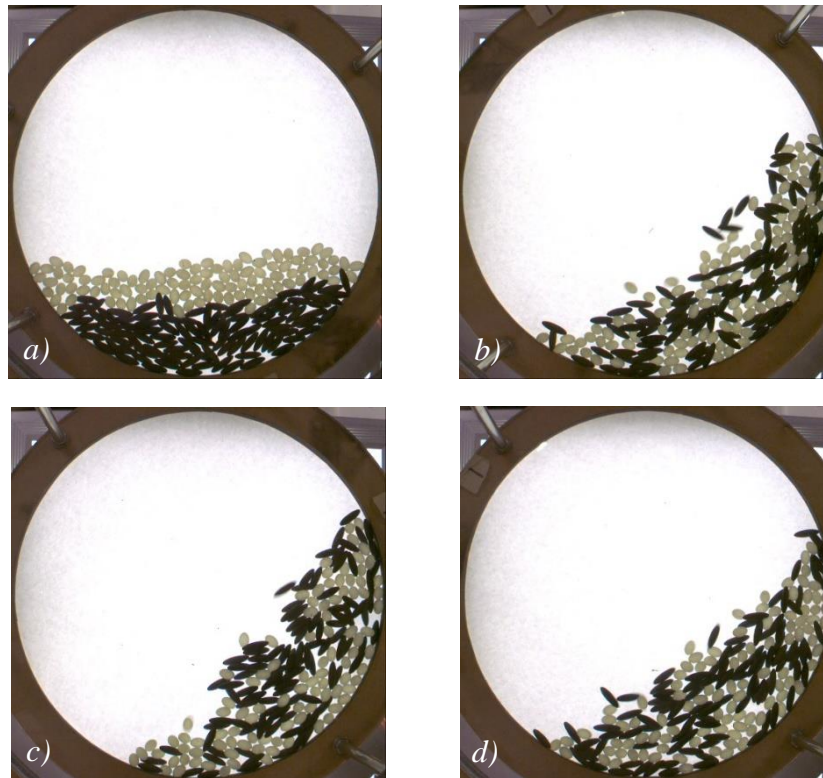


Figure 3.36. Drum at a) $t=0$; b) $t=5$ min; c) $t=15$ min; d) $t=30$ min, ($\omega=4.22$ rpm; $\phi=25\%$; the initial configuration was the E1/E2 one).

The trend of the mean distance of the two types of particles shows that also with the two different initial configurations the same steady state is reached and so the initial configuration of the particles does not affect the final condition of the system.

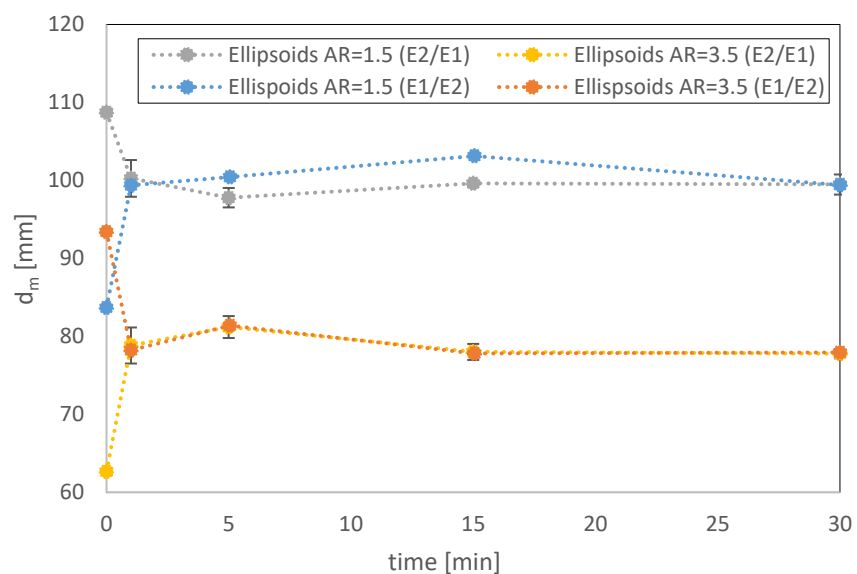


Figure 3.37. Trend of the radial distance vs time for the two initial configurations ($\omega=4.22$ rpm; $\phi=25\%$).

The distribution of the distance of the less elongated ellipsoids (Figure 3.38) shows that a uniform mixing of the particles does not occur, since the ellipsoids with $AR=1.5$ are present in higher number at larger distances; at distance lower than 70 mm a high number of more elongated particles is found. The ellipsoids with $AR=1.5$, instead, are found in higher number at $d=80$ mm and for distances between 100 and 110 mm.

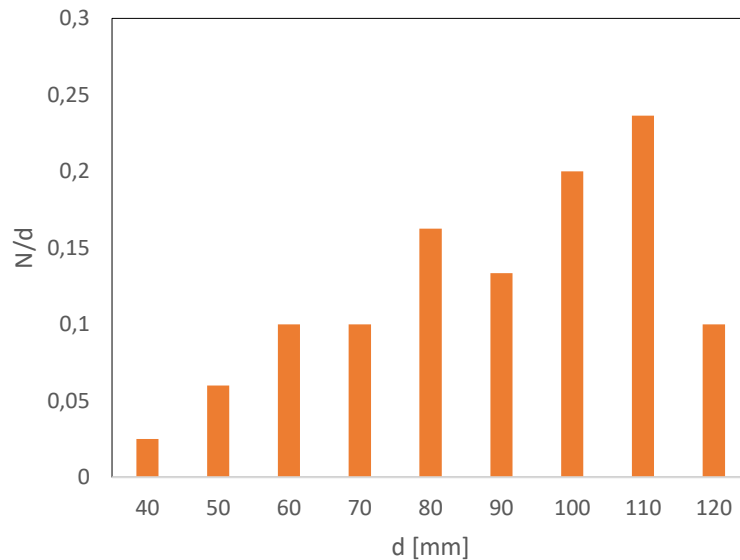


Figure 3.38. Distribution of the radial distance ellipsoids with $AR=1.5$. The histogram refers to the values of radial distance obtained at $t=30$ min ($\omega=4.22$ rpm; $\phi=25\%$; the initial configuration was the E1/E2 one).

Moreover, from Figures 3.34 and 3.37 it can be seen that after one minute the system already reaches the final stable state. So, the transition to the final configuration occurs fast as it is, in fact, reported in Figure 3.39.

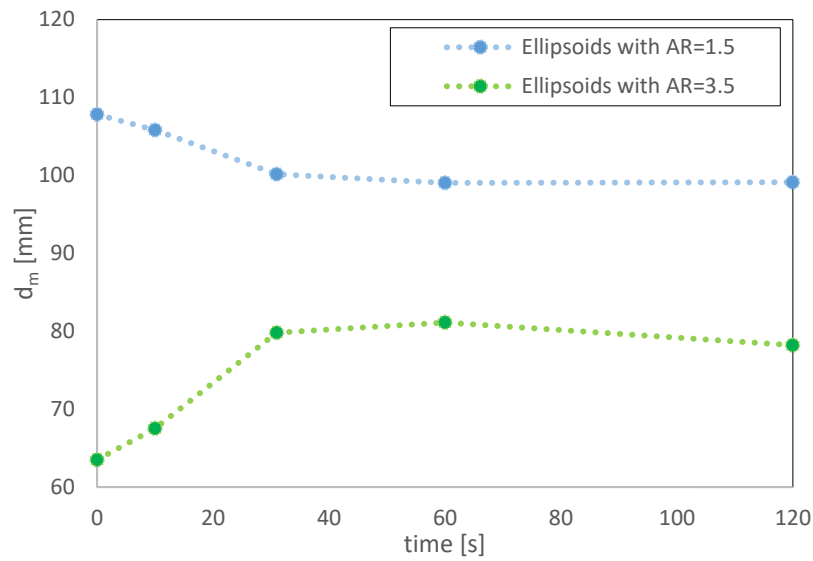


Figure 3.39. Trend of the radial distance vs. time for the 2 minutes test ($\omega=4.22$ rpm; $\phi=25\%$).

After 30 seconds, the radial distance settles to the steady value; the same occurred with the binary mixture made of spheres and ellipsoids with AR=1.5.

The mixture at higher filling level is shown in Figure 3.40.

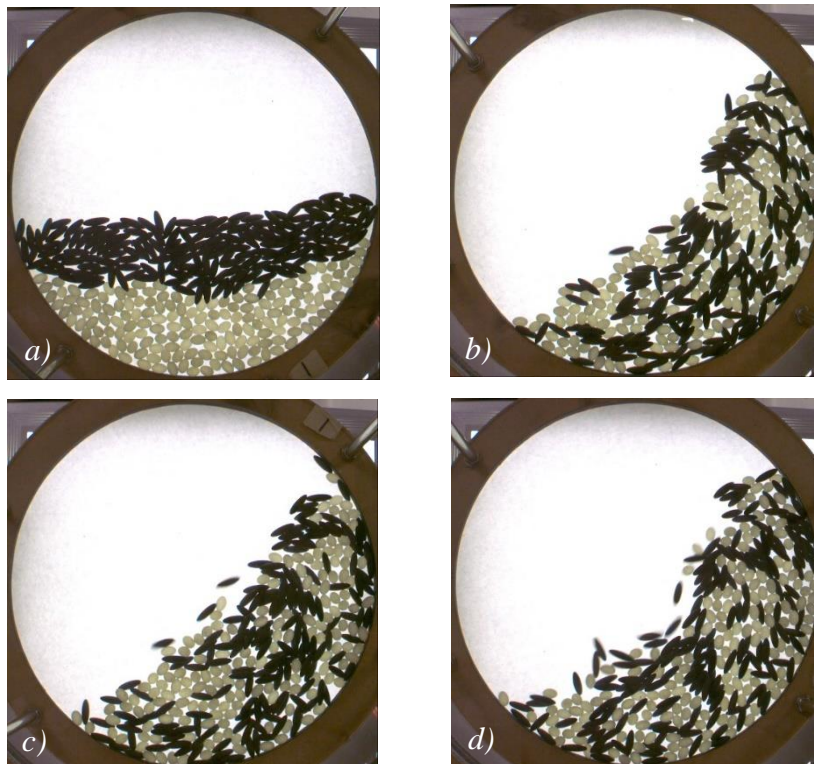


Figure 3.40. Drum at a) $t=0$; b) $t=5$ min; c) $t=15$ min; d) $t=30$ min, (test 2) ($\omega=4.22$ rpm; $\phi=47\%$; the initial configuration was the E2/E1 one).

The radial distance plotted versus time (Figure 3.41) shows again that a stable state is reached in time.

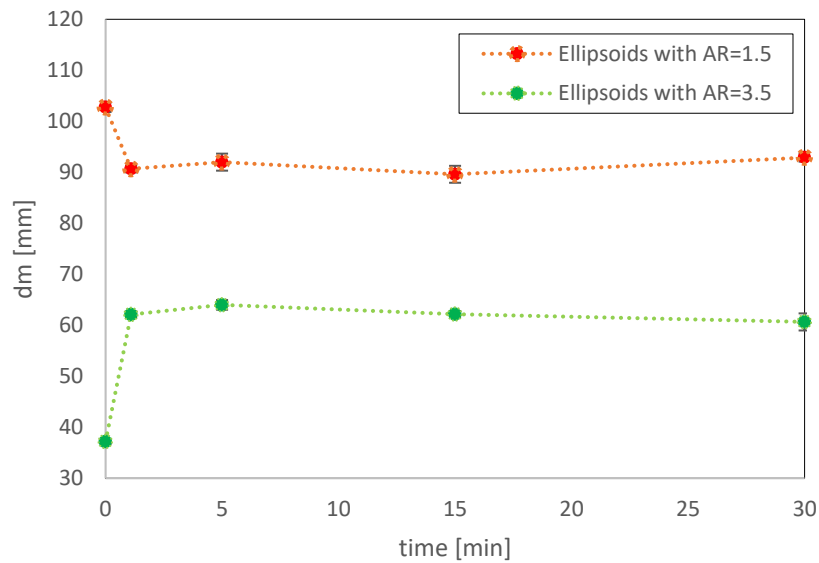


Figure 3.41. Trend of the radial distance vs. time for the mixture of ellipsoids (AR=1.5 and AR=3.5); the graph was obtained by averaging the values of distance of the three tests ($\omega=4.22$ rpm, $\phi=47\%$; the initial configuration was the E2/E1 one).

The distribution of the ellipsoids with AR=1.5 in Figure 3.42 shows that the less elongated particles are mainly distributed at higher distances, so closer to the drum wall.

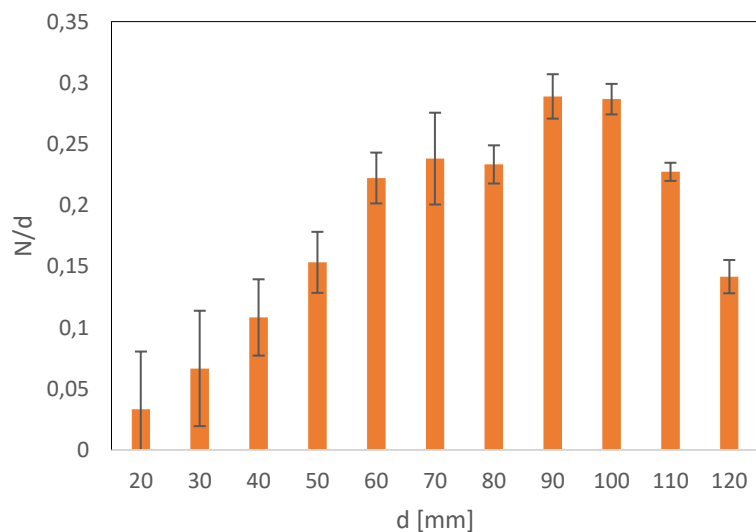


Figure 3.42. Distribution of the radial distance of the ellipsoids with AR=1.5, obtained as the average of the distributions of the three tests. The histogram refers to the values of radial distance obtained at $t=30$ min ($\omega=4.22$ rpm; $\phi=47\%$; the initial configuration was the E2/E1 one).

The binary mixture in the drum at higher level and starting with the E1/E2 configuration is shown in Figure 3.43.

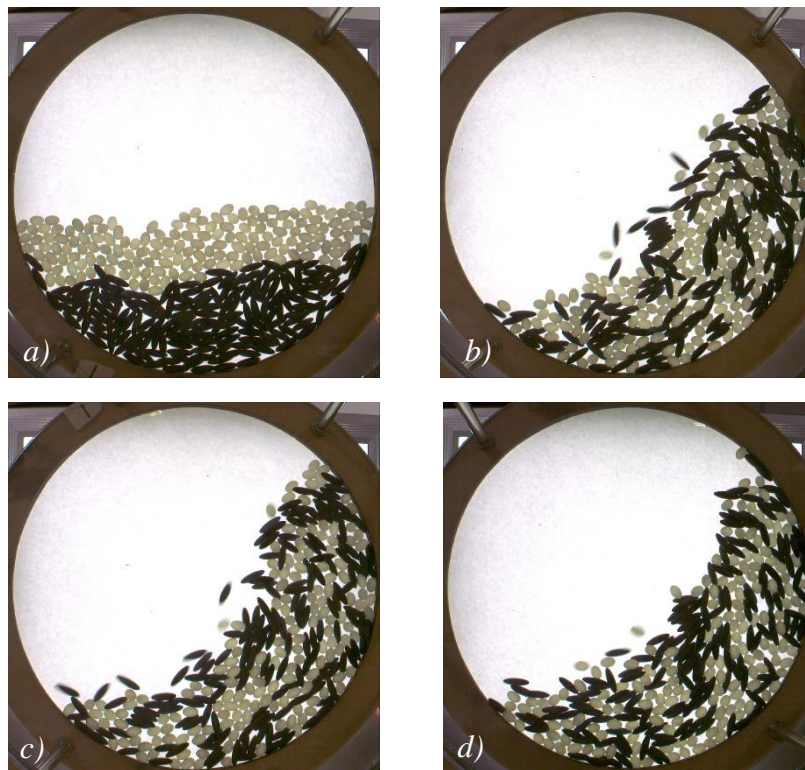


Figure 3.43. Drum at a) $t=0$; b) $t=1$ min; c) $t=15$ min; d) $t=30$ min, ($\omega=4.22$ rpm; $\phi=47\%$; the initial configuration was the E1/E2 one).

The trend of the radial distance and is reported in the following image.

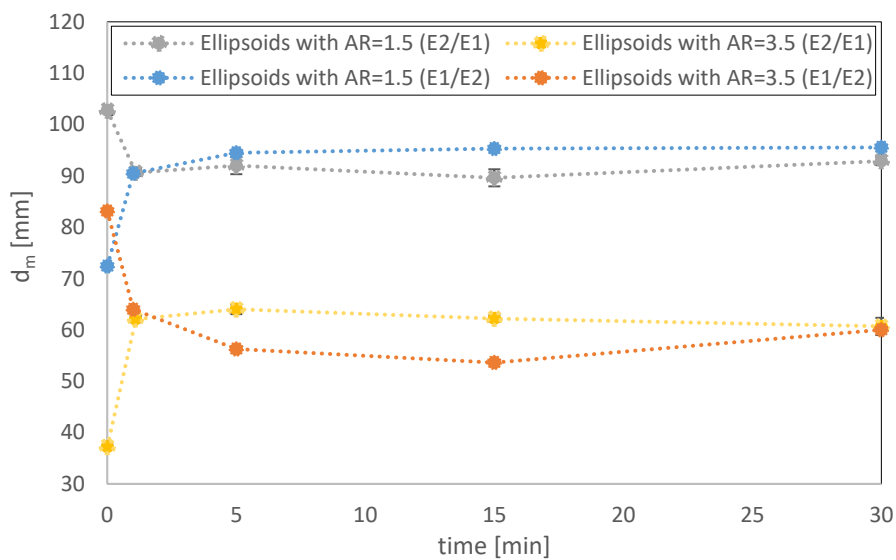


Figure 3.44. Trend of the radial distance vs time for the two initial configurations ($\omega=4.22$ rpm; $\phi=47\%$).

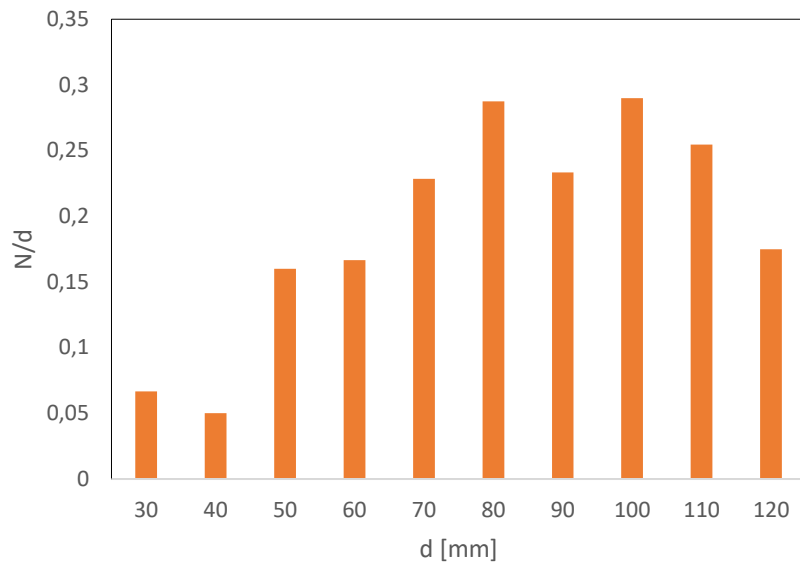


Figure 3.45. Distribution of the radial distance ellipsoids with $AR=1.5$. The histogram refers to the values of radial distance obtained at $t=30$ min ($\omega=4.22$ rpm; $\phi=25\%$; the initial configuration was the E1/E2 one).

So, also for the binary mixture of the two types of particles the filling level of the drum and the initial configuration do not affect the final configuration.

3.1.6 Spheres and ellipsoids $AR=1.5$, $\omega=11.5$ rpm

The experimental tests at higher rotational speed were run at the condition reported in Table 3.6.

Table 3.6. Conditions of the tests with spheres and ellipsoids with $AR=1.5$ at higher rotational speed.

$AR 1$ [-]	$AR 2$ [-]	ω [rpm]	ϕ [-]	initial configuration	time [min]	repetitions
1	1.5	11.51	25%	E/S	30	3
1	1.5	11.51	47%	E/S	30	3

The filling levels of the drum were the same ones considered at lower rotational speed. At lower filling level (25%) the trend of the radial distance was found to be the same of the one found at lower rotational speed, as shown in Figure 3.46.

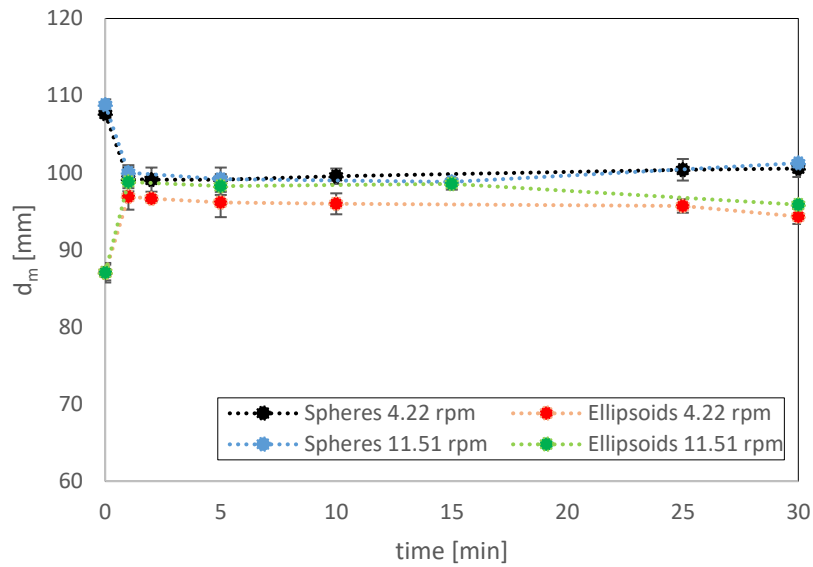


Figure 3.46. Trend of the radial distance vs time for the two rotational speeds of the drum (binary mixture of spheres and ellipsoids with $AR=1.5$, $\varphi=25\%$).

So, also when the drum rotates at higher speed, a steady condition is reached by the binary mixture.

Moreover, from the distribution of the radial distance obtained (Figure 3.47) for the two types of particles it is verified that again the particles do not mix uniformly.

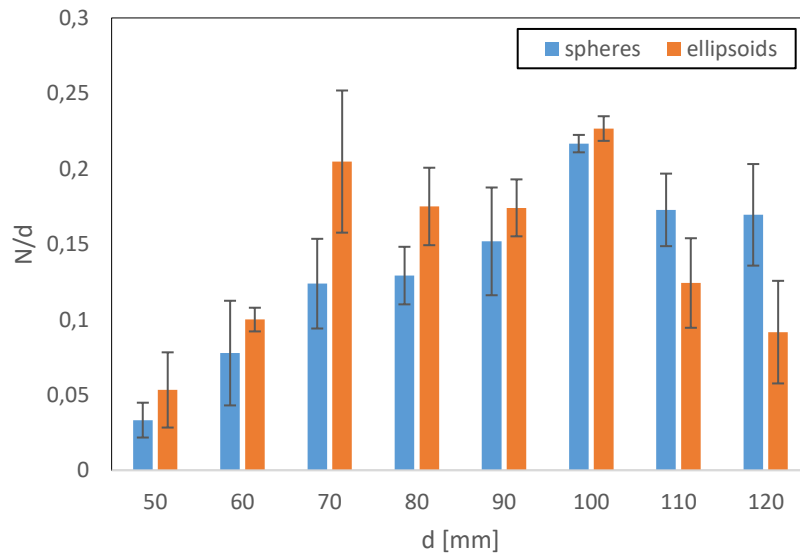


Figure 3.47. Distribution of the radial distance of the two types of particles, obtained as the average of the distributions of the three tests. The histogram refers to the values of radial distance obtained at $t=30$ min ($\omega=11.51$ rpm; $\varphi=25\%$; the initial configuration was the E/S one).

At intermediate distance, in fact, the number of ellipsoids is higher than the number of spheres, especially for distances between 70 and 100 mm; the spherical particles are higher in number very close to the wall.

Also at higher filling level (47%) the behaviour was the same observed at lower rotational speed: the radial distance settle to a steady value and the particles are found not to uniformly mixed, as displayed from the distribution of Figure 3.49.

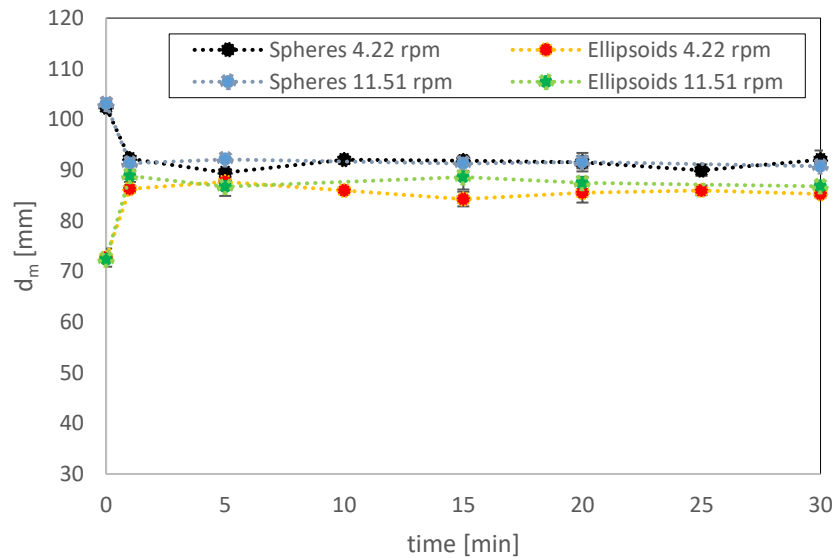


Figure 3.48. Trend of the radial distance vs time for the two rotational speeds of the drum (binary mixture of spheres and ellipsoids with $AR=1.5$, $\phi=47\%$).

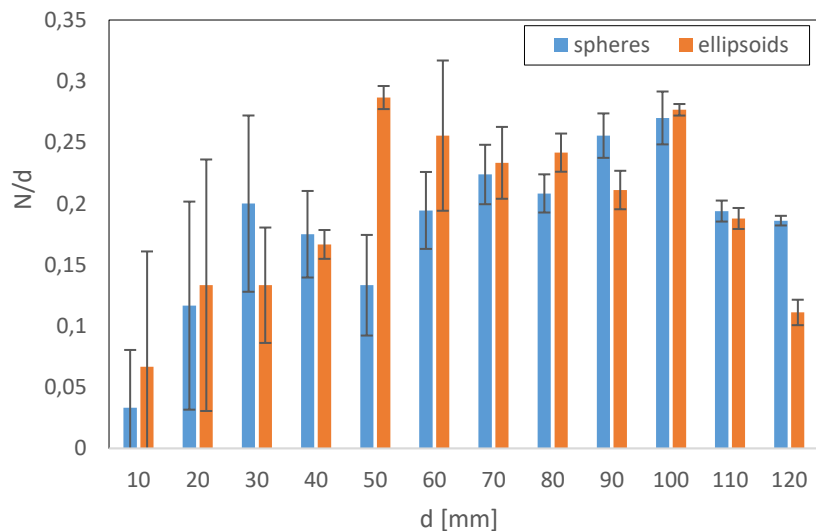


Figure 3.49. Distribution of the radial distance of the two types of particles, obtained as the average of the distributions of the three tests. The histogram refers to the values of radial distance obtained at $t=30$ min ($\omega=11.51$ rpm; $\phi=47\%$; the initial configuration was the E/S one).

The distribution shows that a high number of ellipsoids settles at intermediate distance from the centre of the drum, between 50 and 80 mm and so that the non-spherical particles are distributed, on average, at a lower distance than the spherical particles.

Since at higher rotational velocity the behaviour of the binary mixture is the same found when the drum rotates at lower speed, the drum speed seems not to be a parameter affecting the system.

3.1.7 Spheres and ellipsoids $AR=3.5$, $\omega=11.5$ rpm

The binary mixture of spheres and ellipsoids with $AR=3.5$ was tested at higher rotational speed of the drum, at the conditions specified in Table 3.7.

Table 3.7. Conditions of the tests with spheres and ellipsoids with $AR=3.5$ at higher rotational speed.

$AR 1$ [-]	$AR 2$ [-]	ω [rpm]	ϕ [-]	initial configuration	time [min]	repetitions
1	3.5	11.51	25%	E/S	30	3
1	3.5	11.51	47%	E/S	30	3

At the two rotational speeds, the same steady state is reached; so, also for this binary mixture the speed of the drum does not affect the final configuration.

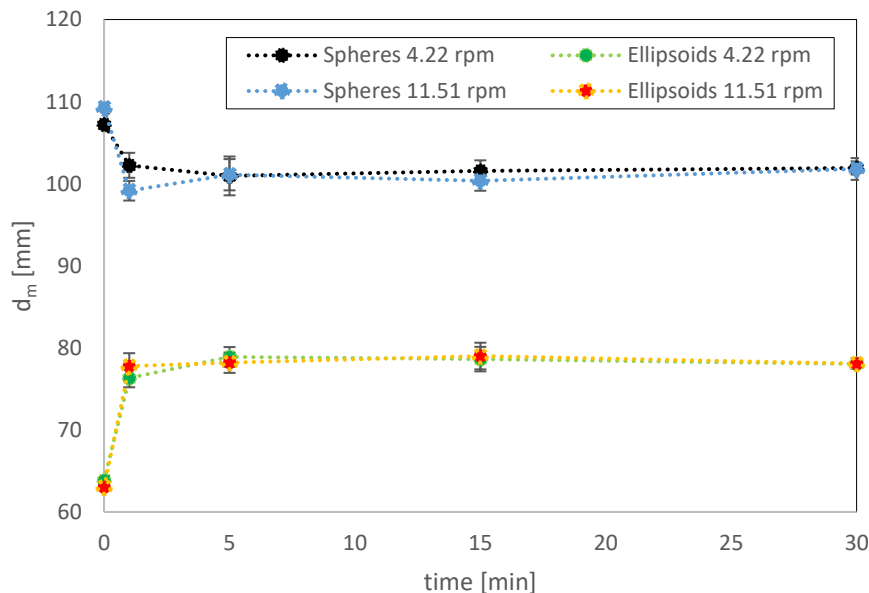


Figure 3.50. Trend of the radial distance vs time for the two rotational speeds of the drum (binary mixture of spheres and ellipsoids with $AR=3.5$, $\phi=25\%$).

At the two rotational speeds, the same steady state is reached; so, also for this binary mixture the speed of the drum does not affect the final configuration.

Moreover, the more elongated particles are found to accumulate at the centre of the granular bed and at lower distance from the centre of the drum, as shown from the distribution.

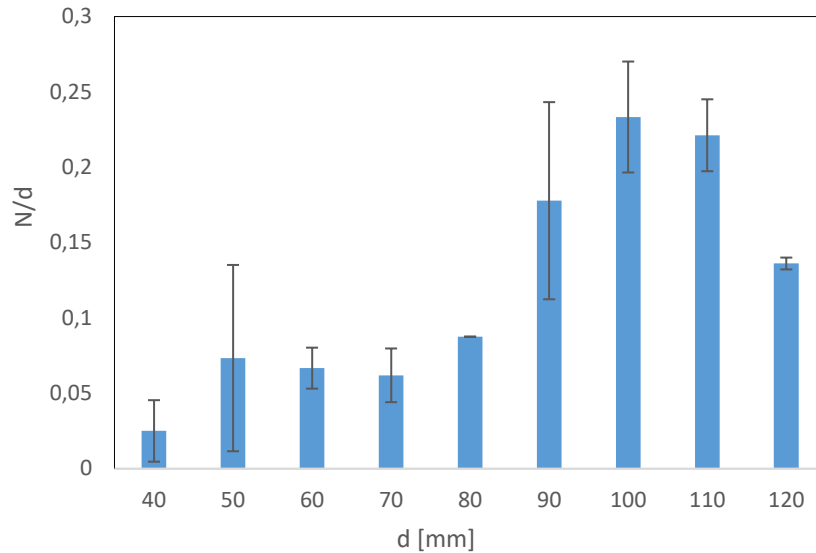


Figure 3.51. Distribution of the radial distance of the spheres, obtained as the average of the distributions of the three tests. The histogram refers to the values of radial distance obtained at $t=30$ min ($\omega=11.51$ rpm; $\varphi=25\%$; the initial configuration was the E/S one).

At higher filling level, the same behaviour is observed.

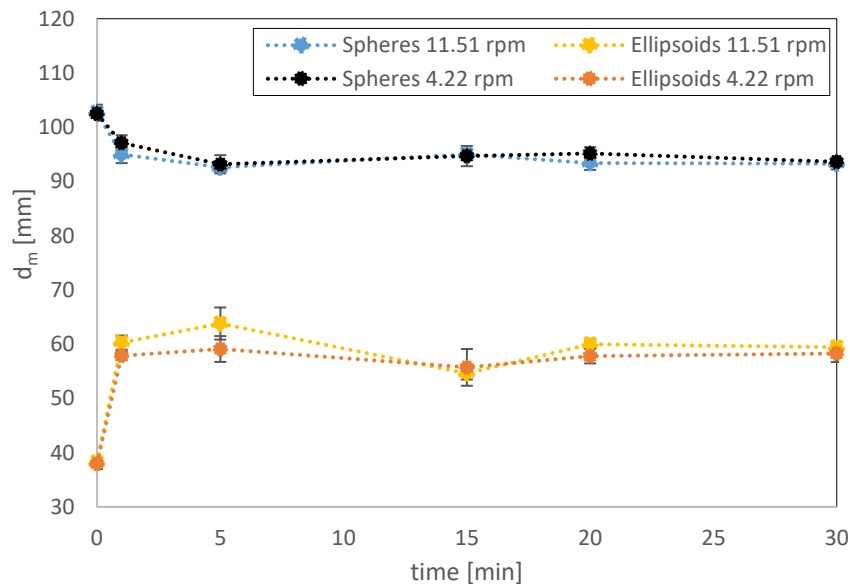


Figure 3.52. Trend of the radial distance vs time for the two rotational speeds of the drum (binary mixture of spheres and ellipsoids with $AR=3.5$, $\varphi=47\%$).

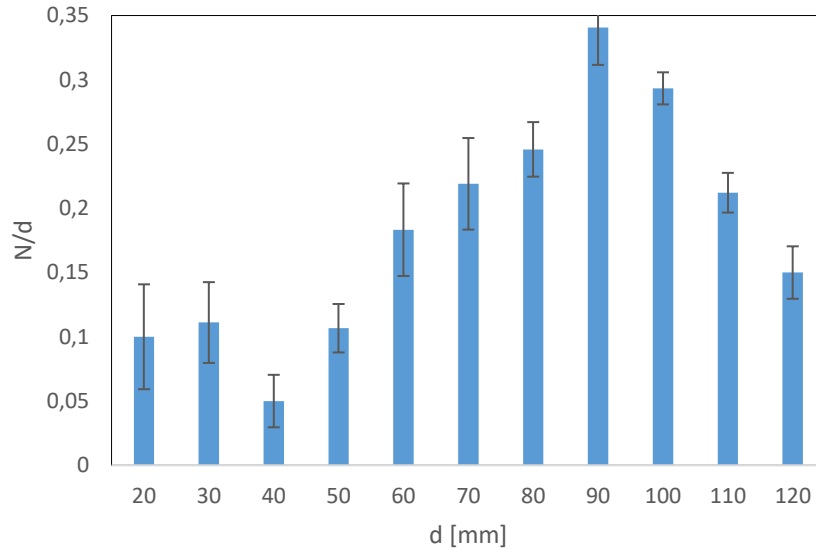


Figure 3.53. Distribution of the radial distance of the spheres, obtained as the average of the distributions of the three tests. The histogram refers to the values of radial distance obtained at $t=30$ min ($\omega=11.51$ rpm; $\varphi=47\%$; the initial configuration was the E/S one).

3.1.8 Discussion

From the experimental tests described in the previous paragraphs, it was found that binary mixtures of particles with different shape but with the same volume do not mix uniformly and segregation was observed. In particular, the particles with lower aspect ratio tend to stay closer to the drum walls, while the more elongated particles are found, on average, mainly at the centre of the granular bed.

The most significant case is represented by the mixture of spheres and ellipsoids with $AR=3.5$; for this mixture, in fact, the segregation is more evident and the non-spherical particles clearly accumulate in the centre of the granular bed. This behaviour can be explained considering that mixing and segregation phenomena in the system occur in the so-called active layer; during the motion of the drum, it was observed that the particles with $AR=3.5$ move in parallel to the granular surface and so they are not able to pass through the void existing between the spherical particles, due to their elongated shape and to their orientation. Therefore, the more elongated particles accumulate on the surface. It has to be considered that the mixture of spheres and ellipsoid with $AR=3.5$ is, among the three considered mixtures, the one that presents the higher difference in shape of its particles. Due to the higher difference in shape, segregation is more evident.

However, the other two binary mixture showed some level of segregation too.

In the case of mixtures of spheres and ellipsoids with AR=1.5 it was shown that the particles did not mix homogeneously, even if the difference in shape is low; the ellipsoids displayed a tendency to settle at the centre of the granular bed, while the spherical particles tended to stay closer to the drum walls.

A not uniform mixing of particles was observed also when the binary mixtures made of ellipsoids with AR=1.5 and ellipsoids with AR=3.5 was considered. The ellipsoids with lower aspect ratio were found to behave similarly to the spherical particles in the other two mixtures; again, it was found that the more elongated particles tend to settle at the centre of the granular bed. The formation of a clear accumulation of more elongated particles was not observed (like it was for the binary mixture of spheres and more elongated ellipsoids) and so the degree of segregation was lower, considering that the difference in shape was smaller.

Furthermore, from the trends of the mean radial distance of the particles it was shown that the three mixtures reach a stable configuration. So, the observed segregation is not a transient phenomenon that vanish after a while, since the segregated configuration is, in fact, kept in time.

When the initial configuration of the particles was inverted, the final configuration of the system was found to be the same. Also, the filling level of the drum and its rotational speed did not affect the final steady state of the mixtures. The particles showed the same behaviour at different filling levels and rotational speed of the drum. Therefore, these two operative variables were found not to affect the phenomena occurring in the rotating drum.

The comparison of the behaviour of the mixtures at the two filling levels can be carried out by normalizing the mean radial distance d_m of the two types of particle on the mean distance of all the particles d_c , calculated according to formula (2.16). The trend of d_m/d_c versus time for the three binary mixtures is shown in the following images:

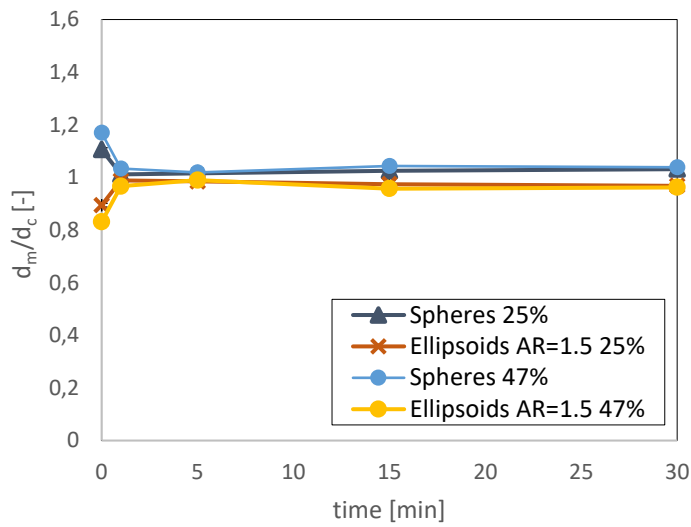


Figure 3.54. d_m/d_c vs. time for the mixture of spheres and ellipsoids with $AR=1.5$.

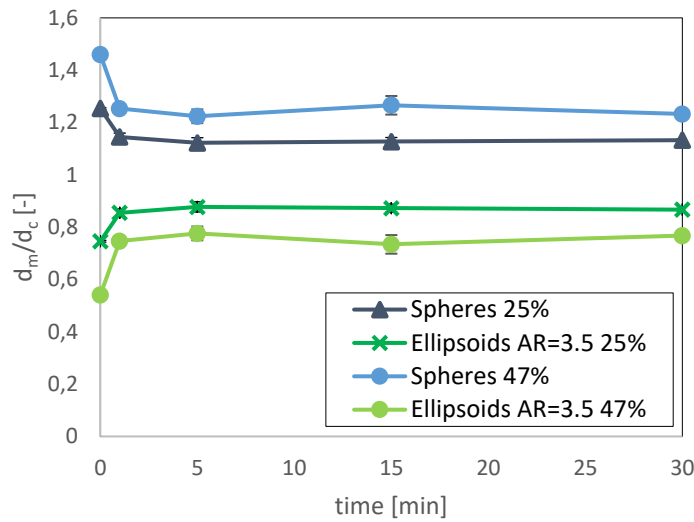


Figure 3.55. d_m/d_c vs. time for the mixture of spheres and ellipsoids with $AR=3.5$.

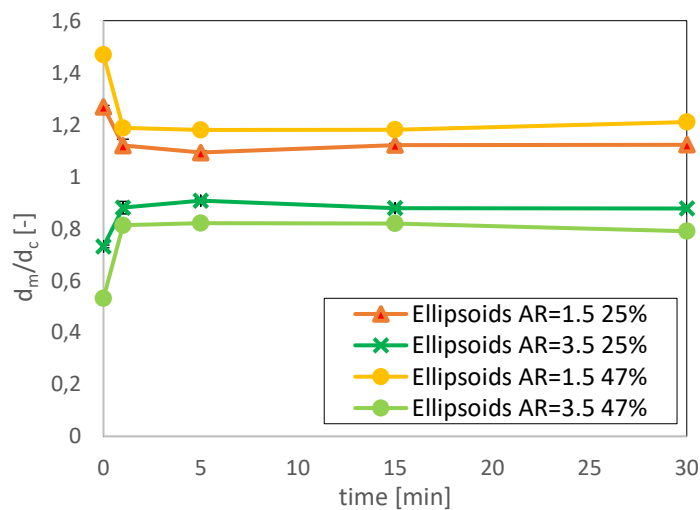


Figure 3.56. d_m/d_c vs. time for the mixture of ellipsoids with $AR=1.5$ and ellipsoids with $AR=3.5$.

In the case of mixture of spheres and ellipsoids with AR=1.5, the curves at different filling levels overlap, showing that the behaviour of the mixture is not affected by the filling levels of the drum. In the case of the other two mixtures, the curves do not overlap exactly, especially in the case of the binary mixture of spheres and ellipsoids with AR=3.5. However, the difference between the curves at different filling levels is not very high.

3.2 Mixtures of particles of different sizes

In this paragraph, the results of the tests performed with mixtures made of particles of different sizes will be presented. It is reminded that, in these tests, the number of particles was defined in order to have binary mixtures with a composition of the 50% of both the components on a base volume and a filling level as equal as possible to 25%.

3.2.1 Spheres with 8 mm and 3.81 mm diameter

The conditions at which the test with 8 mm and 3.81 mm diameter particles was performed are reported in Table 3.8.

Table 3.8. Rotational speed, filling level, number of particles and volume composition of the test.

ω [rpm]	φ % [-]	N big spheres [-]	V big spheres [cm ³]	N small particles [-]	V small spheres [cm ³]
4.22	24.734	115	30.829	1100	31.854

As it is known from the literature, particles of different sizes tend to segregate and the phenomenon occurs quite fast. This was observed in practice; the formation of a segregated core, in fact, is shown in Figure 3.57.

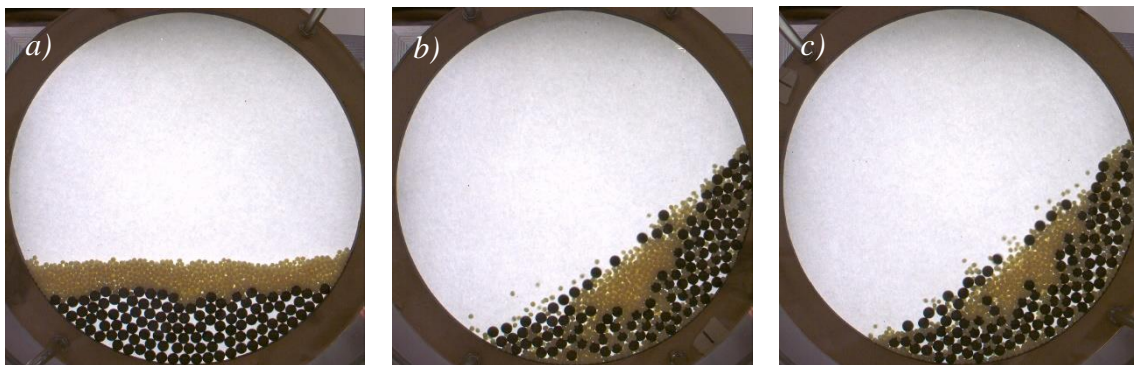


Figure 3.57. a) Drum at the initial condition; b) drum at $t=23$ s; c) drum at $t=120$ s.

From the pictures reported above it can be seen that percolation is not absent at all in this case and some small particles accumulate close to the drum wall, too.

The accumulation of small particles at the centre of the granular bed can be illustrated by plotting the coordinates of the centre of mass of the bigger spheres, as shown in the following pictures.

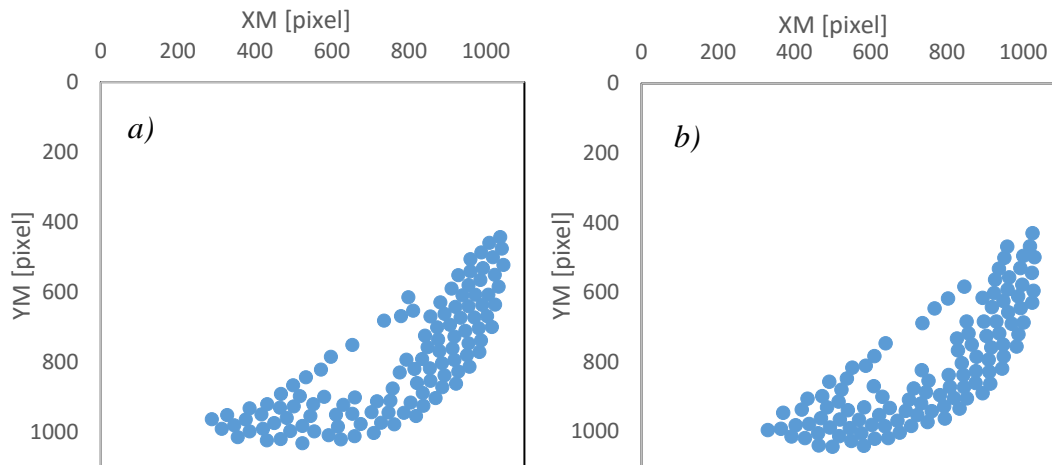


Figure 3.58. Plot of the coordinates of the centre of mass of 8 mm spheres at a) $t=23s$ and b) $t=120s$.

The empty space at the centre of the granular bed is the space unoccupied by the big spheres, where the smaller particles accumulate. Moreover, the radial distance from the centre of the drum (d) of the big spheres was calculated at different time instants and the difference (d_0-d) was plotted in time, where d_0 is the radial distance of the big spheres at the initial time. The trend is displayed in the following figure.

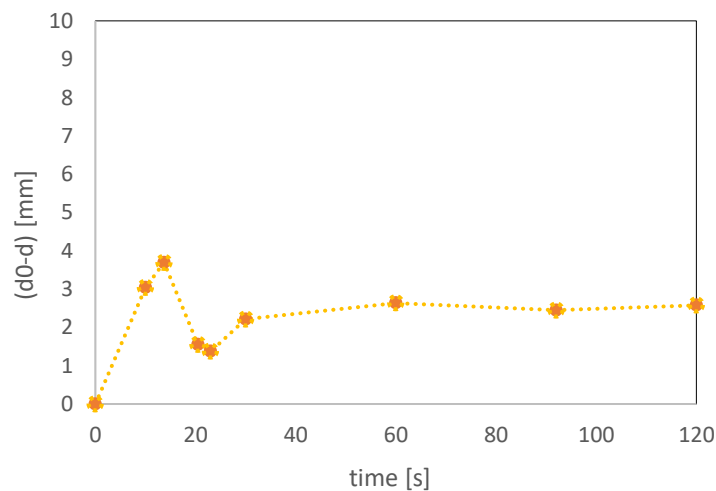


Figure 3.59. (d_0-d) vs time; the radial distance is the one of 8 mm spheres.

The plot shows that a steady state is reached and the transition to the final value is quite fast. As shown previously, in fact, after 23 seconds the system displays a clear segregation that is then kept in time. The oscillations that the trend exhibits at the first seconds are due to the initial motion of the particles before reaching the final steady state value, as Figure 3.60 shows.

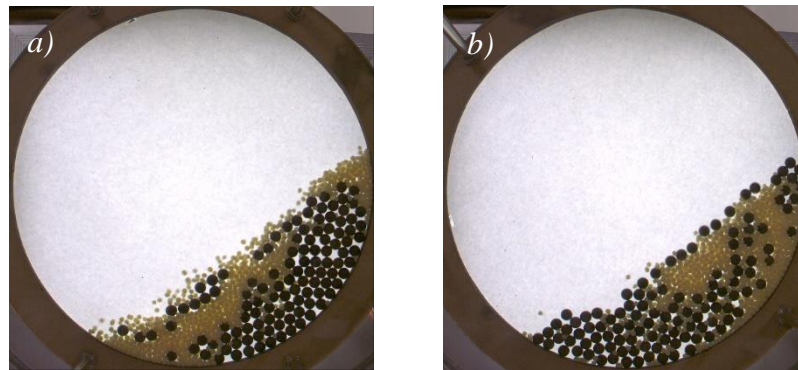


Figure 3.60. a) Drum at $t=10$ s; b) drum at $t=13.7$ s.

Starting from the segregated initial configuration, the particles move and at the very beginning the two types of particles distribute in an opposite way. Then, the segregated core is formed, as shown before.

3.2.2 Spheres with 8 mm and 6 mm diameter

In the same conditions of the previous test but with different small spherical particles another test was performed. The test conditions are reported in Table 3.9.

Table 3.9. Rotational speed, filling level, number of particles and volume composition of the test.

ω [rpm]	ϕ % [-]	N big spheres [-]	V big spheres [cm ³]	N small particles [-]	V small spheres [cm ³]
4.22	24.915	95	25.468	219	24.768



Figure 3.61. a) Drum at the initial condition; b) drum at $t=23$ s; c) drum at $t=120$ s.

Also in this case, the smaller particles tend to settle and the centre of the granular bed. However, the formation of a segregated core is less noticeable, as it can also be seen by plotting the coordinates of the bigger spheres.

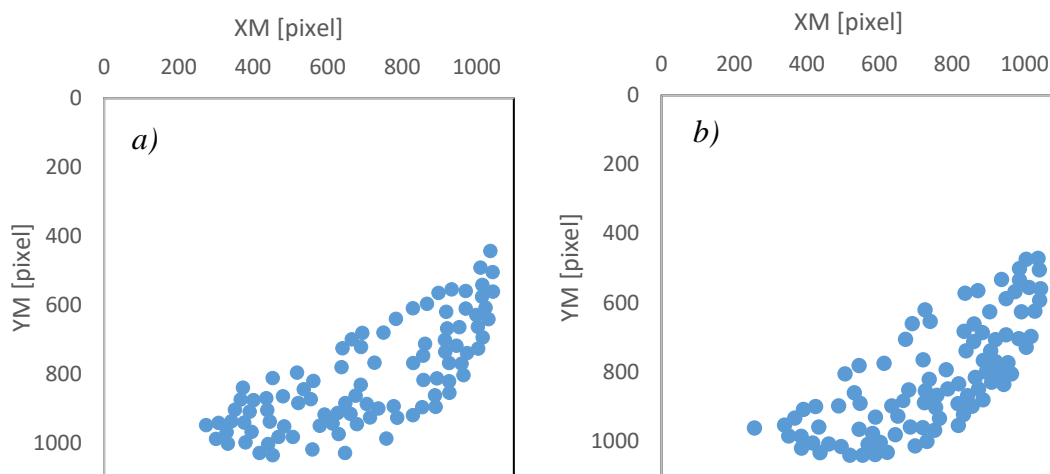


Figure 3.62. Plot of the coordinates of the centre of mass of 8 mm spheres at a) $t=23$ s and b) $t=120$ s

The trend of the difference (d_0-d) is reported in Figure 3.63.

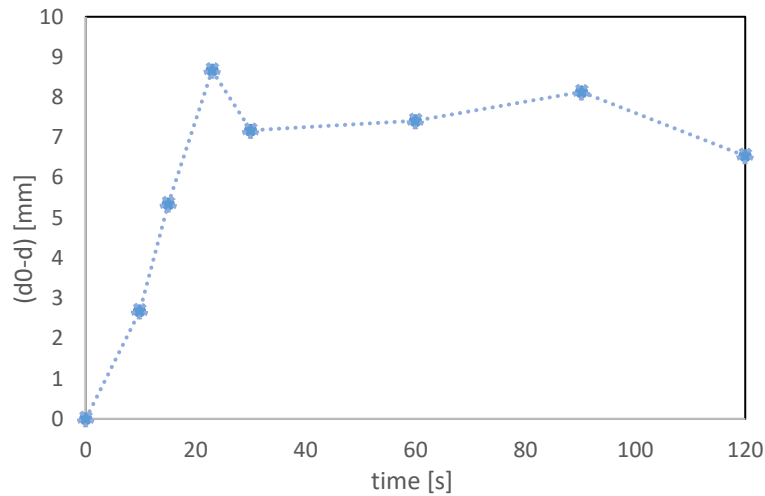


Figure 3.63. (d_0-d) vs time; the radial distance is the one of 8 mm spheres.

As for the mixture previously considered, a steady state is reached, meaning that the mixture stabilizes at a steady condition. Moreover, it can be noticed that after 30 seconds the steady state is already reached, indicating that the achievement of the stable condition for the system is quite fast.

3.2.3 Comparison and discussion

To compare the behaviour of the two binary mixtures the distance of the big spheres is normalized on the distance of the barycentre of the bed from the centre of the drum (d_c) and d/d_c is plotted versus time. The two trends are displayed together in the following image.

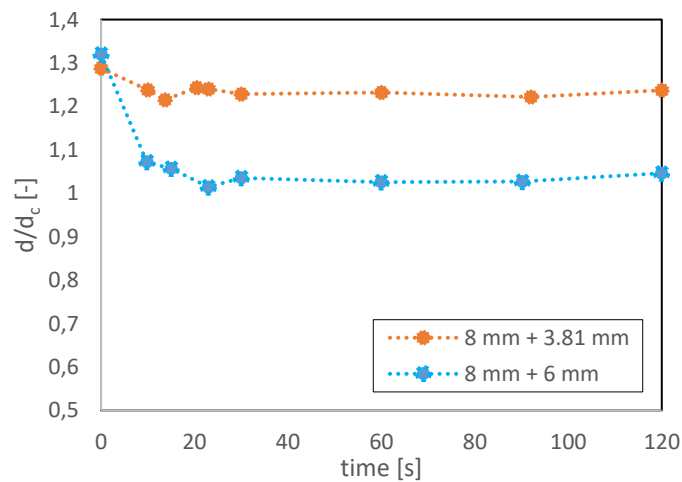


Figure 3.64. Comparison of the two tests with differently sized particles.

As it can be seen, in the case of the binary mixture of 8 mm spheres and 3.81 mm particles, the variation of the normalized radial distance of the bigger spheres with respect to the initial value is not very high; considering that the bigger spheres at the initial time were below the smaller particles and closer to the drum wall, the trend indicates that the big spheres tend to keep a larger radial distance and so to stay closer to the drum wall, as it is in fact observed. The smaller particles, instead, mainly accumulate at lower radial distance, forming a segregated core. As it is known, the motion of the particles occurs only on the surface layer of the granular bed (active layer) and the remaining part of the particles moves as a solid bed. Since voids exist between the big particles during the motion along the surface, the small particles can easily pass through them; however, the deeper big particles are not in motion and so the smaller particles cannot further penetrate in the granular bed and accumulate more superficially.

When 8 mm spheres are placed with 6 mm spheres, instead, the variation of their normalized radial distance is higher. It means that the big spheres have on average a lower distance from the centre of the drum; they change their position from the initial one more than in the previous case and so a higher mixing of particles occurs. The formation of a clear segregated core is, in fact, not observed with this binary mixture, since, due to the lower difference in size, the 6 mm spheres can pass through the voids between the big spheres less easily.

In conclusion, higher is the difference in size of the particles and greater is the observed segregation. When the difference in particle size is lower, instead, particles are more easily mixed. So, the size ratio between the particles constituting the mixture affects the mixing process in the rotating drum and for high size ratios segregation clearly occurs.

3.3 Evaluation of Maximum Angle of Stability, Angle of Repose and Dynamic Repose Angle

The Maximum Angle of Stability (α_{max}), the Angle of Repose (β) and the Dynamic Repose Angle (β_d) were evaluated, with the two methods described in the previous chapter (see § 2.6.3), for all the mixtures considered in this work.

Three values of each angle were estimated with the two methods and the final value was then obtained as the mean value of the three calculated ones.

The drum was rotated at 4.22 rpm, with a filling level of the 25% for all the experiments performed for the angle evaluation.

- **Mixture of spheres and ellipsoids with AR=1.5**

Figure 3.65 shows an example of images used for the evaluation of Maximum Angle of Stability and the Angle of Repose for the binary mixture.

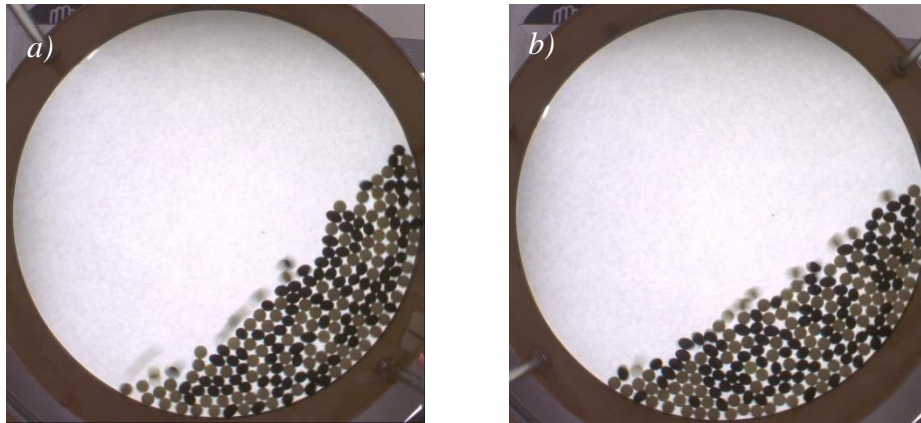


Figure 3.65. Example of images used for the evaluation of a) the Maximum Angle of Stability and b) the Angle of Repose for the mixtures of spheres and ellipsoids with AR=1.5.

The values of angles obtained with the two methods are reported in Table 3.10.

Table 3.10. Maximum Angle of Stability and Angle of Repose evaluated with Method 1 and Method 2.

Mixture of spheres and ellipsoids with AR=1.5				
	Method 1		Method 2	
	α_{max} [degrees]	β [degrees]	α_{max} [degrees]	β [degrees]
1	41.130	30.390	44.230	32.840
2	40.160	31.150	40.760	29.583
3	41.980	31.090	44.663	29.080
mean	41.090	30.887	43.218	30.501
STD [degrees]	0.744	0.345	1.747	1.667

The values obtained with the two methods are very similar. So, in this case both the methods are reliable for the angle evaluation.

The Dynamic Angle of Repose was calculated considering the particles in motion, as reported in Figure 3.66.

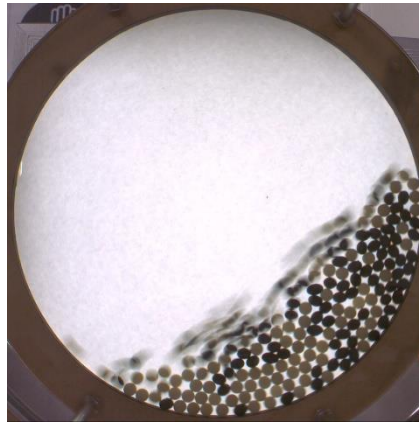


Figure 3.66. Example of image used for the evaluation of the Dynamic Angle of Repose for the mixtures of spheres and ellipsoids with AR=1.5.

The values of the angle obtained with the two methods are reported in Table 3.11.

Table 3.11. Dynamic Angle of Repose evaluated with Method 1 and Method 2.

Mixture of spheres and ellipsoids with AR=1.5		
	Method 1	Method 2
	β_d [degrees]	β_d [degrees]
1	36.830	38.969
2	36.630	38.477
3	36.160	35.615
mean	36.540	37.687
STD [degrees]	0.281	1.479

The values of the Dynamic Angle of Repose calculated with the two methods are very similar.

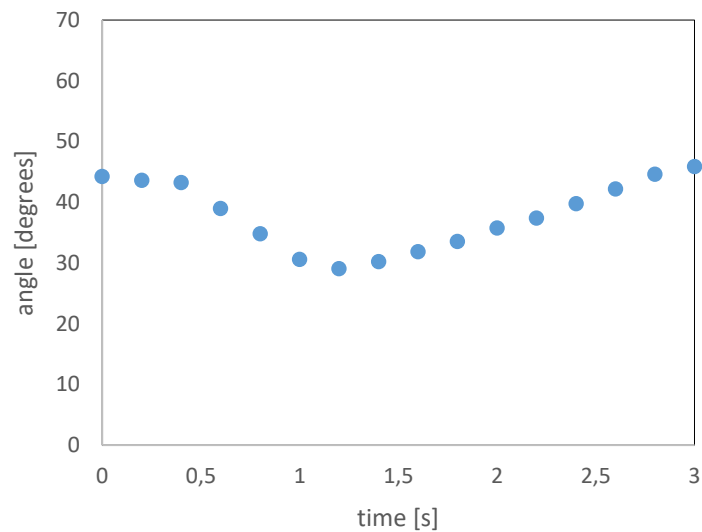
Moreover, the values of Table 3.11 can be compared with the ones obtained calculating the angle as the average of α_{max} and β .

Table 3.12. *Dynamic Angle of Repose calculated as the average of α_{max} and β .*

Mixture of spheres and ellipsoids with AR=1.5		
	Method 1	Method 2
	β_d [degrees]	β_d [degrees]
1	35.760	38.535
2	35.655	35.172
3	36.535	36.872
mean	35.983	36.859
STD [degrees]	0.392	1.373

The values of angle of Tables 3.11 and 3.12 are very similar, differing only for one degree; this confirms that the Dynamic Angle of Repose is computable as the average of the Maximum Angle of Repose and the Angle of Repose.

Furthermore, considering a complete avalanche of the mixture, the value of the angle can be plotted in time.

**Figure 3.67.** *Angle of the surface of the granular bed vs. time (spheres and ellipsoids with AR=1.5).*

The time instant at which the Maximum Angle of Stability is reached is assumed to be the initial time instant ($t=0$). A periodic trend is shown: starting from the maximum angle, after about one second, the angle reaches its minimum value and afterwards the mixture starts to rise again in the drum, and the value of angle returns to maximum one. It takes only three seconds to see a complete avalanche.

- **Mixture of spheres and ellipsoids with AR=3.5**

Two of the images used for the estimation of the angles are reported in Figure 3.68.

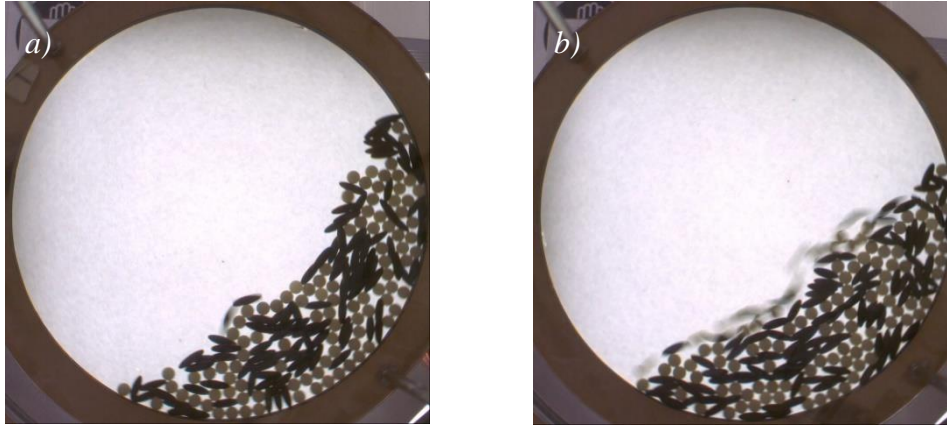


Figure 3.68. Example of images used for the evaluation of a) the Maximum Angle of Stability and b) the Angle of Repose for the mixtures of spheres and ellipsoids with AR=3.5

Table 3.13 contains the calculated values of angle with the two methods.

Table 3.13. Maximum Angle of Stability and Angle of Repose evaluated with Method 1 and Method 2.

Mixture of spheres and ellipsoids with AR=3.5				
Method 1			Method 2	
	α_{max} [degrees]	β [degrees]	α_{max} [degrees]	β [degrees]
1	47.290	35.770	53.108	35.300
2	47.160	36.520	49.140	35.560
3	47.410	35.710	52.183	36.688
mean	47.287	36.000	51.477	35.846
STD [degrees]	0.102	0.369	1.695	0.598

It has to be noted that in this case the values of the Maximum Angle of Stability obtained with the two methods are slightly different. The particles surface was in many cases not exactly flat and the fitting by the straight line was not exactly precise. Moreover, the value of the angles for the mixture of spheres and ellipsoids with AR=3.5 are higher than the ones of the mixtures of spheres and ellipsoids with AR=1.5. The mixtures with more elongated particles are, in fact, able to develop more stable structures that can reach a higher angle before the particles start sliding along the surface.

The Dynamic Angle of Repose was evaluated considering the particles in motion

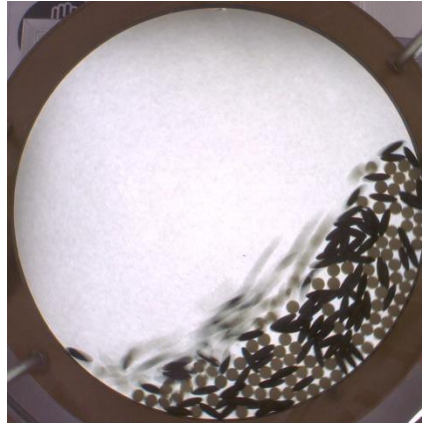


Figure 3.69. Example of image used for the evaluation of the Dynamic Angle of Repose for the mixtures of spheres and ellipsoids with AR=3.5.

The values of β_d obtained with the two methods are reported in Table 3.14.

Table 3.14. Dynamic Angle of Repose evaluated with Method 1 and Method 2.

Mixture of spheres and ellipsoids with AR=3.5		
	Method 1	Method 2
	β_d [degrees]	β_d [degrees]
1	40.050	42.101
2	40.560	37.730
3	41.020	40.754
mean	40.543	40.195
STD [degrees]	0.396	1.828

These values can be compared with the ones obtained evaluating the same angle according to formula (2.23).

Table 3.15. Dynamic Angle of Repose calculated as the average of α_{max} and β .

Mixture of spheres and ellipsoids with AR=3.5		
	Method 1	Method 2
	β_d [degrees]	β_d [degrees]
1	41.530	44.204
2	41.840	42.350
3	41.560	44.431
mean	41.643	43.662
STD [degrees]	0.140	0.932

Also in this case the difference between the values of β_d of Table 3.14 and 3.15 is low. The trend of the angle versus time, for a complete avalanche is shown in the following image.

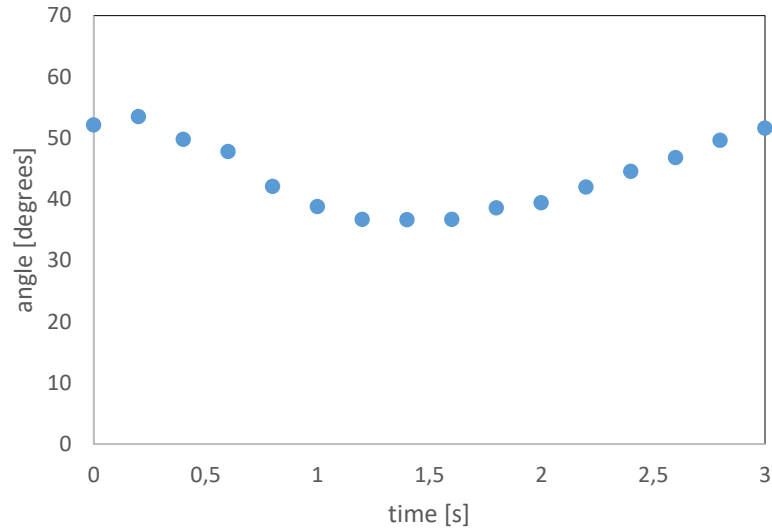


Figure 3.70. Angle of the surface of the granular bed vs. time (spheres and ellipsoids with AR=3.5).

As in the previous case, a complete avalanche occurs in three seconds.

- **Mixture of ellipsoids with AR=1.5 and ellipsoids with AR=3.5**

In Figure 3.71 some pictures of the two angles for the mixtures made of the two types of ellipsoids are shown.

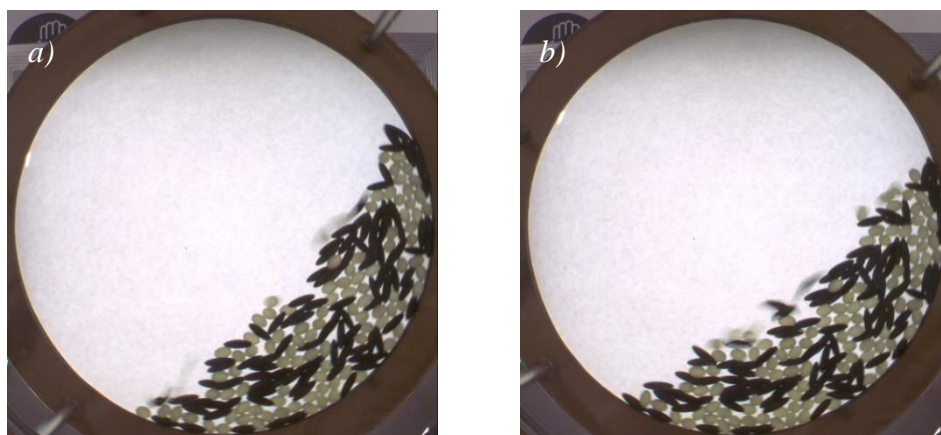


Figure 3.71. Example of images used for the evaluation of a) the Maximum Angle of Stability and b) the Angle of Repose for the mixtures of ellipsoids with AR=1.5 and ellipsoids with AR=3.5.

The estimated values of the angles are reported in the following table.

Table 3.16. Maximum Angle of Stability and Angle of Repose evaluated with Method 1 and Method 2.

Mixture of ellipsoids AR=1.5 and ellipsoids with AR=3.5				
	Method 1		Method 2	
	α_{max} [degrees]	β [degrees]	α_{max} [degrees]	β [degrees]
1	47.700	38.540	56.038	43.111
2	50.090	42.170	48.658	39.275
3	51.500	40.900	52.378	42.498
mean	49.763	40.537	52.357	41.628
STD [degrees]	1.568	1.504	3.014	1.682

Also in this case, Method 1 was less accurate for the evaluation of the Maximum Angle of Stability, since the granular surface is in some cases not exactly flat.

The Dynamic Angle of Repose was also evaluated.

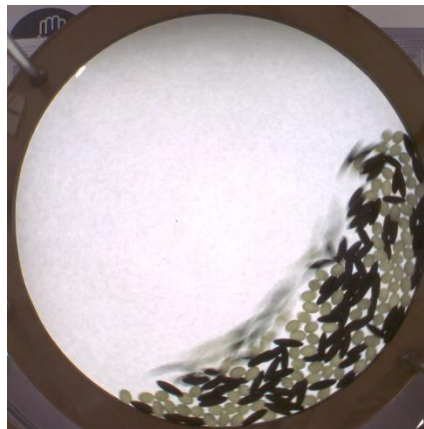


Figure 3.72. Example of image used for the evaluation of the Dynamic Angle of Repose for the mixtures of ellipsoids with AR=1.5 and ellipsoids with AR=3.5.

It was verified that the values of the angle computed from images of the particles in motion (Table 3.17) were very similar to the values obtained according to formula (2.23) (Table 3.18).

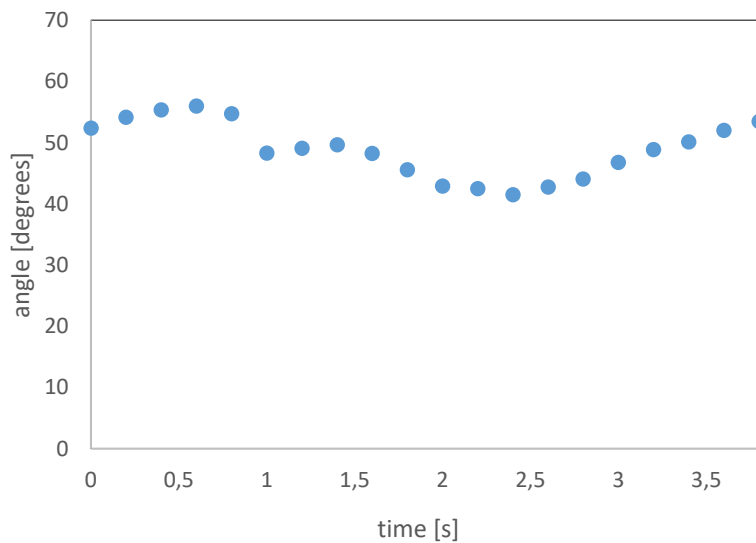
Table 3.17. *Dynamic Angle of Repose evaluated with Method 1 and Method 2.*

Mixture of ellipsoids AR=1.5 and ellipsoids with AR=3.5		
	Method 1	Method 2
	β_d [degrees]	β_d [degrees]
1	41.790	45.561
2	45.710	46.787
3	43.650	48.256
mean	43.717	46.868
STD [degrees]	1.601	1.102

Table 3.18. *Dynamic Angle of Repose calculated as the average of α_{max} and β .*

Mixture of ellipsoids AR=1.5 and ellipsoids with AR=3.5		
	Method 1	Method 2
	β_d [degrees]	β_d [degrees]
1	43.120	49.574
2	46.130	43.965
3	46.200	47.438
mean	45.150	46.993
STD [degrees]	1.436	2.312

The trend of the angle versus time for the mixture made of the two types of ellipsoids is reported in Figure 3.73.

**Figure 3.73.** *Angle of the surface of the granular bed vs. time (ellipsoids with AR=1.5 and AR= 3.5)*

For the mixture of ellipsoids, the trend of the angle is more oscillating before the minimum value is reached. Also, it takes more time (almost four seconds) for the angle to return to the maximum value.

Furthermore, the obtained values of angle for the mixtures of the two types of ellipsoids are the highest ones among the three mixtures of differently shaped particles that were taken into account.

The values of the two angles for the three mixtures are visually shown in the following histograms.

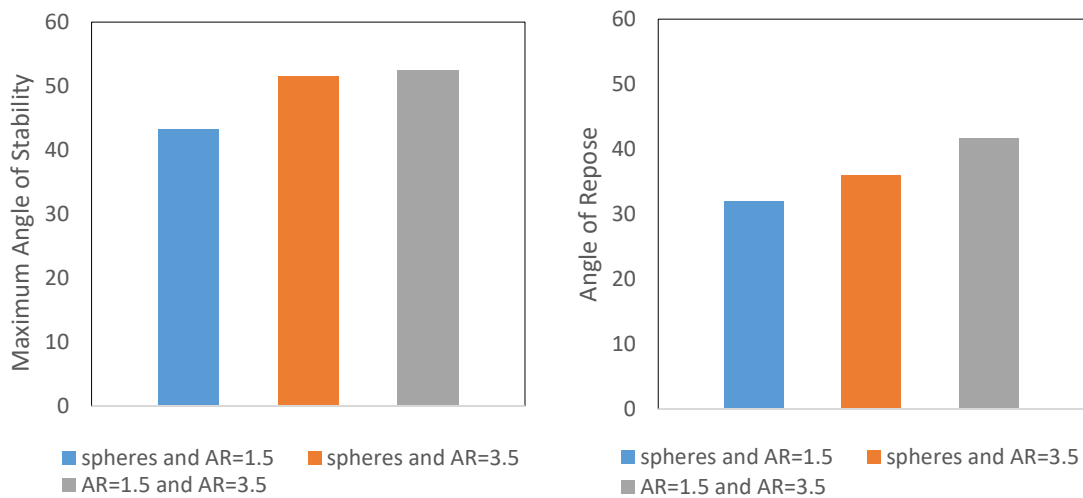


Figure 3.74. Maximum Angle of Stability and Angle of Repose for the three mixtures.

The evaluation of the angles for the three mixtures highlights that different behaviours occur according to particles shape. As it was already said, the elongated particles are able to partly overlap each other and, due to their shape and also due to the presence of the drum walls, the mixtures they form are more stable. Consequently, the Maximum Angle of Stability and the Angle of Repose assume higher values for the mixtures containing particles with AR=3.5. Moreover, the mixture made of ellipsoids with AR=1.5 and AR=3.5 demonstrate even higher angles. This means again that non-spherical particles give more stable mixtures due to their shape.

- **Spheres with 8 mm and particles with 3.81 mm diameter**

The formed by the binary mixtures are illustrated in Figure 3.75.

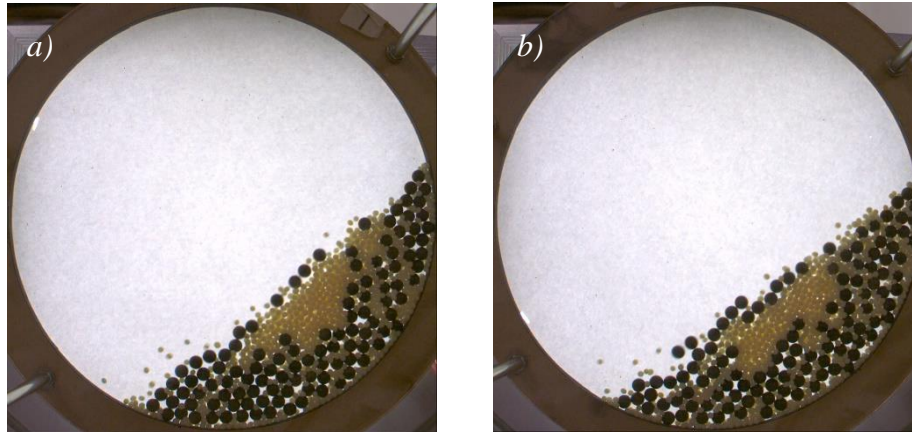


Figure 3.75. Example of images used for the evaluation of a) the Maximum Angle of Stability and b) the Angle of Repose for the mixtures of 8 mm spheres and 3.81 mm particles.

The values of angles are reported in the following table:

Table 3.19. Maximum Angle of Stability and Angle of Repose evaluated with Method 1 and Method 2.

Mixture of 8 mm spheres and 3.81 mm particles				
	Method 1		Method 2	
	α_{max} [degrees]	β [degrees]	α_{max} [degrees]	β [degrees]
1	38.750	36.750	39.327	37.282
2	38.380	36.510	38.259	36.658
3	38.590	36.340	38.431	35.983
mean	38.573	36.533	38.672	36.641
STD [degrees]	0.152	0.168	0.468	0.530

The values obtained with the two methods are very similar. Moreover, the difference between the Maximum Angle of Stability and the Angle of Repose is very low. The angle that the granular bed forms in the drum does not change very much during the motion, meaning that with mixture of particles of the same shape the motion is more regular and stable.

The Dynamic Angle of Repose was evaluated from pictures of the mixture in motion. An example is displayed in Figure 3.76.

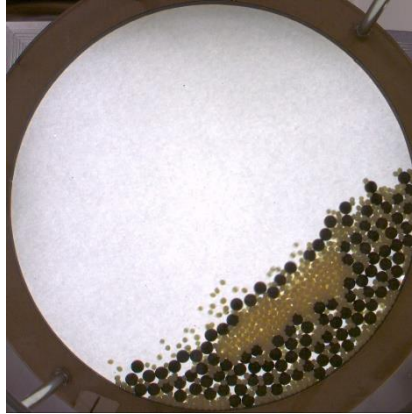


Figure 3.76. Example of image used for the evaluation of the Dynamic Angle of Repose for the mixtures of 8 mm spheres and 3.81 mm particles.

The values of the Dynamic Angle of Repose computed as before are reported in Table 3.20 and 3.21.

Table 3.20. Dynamic Angle of Repose evaluated with Method 1 and Method 2.

Mixture of 8 mm spheres and 3.81 mm particles		
	Method 1	Method 2
	β_d [degrees]	β_d [degrees]
1	37.180	39.054
2	37.670	37.118
3	37.750	38.170
mean	37.533	38.114
STD [degrees]	0.252	0.791

Table 3.21. Dynamic Angle of Repose calculated as the average of α_{max} and β .

Mixture of 8 mm spheres and 3.81 mm particles		
	Method 1	Method 2
	β_d [degrees]	β_d [degrees]
1	37.750	38.304
2	37.455	37.459
3	37.465	37.207
mean	37.553	37.657
STD [degrees]	0.139	0.469

The values obtained are very similar, confirming the validity of formula (2.23).

- **Spheres with 8 mm and 6 mm diameter**

An example of angles is reported below.

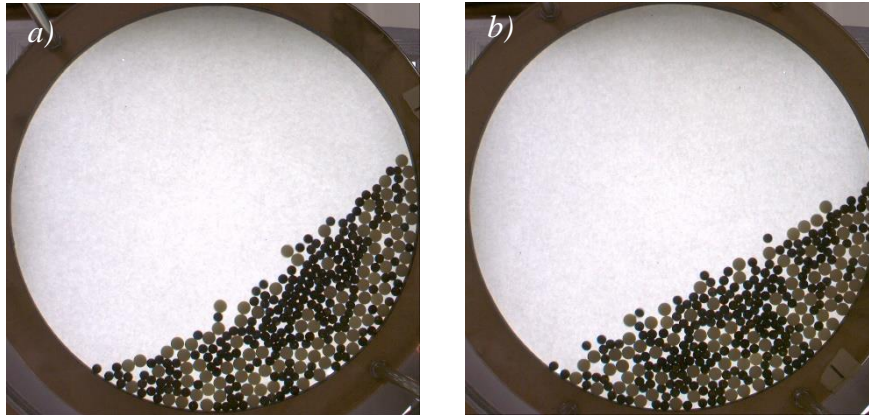


Figure 3.77. Example of images used for the evaluation of a) the Maximum Angle of Stability and b) the Angle of Repose for the mixtures of 8 mm spheres and 6 mm spheres.

Table 3.22 reports the calculated values of α_{max} and β .

Table 3.22. Maximum Angle of Stability and Angle of Repose evaluated with Method 1 and Method 2

Mixture of 8 mm spheres and 6 mm spheres				
Method 1			Method 2	
	α_{max} [degrees]	β [degrees]	α_{max} [degrees]	β [degrees]
1	37.240	35.720	36.012	33.817
2	37.180	35.280	37.041	30.809
3	37.840	32.590	37.100	30.803
mean	37.420	34.530	36.717	31.809
STD [degrees]	0.298	1.383	0.499	1.419

The angles calculated with the two methods are slightly different in this case; also, the angles for this binary mixture are slightly lower than the angles calculated for the other binary mixture of differently sized particles.

The Dynamic Angle of Repose was calculated, too.



Figure 3.78. Example of image used for the evaluation of the Dynamic Angle of Repose for the mixtures of 8 mm spheres and 6 mm spheres.

The values of the Dynamic Angle of Repose are presented in the following tables.

Table 3.23. Dynamic Angle of Repose evaluated with Method 1 and Method 2.

Mixture of 8 mm spheres and 6 mm spheres		
	Method 1	Method 2
	β_d [degrees]	β_d [degrees]
1	34.720	34.415
2	35.320	33.771
3	37.730	33.910
mean	34.923	34.032
STD [degrees]	0.281	0.277

Table 3.24. Dynamic Angle of Repose calculated as the average of α_{max} and β .

Mixture of 8 mm spheres and 6 mm spheres		
	Method 1	Method 2
	β_d [degrees]	β_d [degrees]
1	36.480	34.915
2	36.230	33.925
3	35.215	33.951
mean	35.975	34.263
STD [degrees]	0.547	0.461

It has to be noted that the Maximum Angles of Stability calculated for the mixtures of particles with different size are significantly lower than the ones obtained for the mixtures of differently shaped particles, especially with respect to the values obtained for the

mixtures containing the more elongated particles. This suggest that with particles of the same shape the motion in the drum is different; the maximum angle that the granular bed reaches before one avalanche occurs is lower so the mixtures form less stable structures and flow more easily in the rotating drum.

So, also from the angle evaluation it can be concluded that the particles shape has a strong influence on the mixture behaviour un the drum.

Conclusions

The aim of this work was the study of mixing and segregation phenomena occurring in a rotating drum loaded with particles of different shapes. Two types of ellipsoids were used as non-spherical particles; they were considered together with spherical particles having the same volume.

It was shown that shape segregation phenomena are not transient ones, but the segregated configurations reached by the considered mixtures are kept in time. The phenomenon occurs also when the difference in shape is very low and it does not depend neither on the initial configuration of the system nor on the filling level of the drum and its rotational speed. Furthermore, shape segregation occurs very fast and the kinetic of the phenomenon is comparable to the one of size segregation phenomena.

The influence of the particles shape was also underlined by the calculation of the Maximum Angle of Stability, the Angle of Repose and the Dynamic Angle of Repose. Mixtures of differently sized particles show lower values of angles than the mixtures of differently shaped particles. The shape of the particle strongly influences the dynamics of the mixture in the drum and mixtures of differently shaped particles can develop stable structures showing high values of angles. Also, among the three mixtures made of particles of different shapes, the one made of the two types of non-spherical particles shows the highest values of angles, indicating that when both the components in the mixtures are non-spherical the dynamic is even different.

As a conclusion, the shape is a relevant particles property not only with respect to the mixing process but also with respect to the dynamic of the particle in the rotating drum. Considering the relevance of non-spherical particles in common practical application, the phenomenon has to be clearly taken into account and further investigated to completely characterize it.

The study was limited to radial phenomena and has considered two types of non-spherical particles only. As next steps, also different geometries of the drum should be considered; in particular, increasing the thickness of the drum would allow to investigate also axial phenomena. Moreover, the study should be extended also to other types of non-spherical particles.

Appendix

In this Appendix, some information about the ImageJ program are reported; they can be useful to better understand the image processing procedure followed in this work and presented in Chapter 2. Also, the main options and plugins used for the image analysis are described.

ImageJ is an open source Java image processing program that allows to display, modify, process and save 8-bit, 16-bit and 32-bit pictures.

The program has thousands of plugins that extend its functionality. Some of them are already installed, some can be installed from the ImageJ update site and some more can be manually installed from online sources.

When the program runs, the main ImageJ window opens. The window presents eight menus: *File*, *Edit*, *Image*, *Process*, *Analyze*, *Plugins*, *Window* and *Help*, as shown in Figure A1.

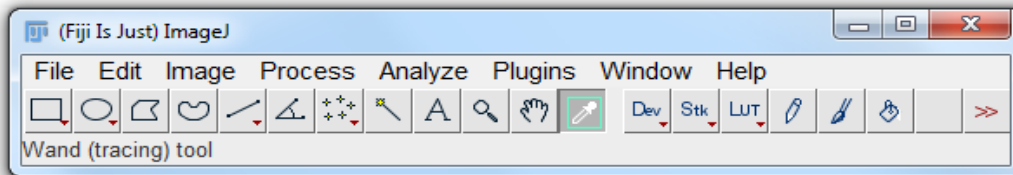


Figure A1. *ImageJ* interface.

Image types

Digital images are two-dimensional grids of pixel intensities values; the width and height of the image are defined by the number of pixel in x (rows) and y (columns) directions. Pixels are the smallest single components of images, with a numeric value – pixel intensity – that range between black and white. In this range, the number of unique intensity vales that can exist in the image is defined as the bit-depth of the image and specifies the level of precision in which intensities are coded. For example, a 2-bit image has $2^2= 4$ tones, a 4-bit image has $2^4= 16$ tones.

In terms of bits per pixels (bpp), the main types of images are:

- 8-bit: images that can display $2^8 = 256$ grey levels. Each pixel is represented in the *byte* format.
- 16-bit: images that can display $2^{16} = 65536$ grey level.
- 32-bit: images that can display $2^{32} = 4294967296$ grey levels. Each pixel is represented in *short* format
- RGB colour: colour images that can display 256 values in the Red, Green and Blue channel. These are $2^{3 \times 8} = 24$ -bit images.

After opening a new image, the image type can be set in the *Image* menu (*Image* → *Type*). The images can be saved in different formats. The TIFF format is usually used in this work to save the modified pictures.

Split Channels

The option is included in the *Image* menu (*Image* → *Color* → *Split Channels*) and splits an RGB image into three greyscale images containing the blue, green and red components of the original image. Three images are obtained: (*blue*), (*green*) and (*red*).

Duplicate

The command *Duplicate* creates a new window with a copy of the original image. Also, if a rectangular part of the original image is selected with the *Rectangle Selection Tool*, the command creates a copy of the rectangular selection. The command is in the *Image* menu (*Image* → *Duplicate*).

Smooth and Sharpen

The *Smooth* and *Sharpen* commands are in the *Process* menu (*Process* → *Smooth*, *Process* → *Sharpen*). The first one blurs the active image or selection, replacing each pixel with the average of its 3×3 neighbourhood. The second option increases contrast and accentuates detail in the image or election, but may also increase the noise; it replaces each pixel with a weighted average of the 3×3 neighbourhood.

Threshold

The *Threshold* option is contained in the *Image* menu (*Image* → *Adjust* → *Split Channels*). The *Threshold* is a segmentation of the image that is needed to separate the object of

interest (particles in this case) from the background. The command only works with greyscale images and generates a binary image in which the black areas are the interest objects on a white background, or vice-versa.

The threshold operation can be guided by the grey colour histogram displayed in the *Threshold* window; it represents a bimodal distribution with on its left the pixel belonging to the background and on the right those belonging to the object of interest. The minimum and maximum threshold values can be set by two sliders: the upper slider adjusts the minimum threshold value and the lower slider sets the maximum threshold value. There is also the chance to apply an *Auto* threshold that automatically sets the threshold levels based on an analysis of the histogram of the image or selection.

Erode, Dilate and Close

These commands are in the *Process* menu and in particular in the *Binary* submenu which contains commands to process black and white images (*Process*→*Binary*→*Erode*, *Process*→*Binary*→*Dilate*, *Process*→*Binary*→*Close*). They assume that the objects are black and the background is white.

The command *Erode* removes pixels from the edges of the black objects in a binary image. Pixels can be instead added to the edge of objects by the command *Dilate*.

With the *Close* command, a dilation operation, followed by erosion is performed, smoothing objects and removing isolated pixels. This can help to eliminate undesired surface irregularities of the objects.

Watershed

The *Watershed* segmentation (*Process*→*Binary*→*Watershed*) is a way of automatically separate touching objects or cutting apart particles that touch. It first calculates the Euclidian distance map (EDM) and find the ultimate eroded points (UEPs). To obtain the EDM each foreground pixel in the binary image is replaced with a grey value equal to that pixel's distance from the nearest background pixel. The ultimate eroded points are maxima of the EDM and their value is equal to the radius of the largest circle that fits into the binary object, with the UEP as the centre. The *Watershed* command dilates each of the UEPs as far as possible, either until the edge of the object is reached or the edge touches a region of another growing UEP.

Adjustable Watershed

The *Adjustable Watershed* is an additional ImageJ plugin that can be installed from online sources. The *Watershed* command described above has not parameters to adjust and especially in the case of touching objects the segmentation can be not correct. In the *Adjustable Watershed*, instead, there is the possibility to set the tolerance that in the standard *Watershed* is equal to 0.5. The tolerance determines the difference of radius between the smaller of the largest inscribed circles and a circle inscribed at the neck between the particles.

Analyze Particles

The *Analyze* menu contains commands related to the measurements on image data and plugins related to image analysis. In particular, *Analyze Particles* (*Analyze*→*Analyze Particles*) is the command that counts and measures objects in a binary or thresholded image. A range of size (in pixel²) and a range of circularity can be set for the analysis of the objects.

In output the results of the analysis are displayed in a tabular form: the parameters reported in the table are those that are set in *Analyze*→*Set Measurement*. The interesting parameters are in this case the area, the centre of mass, the shape descriptors, the perimeter and the Feret's diameter. So, area, x and y coordinates of the centre of mass, perimeter, circularity, Feret's diameter, solidity and aspect ratio of the particles are reported in the results table. Moreover, in output also the *Outlines* or the *Overlay Outlines* can be shown. The *Outlines* image contains numbered outlines of the measured particles, displayed in a new image. The *Overlay Outlines* are instead outlines overlaid in the original image.

Finally, it is possible to record a *Macro* with all the commands so that the same procedure can be repeated on each image automatically.

References

- Boateng A.A., Barr P.V. (1997). Granular flow behaviour in the transverse plane of a partially filled rotating cylinder, *Journal of Fluid Mechanics*, Vol. 330, pp. 233–249.
- Cantelaube F., Bideau D. (1995). Radial Segregation in a 2d Drum: an Experimental Analysis, *Europhysics Letters*, Vol. 30 (3), pp. 133-138.
- Cheng N. S. (2016). Difference between static and dynamic angle of repose of uniform sediment grains, *International Journal of Sediment Research*, Vol. 32 (2), pp. 149-154.
- Clément E., Rajchenbach J., Duran J. (1995). Mixing of a Granular Material in a Bidimensional Rotating Drum, *Europhysics Letters*, Vol. 30 (1), pp. 7-12.
- Dubè O., Alizadeh E., Chaouki J., Bertrand F. (2013). Dynamics of non-spherical particles in a rotating drum, *Chemical Engineering Science*, Vol. 101, pp. 486-502.
- Henein H., Brimacombe J.K, Watkinson A.P. (1983). Experimental study of traverse bed motion in rotary kilns, *Metallurgical Transaction B*, Vol. 14 (2), pp. 191-205.
- Henein, H., Brimacombe, J.K, Watkinson, A.P. (1985). An experimental study of segregation in rotary kilns,” *Metallurgical Transaction B*, Vol. 16 (4), pp. 763-774.
- Ferreira T., Rasband W. (2012). *ImageJ User Guide*.
- Ingram A., Seville J.P.K, Parker D.J., Fan X., Forster R.G. (2005). Axial and radial dispersion in rolling mode rotating drums, *Powder Technology*, Vol. 158 (1-3), pp. 76-91.
- Mellmann J. (2001). The transverse motion of solids in rotating cylinders – forms of motion and transition behaviour, *Powder Technology*, Vol 118, pp 251-270.
- Prigozhin L. (1993). A variational problem of bulk solids mechanics and free-surface segregation, *Chemical Engineering Science*, Vol. 48, pp. 3647-3656.
- Prigozhin L., Kalman H. (1998). Radial mixing and segregation of a binary mixture in a rotating drum: Model and experiment, *Physical Review*, Vol. 57 (2), pp 2073-2080.
- Rhodes, M. (2008). *Introduction to Particle Technology* (Second Edition), John Wiley & Sons Ltd, Bognor Regis (U.K), pp. 293-301.
- Rutgers, R., (1965). Longitudinal mixing of granular material flowing through a rotating cylinder, *Chem. Eng. Sci.* 20, pp 1079-1087, 1089-1100.
- Santomaso, A.C., Petenò, L., Canu, P. (2006). Radial segregation driven by axial convection, *Europhysics Letters*, Vol. 75 (4).
- Santomaso, A.C., Canu, P. (2007). Single particles properties vs. bulk flowability, *Proceedings of 5th International Conference for Conveying and Handling of Particulate Solids*.

- Santos D.A., Scatena R., Duarte C.R., Barrozo M. A. S. (2016). Transition phenomenon investigation between different flow regimes in a rotary drum, *Brazilian Journal of Chemical Engineering*, Vol. 33 (3), pp 491-501.
- Thomas N. (2000). Reverse and intermediate segregation of large beads in a dry granular media, *Physical Review*, Vol. 62 (1), pp 961-974.
- Van Puyvelde D.R., Young B.R., Wilson M.A., Schmidt S.J. (2000). Modelling transverse segregation of particulate solids in a rolling drum, *Chemical Engineering Research and design*, Vol. 78 (4), pp 643-650.
- Woodle G.R., Munro J.M. (1993). Particle motion and mixing in a rotary kiln, *Powder Technology*, Vol. 76 (3), pp 241-245.
- Yang H., Zhang B.F., Li R., Zhen G., Zivkovic V. (2017). Particle dynamics in avalanche flow of irregular sand particles in the slumping regime of a rotating drum, *Powder Technology*, Vol. 311, pp 439-448.

Web Sources

<https://www.freecadweb.org/?lang=it> (06.05.2017)

<http://imagej.net/Plugins> (11.05.2017)

http://imagejdocu.tudor.lu/doku.php?id=plugin:segmentation:adjustable_watershed:start
(16.05.2017)